Multi-Hazard Lifecycle Methods for Aging Structures and Infrastructure Systems

DISSERTATION

Presented in Partial Fulfillment of the Requirements for the Degree Doctor of Philosophy in the Graduate School of The Ohio State University

By

SeyedEhsan Fereshtehnejad

Graduate Program in Civil Engineering

The Ohio State University

2018

Dissertation Committee:

Dr. Abdollah Shafieezadeh, Advisor

Dr. Rabi Mishalani

Dr. Halil Sezen

Dr. Can Emre Koksal

Dr. Steve Hovick

Abstract

Extreme hazards such as earthquakes, floods, and hurricanes can significantly affect the performance and serviceability of structures and infrastructure systems during their lifetime. Recent prominent examples include the 2017 earthquake in the vicinity of Iran-Iraq border and the 2017 earthquake in Mexico that led to hundreds of fatalities. Hurricane Matthew (2016), Harvey (2017), Irma (2017), and Jose (2017) caused significant damage to critical infrastructure systems in a number of south-eastern states in the U.S. Such hazards can occur multiple times during the lifetime of infrastructure systems. Each event is accompanied by a set of adverse consequences including, among others, human casualties, physical damage, and downtime due to the repair of damage and restoration of the functionality of the system. In addition, as infrastructure assets are exposed to environmental stressors and service loads, they undergo gradual aging and deterioration over their lifetime. The subsequent degradations in the capacity of the systems increase their vulnerability against hazards over time. These compounding effects, among others, pose a tremendous challenge for evaluating the performance of structures and infrastructure systems, and managing their performance. In the light of such challenges and budget limitations, it is important to evaluate the lifecycle cost of infrastructure systems in order to minimize the potential losses over their service lifetime.

For structures or infrastructure systems that are exposed to multiple hazards during their lifetimes, damage accumulation is a critical issue. As supported by historical records, the accumulation of damage from prior events can considerably increase the vulnerability of structures and infrastructure systems to future hazards. However, this phenomenon is either disregarded or addressed inadequately in existing risk management frameworks. In addition, these frameworks do not incorporate effects of gradual deterioration on the reduced capacity of infrastructure systems against hazards, or they make significant simplifications in doing so. This limitation may lead to unrealistic assessments of the lifecycle performance of these critical assets, and subsequently, ineffective retrofit or repair decisions.

This doctoral research proposes probabilistic lifecycle cost and resilience analysis methods that properly incorporate the foregoing effects in order to arrive at optimal design or retrofit decisions among a list of pre-specified alternatives for individual structures and infrastructure systems. In the developed methods, design or retrofit alternatives are considered to be applied at the current time for a specified lifetime, where the state of the system is known perfectly at the current time. In addition, hazards of the same or different types are considered to be independently occurring. The new contributions of the proposed frameworks in this research include:

- Probabilistic consideration of the impact of damages induced by prior hazards on the increased vulnerability of systems against future potential hazards for lifecycle cost and resilience assessments when hazards are of the same type.

- Incorporation of the dependencies between different types of damages that are induced by multiple types of hazards in the lifecycle cost analysis.
- Integration of the impact of gradual deterioration on the reduced capacity of the system over time in lifecycle cost analysis with multiple types and occurrences of hazards.

Dedication

To

My brilliant beloved wife, Saeideh

For being a constant source of unwavering encouragement and support in my life.

My parents, Jila and Mehdi

For not only raising me with unconditional love but also teaching me how to work hard for the things that I aspire to achieve.

My brothers, Mohammad and Milad

For always being my support over the years.

Acknowledgments

I would like to acknowledge the National Science Foundation (NSF) to have partly funded my research through award CMMI 1333943. Any opinions, findings, and conclusions or recommendations expressed in this dissertation are those of the author and do not necessarily reflect the views of the National Science Foundation.

I would like to thank my advisor, Dr. Shafieezadeh, for his unwavering support, encouragement, patience, time and envision in the course of the past five years of my PhD studies. More importantly, I am grateful to him for instructing me how to think critically to be able to find effective solutions for challenging and complex problems. I benefit tremendously from his enthusiasm, skepticism in research, and technical and editorial advice for completing this dissertation. He is a great professor who really cares about his students and their future. For these I am always indebted to him.

I want to thank my thesis committee member, Dr. Rabi Mishalani, for what I learned from his instructive course, Infrastructure System Analysis, which contributed to my PhD research. I would like to also thank his beneficial advices during my PhD candidacy exam and his guidance and insightful feedback during the preparation of this dissertation.

I would like to thank Dr. Emre Koksal for offering his great course, Discrete Stochastic Process, in which I gained deep knowledge on probability topics and stochastic

processes. This greatly assisted me in developing new probabilistic methods presented in this dissertation for risk-based optimal management of structures and infrastructure system. I also appreciate him to kindly serve on my PhD candidacy and Dissertation committee.

I want to express my gratitude to Dr. Halil Sezen for being on my candidacy and dissertation committee, and for his great course "Prestressed Concrete Design". I am especially thankful for his insightful suggestion that encouraged me to be always considerate about the practicality of my research on real world problems.

I am also grateful to my colleagues and caring friends at RAMSIS lab who kindheartedly gave their help, support and made my PhD life wonderful.

I want to thank my parents who gave me their unconditional blessing and support through every stage of my education.

I owe a special thanks to my wife, Saeideh, for her love, patience, self-sacrifice, and amazing support and help.

Last and foremost, I would like to thank God Almighty, without whose will and grace this achievement would not have been possible.

Vita

Sep. 2004 to Sep. 2008	B.Sc. in Structural Engineering, Civil Engineering, Isfahan University of Technology, Iran
Sep 2008 to Feb. 2011	M.Sc. in Earthquake Engineering, Civil Engineering, Amirkabir University of Technology, Iran
Sep. 2009 to Sep. 2011	Structural Engineer, Boland-Payeh Inc., Iran
Sep. 2010 to Sep. 2012	Graduate Research Assistant, Department of Civil Engineering, Amirkabir University of Technology, Iran
Aug. 2013 to Present	PhD in Structural Engineer, Civil Engineering, The Ohio State University
August 2013 to July 2014	Graduate Fellow, Graduate School, The Ohio State University
August 2014 to Present	Graduate Research Assistant, Department of Civil Engineering, The Ohio State

University (Funded by Ohio Department of Transportation)

Publications

Journal Papers

J1. Fereshtehnejad, E. and Shafieezadeh, A., 2018. A Multi-Type Multi-Occurrence Hazard Lifecycle Cost Analysis Framework for Infrastructure Management Decision Making, Engineering Structures, 167: 504-517.

J2. El-Khoury O, Shafieezadeh A, Fereshtehnejad E., 2018. A risk-based life cycle cost strategy for optimal design and evaluation of control methods for nonlinear structures. Earthquake Engineering & Structural Dynamics.

J3. Fereshtehnejad, E. and Shafieezadeh, A., 2017. A randomized point-based value iteration POMDP enhanced with a counting process technique for optimal management of multi-state multi-element systems. Structural Safety, 65, pp.113-125.

J4. Fereshtehnejad, E., Hur, J., Shafieezadeh, A. and Brokaw, M., 2017. Ohio Bridge Condition Index: Multilevel Cost-Based Performance Index for Bridge Systems. Transportation Research Record: Journal of Transportation Research Board, pp.274-286.

J5. Fereshtehnejad, E. and Shafieezadeh, A., 2016. Multiple hazard incidents lifecycle cost assessment of structural systems considering state-dependent repair times and

fragility curves. Earthquake Engineering and Structural Dynamics, 45(14), pp.2327-2347.

J6. Fereshtehnejad, E., Banazadeh, M. and Shafieezadeh, A., 2016. System reliability-based seismic collapse assessment of steel moment frames using incremental dynamic analysis and Bayesian probability network. Engineering Structures 118 (2016): 274-286.

J7. Banazadeh, M. and Fereshtehnejad, S.E., 2014. Probabilistic Assessment of Collapse Limit-State in Steel Frames by Simulating Failure Modes Using Bayesian Probability Network. Amirkabir Journal of Civil and Environmental Engineering. 45 (2): 83-96.

J8. Fereshtehnejad, E., Hur, J., Shafieezadeh, A. Brokaw, M., Noll, B., Backs, J., and Waheed, A. Systematic Procedures for the analysis of Agency- and User- Costs of Bridge Repair Actions. Transportation Research Record: Journal of Transportation Research Board, 118, Accepted for publication.

Peer Reviewed Conference Publications

C1. Fereshtehnejad, E., and Shafieezadeh, A., 2018. Optimal Bridge Repair Actions Considering the Potential for Multiple Earthquake Occurrence. Presenting in 11th National Conference on Earthquake Engineering. Los Angeles, California, June 25-29, 2018.

C2. Fereshtehnejad, E. and Shafieezadeh, A., 2017. Optimal Retrofit Decision-Making for Bridge Systems Based on Multi-Hazard Lifecycle Cost Analysis. 11th international Bridge and Structure Management Conference. Mesa, Arizona, USA.

C3. Fereshtehnejad, E., Hur, J., Shafieezadeh, A. and Brokaw, M., 2017. Ohio Bridge Condition Index: A Novel Cost and Condition Based Index for Assessment of Bridges. 11th international Bridge and Structure Management Conference. Mesa, Arizona, USA.

C4. Shafieezadeh, A. and Fereshtehnejad, E., 2015. Risk management of multi-state multi-component bridge systems using partially observable Markov decision processes. International Conference on Applications of Statistics and Probability in Civil Engineering (ICASP). Vancouver, Canada.

Other Conference Publications

C5. Fereshtehnejad, E., Hur, J., Shafieezadeh, A. Brokaw, M., Noll, B., Backs, J., and Waheed, A. A Bridge Performance Index with Objective Incorporation of Safety Risks. 97th Transportation Research Board Annual Meeting. Washington DC., January 7-11, 2018.

C6. Fereshtehnejad, E., Hur, J., and Shafieezadeh, A., 2017. Performance Measures for The Assessment of the Condition of Bridges: A Critical Review. 96th Transportation Research Board Annual Meeting. 17-05179.

C7. Fereshtehnejad, S.E., and Banazadeh, M., 2012. A Combination of the IDA-based Bayesian Probability Network and the Response Surface Method in System Reliability Assessment of Steel Frames. 15th World Conference on Earthquake Engineering, Lisbon, Portugal, 24-28.

Fields of Study

Major Field: Civil Engineering

Table of Contents

List of Tables

List of Figures

Chapter 1: Introduction

1.1. Motivation

Extreme hazards such as earthquakes, floods, and hurricanes can significantly affect the performance and serviceability of structures and infrastructure systems during their lifetime. Despite their low probability of occurrence, the consequences of these extreme events can be catastrophic. Recent prominent examples include the 2017 earthquake in Iran-Iraq border and the 2017 earthquake in Mexico that led to hundreds of fatalities. Hurricane Matthew in 2016, and hurricanes Harvey, Irma, and Jose in 2017 caused significant damage to critical infrastructure systems in a number of south-eastern states in the United States. Only the insured losses amounted to between $1~5 billion (1–3), and the total losses are expected to be considerably higher. Such hazards can occur multiple times during the lifetime of structures and infrastructure systems, especially in hazard prone areas. Each event has the potential to incur a set of losses including, among others, human casualties, physical damage, and downtime due to the repair of damage and restoration of the functionality of the system. The incurred losses may considerably increase if hazards occur within a short period of time from previous events, leaving insufficient time for the repair of the induced damages from prior hazards. This can have catastrophic consequences, as it increases the vulnerability of structures and infrastructure systems

against hazards. A number of historical examples that support this view are elaborated below:

- A chain of three consecutive major earthquakes occurred in Central Italy from August 2016 to October 2016 (4). The first event on August 24 had a magnitude of 6.1, the second on October 26 occurred with a magnitude of 5.9, and the third one on October 30 had a magnitude of 6.5. Following reconnaissance investigations on the extent of structural damage after each of these earthquakes, it was observed that many structures in the affected villages and hamlets sustained significant accumulation of damage after the earthquakes in October (4). Considering that the three earthquakes were almost similar in magnitude with short inter-arrival times, it is inferred that untreated hazard-induced damages reduced the capacity of structural systems resulting in their higher vulnerability against the next events.
- Following the damaging Northridge earthquake on January 1994 in San Fernando Valley, affected structures sustained additional damage during the subsequent aftershocks (5). Considering that the aftershocks were all smaller in magnitude compared to the main-shock (6), the additional damage sustained by structures during aftershocks is in part attributed to the reduced capacity of structures because of the main-shock.
- In September 2010, an earthquake with the magnitude of 7.1 caused widespread damage to structures and infrastructure systems in Christchurch, New Zealand (7). Six months later, an aftershock with the magnitude of 6.3 shook the same region and induced further damage in already damaged structures and infrastructure

systems. 185 casualties were reported due to the aftershock (8), among which 115 were due to the collapse of the Canterbury television building. The collapse has been attributed to the non-ductile design of the building and the accumulated damage from the previous earthquake on September 10th and its aftershocks (9,10).

- In 2011, in the east coast of Honshu, Japan, a devastating tsunami took place due to a strong earthquake that happened just before the tsunami (11). The sequence of earthquake and tsunami caused massive destructions to the region's infrastructure (12).
- In 2017, hurricane Harvey struck regions close to Cameron, Louisiana two times in less than a week, and caused notable damage to the transportation infrastructure (13,14).

Risk analysis for such circumstances is further exacerbated by uncertainties in structural response and randomness in the intensity of hazards and their times of occurrence.

Another source of complexity is the aging and deterioration of infrastructure systems over their lifetime due to exposure to environmental stressors and service loads. The subsequent degradations in the capacity of the systems increase their vulnerability against hazards over time. These compounding effects, among others, pose a tremendous challenge for evaluating the performance of structures and infrastructure systems, and managing their safety and serviceability. In light of budget limitations, it is important to accurately evaluate the lifecycle cost and resiliency of structures and infrastructure systems in order to minimize the potential losses over their service lifetime. Considering individual

structures and infrastructure systems, this doctoral research proposes probabilistic lifecycle cost and resilience analysis methods that properly incorporate the foregoing effects in order to arrive at optimal decisions for these assets.

1.2. Background

A proper decision-making framework should take into account all possible hazard incidents and the corresponding consequences. In performance-based design engineering, for different levels of the frequency of hazard events, different performance objectives in terms of acceptable damage-states are recommended. For instance, FEMA 445 (15) specifies that only little or no damage is acceptable for frequently happening events, whereas considerable damage is allowed to occur in case of extremely large and rare hazard events. The logic behind the acceptability of such performance levels is the risk associated with each damage-state. This risk is normally expressed as the product of the damage-state likelihood by its implications. The implications are often articulated in terms of monetary loss. The foregoing product is also referred to as the *risk cost*.

Lifecycle cost (LCC) of infrastructure systems is a capable and comprehensive performance measure that incorporates the associated risk costs of the entire set of considered damage-states during the lifetime of the system. In the literature of risk analysis for infrastructure systems, LCC is considered as one of the most appropriate performance measures for infrastructure decision-making (16–19). In addition to hazard-induced risk costs, LCC can include the initial construction or retrofit costs, as well as the costs of routine maintenance and inspections that are periodically performed. A number of studies

have developed and applied LCC frameworks to investigate effects of a single type of hazard on an infrastructure and identify optimal strategies for managing risks to the system. Examples of such studies include (20–26). In these studies that consider multiple hazard incidents, it is assumed that repairs following hazard occurrences are instantaneous or there are no repair actions after each incident of hazards. In reality, however, the time required for repairing damage to infrastructure systems depends on the extent of damage, type of repair action, availability of materials and crew, and socio-economic factors, among others. When repair times are long, the possibility of next hazards happening before the damage arising from previous hazards are repaired increases. This results in accumulation of damage and represents a vulnerable condition for infrastructure systems.

When looking at infrastructure systems located in regions that are exposed to more than one type of hazard, many studies, such as (27,28), disregarded the dependency between damage conditions induced by various hazard types. Jalayer et al. (29) attempted to address such dependencies for multiple hazard types in a framework that requires simulating all possible scenarios for the order of hazard events of various types and intensities. In addition, each of these scenarios requires time-consuming structural pushover and dynamic analyses. These requirements make the framework computationally prohibitive for a comprehensive LCC analysis. Moreover, there are a number of assumptions in that framework that may not accurately represent the performance of actual systems (30). These assumptions will be elaborated in Chapter 2.

Very few studies have investigated LCC analysis for structures and infrastructure systems subjected to both random hazard occurrences and gradual deterioration due to

environmental stressors. Some of these studies include (31–34). In these studies, either the potential of damage accumulation induced by successive hazards are overlooked or major simplifications are made in the suggested frameworks that can impose considerable error to LCC calculations. These simplifications are elaborated in Chapter 4. In addition, none of the proposed methods incorporate more than one type of hazard, which is essential for proper management of many infrastructure systems.

Besides LCC analysis, resilience has also gained considerable attention as a prominent measure for the functionality performance of structures and infrastructure systems against hazards. Proper estimation of this metric for structures and infrastructure systems can assist in disaster management. For problems where hazard occurrences are considered over the lifetime of the infrastructure systems, a number of research studies have proposed expected lifecycle resilience indexes (35–38). However, these measures neglect the following two primary factors:

- The relative time between hazard occurrences, which can be less than the considered control time in the resilience index formulation.

- The possibility of a weakened system due to the incomplete repair of damages induced by previous hazards, or leaving those damages untreated.

In summary, the potential of damage-accumulation is either disregarded or addressed inadequately in existing risk management frameworks. In addition, these frameworks do not incorporate the effects of gradual deterioration due to environmental stressors on the reduced capacity of infrastructure systems against hazards, or they make major simplifications. These limitations may lead to unrealistic assessments of the lifecycle

performance of these critical assets, and subsequently, ineffective retrofit or repair decisions.

1.3. Objectives and Scope of the Research

The objective of this doctoral research is to develop comprehensive probabilistic methods that can minimize the lifecycle cost of individual structures and infrastructure systems considering potential exposures to multiple extreme events in the lifetime of these systems and the compounding effects of aging and deterioration. This goal has been achieved here through development of probabilistic lifecycle cost and resilience analysis methods that properly incorporate the foregoing effects in order to arrive at optimal design or retrofit decisions among a list of pre-specified alternatives for structures and infrastructure systems. The new contributions of the proposed frameworks in this research include:

- Probabilistic consideration of the impact of damages induced by prior hazards on the increased vulnerability of systems against future potential hazards for lifecycle cost and resilience assessments when hazards are of the same type.
- Incorporation of the dependencies between different types of damages that are induced by multiple types of hazards in the lifecycle cost analysis.
- Integration of the impact of gradual deterioration on the reduced capacity of the system over time in lifecycle cost analysis with multiple types and occurrences of hazards.

In the developed methods, the following assumptions and considerations exist:

- Design or retrofit alternatives are exogenously predetermined.

- Design or retrofit alternatives are considered to be applied at the current time for a specified lifetime.
- The damage-state of the system at the current time is known perfectly (with probability one).
- Hazards of the same or different types are considered to be independently occurring.

Whereas the developed frameworks in this dissertation have attempted to more realistically and accurately estimate the expected LCC of individual structures and infrastructure systems compared to the existing methods in the field of multi-hazard LCC analysis, the foregoing limitations may limit the reliability and accuracy of the calculated LCCs and the scope of the identified findings. Further research studies can be conducted in the future to relax these assumptions to arrive at more reliable and accurate estimates for LCC analyses and widen the scope of the applicability of the corresponding findings.

1.4. Dissertation Agenda

Chapter 1 presents an introduction to multi-hazard risk management of infrastructure systems and describes the motivations for carrying out this research study. In Chapter 2, a lifecycle cost analysis framework for decision-making across predetermined design or retrofit alternatives is developed that probabilistically incorporates the possibility of multiple occurrences of one type of hazard during the lifetime of the structure or infrastructure system. Unlike other methods, this method accounts for the dependencies of damages from consecutive hazards, which can increase the vulnerability of the system due to the potential of damage accumulations. These damage-dependencies are incorporated

through a recursive function to significantly reduce the computational demand of the framework. Chapter 2 also presents a comprehensive framework for the assessment of the lifecycle resilience of structures and infrastructure systems considering damage-dependencies from consecutive hazards of one type. As mentioned earlier, resilience index is a prominent measure of the functionality performance of structures and infrastructure systems against hazards, and thus proper estimation of this index is important for disaster management. Chapter 3 extends the probabilistic framework proposed for one hazard type in Chapter 2 to multiple types of hazards that may occur at any time and order during the lifetime of the system. In Chapter 4, effects of gradual deterioration due to environmental stressors are probabilistically integrated with the potential of multiple types of hazards. This new framework facilitates reliable lifecycle cost assessment for aging infrastructure systems against extreme hazards. Finally, the overall conclusions of this study and the future research directions are discussed in Chapter 5.

Chapter 2: Risk-Based Lifecycle Cost and Resilience Analysis Considering Multiple Occurrences of one Hazard Type

2.1. Summary

The performance and serviceability of structural systems during their lifetime can be significantly affected by the occurrence of extreme events. Despite their low probability, there is a potential for multiple occurrences of such hazards during the relatively long service life of systems. This chapter proposes a comprehensive framework for the assessment of LCC of structures and infrastructure systems subject to multiple hazard events throughout their lifetime. The framework entails the LCCs of maintenance and repair, as well as the salvage value of the structure at the end of the lifetime. The primary feature of the proposed framework is the incorporation of effects of incomplete repair actions on the accumulated damage through damage-state dependent repair times, considering the possibility of multiple occurrences of a single type hazard. In addition, the developed method requires limited resources in terms of input data and computational costs. A dynamic programming procedure is proposed to calculate the expected damage-condition of the structure for each possibility of the number of hazard incidents based on state-dependent fragility curves. Based on the proposed LCC analysis method optimal decision-making can be made across predetermined design or retrofit alternatives.

The foregoing features are also integrated in the resilience index formulation, which is a common measure in the field of disaster recovery assessment following hazard occurrences. Resilience index is a capable measure that properly reflects the serviceability performance of infrastructure systems against hazards. This chapter proposes a new formulation of the resilience index that accurately accounts for the possibility of multiple hazard occurrences in the lifetime of a structure or an infrastructure system. Unlike existing resilience indexes, the proposed index, called Risk-based Lifecycle Resilience Index (RLRI), probabilistically accounts for 1) the inter-arrival time between stochastic hazard occurrences, and 2) damage accumulations due to plausible incomplete repairs, or untreated structural damages. These factors are incorporated using the theorem of total probability, conditional probability chain rule at multiple levels, Bayes rule, the foregoing dynamic programming procedure for damage-state transition probabilities, and time-variant reward functions for system recovery at different damage-states.

The proposed LCC framework is first applied to a moment-frame building located in a region with high seismicity and LCCs are evaluated for six retrofit plans. The results displayed variation in the ranking of the retrofit actions with respect to lifetime. Furthermore, sensitivity analyses demonstrated that disregarding repair time in the LCC analysis can result in false identification of unsafe retrofit actions as optimal and reliable strategies. In a second case study, the developed framework in this chapter is applied to a realistic bridge system located in a seismic region. Six alternatives for the repair of earthquake-induced damages corresponding to the extent and speed of performing such repairs are evaluated. Results show that not performing repair actions for slight damages

results in less incurred expected lifecycle hazard costs compared to the case where all extents of damage are repaired following an earthquake. This is attributed to the high traffic demand, and consequently considerable traffic disruption on the bridge due to repairs, while the improvement on the capacity of the bridge caused by repairs on slight damages is insignificant. Furthermore, investing on fast repair technologies decreases the expected lifecycle hazard costs, despite the higher costs of implementing these methods.

Implementation of the proposed lifecycle resilience index for the realistic case study bridge shows that for a region with a moderate chance of high-intensity earthquakes, avoiding repairs for slight damages and subsequent reduced traffic disruptions result in higher lifecycle functionality for the bridge. However, when the bridge is located in a region with a more chance of high-intensity earthquakes, for service lifetimes more than 35 years, the agency is recommended to conduct repairs for all extents of damages. A comparison between these optimal alternatives that are recognized following the lifecycle resilience index framework with those determined according to the proposed total LCC framework shows that repair plans that lead to maximum functionality do not necessarily incur minimum expected lifecycle hazard-induced costs. The latter focuses only on the serviceability performance of the system, while the former incorporates all consequences objectively through the unified metric of cost.

The results of the lifecycle resilience index also indicate that disregarding couplings between damages from consecutive earthquakes can result in significant overestimation of the resilience index, as well as false identification of the optimal repair

policy. This improper policy may impose considerable adverse consequences on the community.

2.2. Introduction

Extreme natural and manmade hazards can significantly impact the performance and serviceability of structures and infrastructure systems during their lifetime. While these extreme events may rarely happen, there is a possibility for multiple occurrences of such events throughout the service life of infrastructure systems. For instance, a building in a seismic region is prone to experience multiple earthquake occurrences throughout its lifetime. Each occurrence of an extreme event is accompanied by a set of advert consequences including, among others, human casualties, physical damage, and downtime due to the repair of damage and restoration of the functionality of the system. This highlights the need for efficient frameworks that enable identification of proper maintenance and retrofit strategies to reduce the potential of such negative implications and ensure an acceptable level of safety and serviceability throughout the service life of the system.

2.2.1. Existing and the Proposed Lifecycle Cost Analysis Frameworks

A proper decision-making framework should take into account all possible hazard incidents and the corresponding consequences. In performance-based design engineering, for different levels of the frequency of hazard events, different performance objectives in terms of acceptable damage-states are recommended. For instance, FEMA 445 (15)

specifies that only little or no damage is acceptable for frequently happening events, whereas considerable damage is allowed to occur in case of extremely large and rare hazard events. The logic behind the acceptability of such performance levels is the risk associated with each damage-state. This risk is normally expressed by the product of the damage-state likelihood by its implications. The implications are often articulated in terms of monetary loss. Hereafter, the foregoing product is referred to as *risk cost*. LCC of infrastructure systems is a capable and comprehensive performance measure (16,17,19) that incorporates the associated risk costs of the entire set of considered limit-states during the lifetime of the system. This metric has found many applications for management of civil infrastructure systems. For example, Frangopol and Estes (39) determined the optimal periodic inspection and maintenance strategies of a bridge by minimizing the expected LCC of the system. The only considered limit-state in that research was failure of the bridge. In addition, deterioration in structural elements was the sole cause of strength degradation. Considering random hazards, a number of studies have developed and applied LCC frameworks to investigate effects of multiple occurrences of a single type of hazard on a structures or an infrastructure and identify optimal strategies for managing risks to the system. Examples of such studies include Vanmarcke et al. (20–26). In these investigations, for all possible damage-states that the system may experience, the repair following each hazard occurrence was considered to be instantaneous or it was assumed that no repair action is performed after such events. In reality however, the repair time and the time of preparing for the repair actions vary depending on the damage-state that the system experiences, type of rehabilitation/repair strategies, and socio-economic

factors, among others. In case of long repair times in the aftermath of severe damage-states, the likelihood of next hazards occurring before the system is completely repaired increases. In this case, the existing damage very likely aggravates the level of damage that the next hazard can induce, therefore increasing the vulnerability of the infrastructure system. On the other hand, if the structure sustains a less severe damage following an extreme event, there is a high probability that the repair action is complete and the system is back to the intact damage-state before next hazard events affect the system. Jalayer et al. (29) proposed a procedure for the LCC assessment of structures against multiple types of hazards by considering the possibility of incomplete repair scenarios as a function of structural damage-states. The discounted maintenance costs, the possibility of multiple hazard occurrences and the repair costs following each hazard event were considered in the expected lifetime cost of the system. The damage-state at the occurrence of each hazard event was assumed dependent on the repair strategies and the sequence of the occurrence of different types of previous hazard scenarios. Considering all possible combinations of these ordered-event scenarios can make the problem exponentially large and significantly time-consuming. Furthermore, the procedure for deriving such conditional damage-states requires numerous static pushover and dynamic time history analyses. The process should be repeated for all of the sequences of hazard events which significantly increases the computational demand when the number of combinations is large. In addition, the formulation of the framework is based on a set of assumptions that may not truly represent the behavior of actual systems. For instance, the probabilistic event of exceeding a particular damage-state i at jth occurrence of a hazard incident is

considered independent of the previously exceeded damage-states other than *i*. However in reality, the damage-state of the system after each hazard incident directly depends on the extent of damage that the structure has experienced from prior events. Furthermore, when breaking down the probability of exceeding a damage-state *i* into events of prior damaged and undamaged states, the repair time for damage-state *i* is assigned to all prior damage sustained in past events independent of the damage condition of the system following those events.

This chapter proposes a new method for probabilistic LCC assessment of individual structural systems exposed to multiple occurrences of a hazard type. It is worthy to note that in the literature of structures and infrastructure management, occurrences of multiple types of hazards such as earthquake, scour, and flood are referred to as "multi-hazard" occurrences, which will be investigated in Chapters 4 and 5. The focus of this chapter however, is on multiple occurrences of a particular hazard type e.g. multiple earthquake events. The cost elements in the proposed framework include the expected annual maintenance cost, the expected incurred costs due to multiple hazard incidents, and the expected salvage value as a function of the hazard-induced damage-state of the system at the end of its service life. The expected hazard-induced cost is calculated by considering all scenarios of hazard events. Probabilities of damage-states of the system are determined recursively and the associated risk costs are computed using damage-state dependent fragility curves for multiple structural limit-states considering the possibility of incomplete repair actions at the time of occurrence of the next hazard incident. The framework is comprehensive yet time-efficient due to a dynamic programming method

that is proposed to estimate the damage-state at a hazard incident through consideration of possible sequences of prior hazard events.

In Section 2.3, the analytical framework of the proposed LCC method is elaborated. This framework is applied to a case study frame building with six retrofit options introduced in Section 2.5. In this section, the optimal strategy with the least expected LCC is identified, and the effect of repair time on the identification of the optimal decision is evaluated. In Section 2.6, the developed method is implemented on a second case study; a bridge system which is located in a seismic region. This section provides characteristics and other case study bridge data required for the application of the proposed LCC analysis framework. This is followed by the LCC results evaluated for six alternatives for the repair of earthquake-induced damages corresponding to the extent and speed of performing such repairs.

2.2.2. Existing and the Proposed Lifecycle Resilience Analysis Frameworks

As mentioned in the previous section, it is significant to integrate effects of incomplete repair actions on the accumulated damage into LCC analysis. This can be achieved using damage-state dependent repair times, considering the possibility of multiple hazard occurrences. These effects are also integrated in the resilience index formulation, which is a common measure in disaster recovery assessment following hazard occurrences.

Among various infrastructure performance measures, resilience index is a capable measure that properly reflects the serviceability performance of structures and infrastructure systems against hazards. This index can be particularly useful for risk-

informed decision-making when recovering the functionality of systems is the priority. Resilience index incorporates the track of system recovery after a hazard, and various resilience properties of a system including robustness, rapidity, resourcefulness, and redundancy (40,41). For a single hazard event, resilience index, R, is defined as the area under the functionality curve of the system from the time of hazard occurrence, t_0, to the end of a considered control time, $t_0 + t_h$, i.e. the gray area in Figure 2-1, over the functionality area during this period when the system is fully operational. In mathematical terms:

$$R = \frac{\int_{t_0}^{t_0+t_h} F(t)dt}{100\% \times t_h} \tag{2-1}$$

where $F(t)$ is the percentage-wise recovery function (or functionality) of the system at time t ($t_0 < t < t_h$). Noticeably, in the resilience index formulation in Equation (2-1), functionality of the system after a hazard incident is compared with the full functionality of this system before the occurrence of the hazard. Control time, t_h, is commonly considered as a time, during which the full recovery of the system can be achieved. For structures and infrastructure systems, this value is often considered as a value between one and two years (35,38,41–43). In hazard prone regions during the service lifetime of structures or infrastructure systems, they may experience multiple hazards. For instance, the rate of earthquake occurrence is approximately one per 2.7 years for the cities of Sacramento and Sierra Madre in California (calculated from U.S. Geological Survey (44)). This translates to 28 expected earthquakes for an infrastructure located in either of these cities with a service lifetime of 75 years. Thus, a realistic and accurate resilience

index should account for the potential of multiple hazard occurrences. To comply with this need, some research studies have suggested expected resilience indexes that account for multiple hazard occurrences in the lifetime of infrastructure systems and uncertainties in the robustness and recovery functions of these systems (35–38). However, these methods face the following two primary limitations:

1) The inter-arrival time between hazard occurrences is neglected, which affects the accuracy of resilience estimates. For more clarification, let's consider a scenario where a hazard takes place at time t_1 following the occurrence of a previous hazard at time t_0. There can be cases where the time difference between these two hazards is less than the considered control time for the evaluation of the resilience index (see Figure 2-1). However in existing resilience index formulations based on Equation (2-1), functionality of the system is evaluated until the end of the control time, which as noted, may be longer than the occurrence time of the next hazard event. In addition, there is a potential for multiple occurrences of such a scenario, since multiple hazard incidents with random inter-arrival times may hit the system during its lifetime. Thus, to accurately calculate the lifetime resilience index of the system with regard to these issues, both the system functionality and the full functionality areas in the resilience index formulation should probabilistically account for the inter-arrival times between hazard occurrences.
2) The possibility of a weaker system due to incomplete repairs of damages induced by previous hazards or due to leaving those damages untreated is

neglected. Agencies responsible for management of infrastructure systems may decide to repair hazard-induced damages or leave them untreated in the aftermath of an event. In the latter case, or the former when the repair actions are interrupted by the next hazard, the system is at a damage-state more severe than the intact condition at the time of the next hazard. In such circumstances, the system is more vulnerable to hazard-induced damages compared to the situation where the system is in the intact state. This issue is also extensively discussed in the previous chapter. An accurate and reliable resilience index should properly account for such dependencies between the damages from successive hazards.

The foregoing issues are probabilistically integrated in a risk-based lifecycle resilience index (RLRI) that is proposed in this chapter. The rest of this chapter is organized as follows: In Section 2.4, the development of the proposed RLRI formulation is presented. This index is then evaluated for the case study bridge system that is explained in the previous chapter. Section 2.7.1 and 2.7.2 explain the required data for the implementation of the proposed resilience index on the case study bridge. In Section 2.7.3, the results of the RLRI for the case study bridge are presented. In addition, the significance of stochastically incorporating the dependencies between damages from consecutive hazards, as well as their inter-arrival times in the resilience assessment are analyzed. Moreover, the proposed expected RLRI is employed to determine the best option among various repair alternatives based on their expected incurred LCCs and the agency's

available budget. Finally, Section 2.8 summarizes the findings of the entire chapter and presents the concluding remarks.

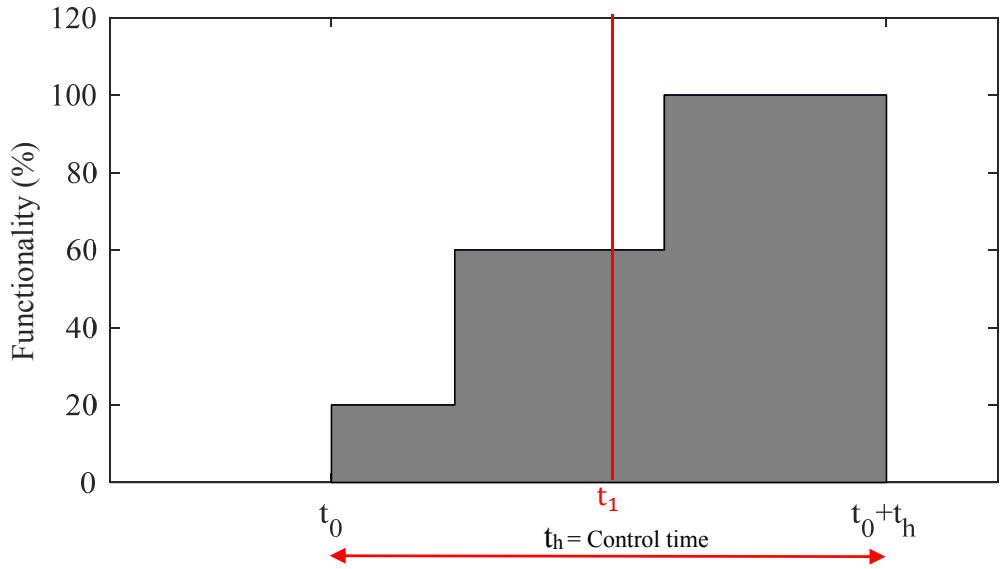

Figure 2-1 Functionality recovery of an infrastructure after the occurrence of a hazard

2.3. Analytical Framework for Lifecycle Cost Assessment

For a structure or an infrastructure system exposed to multiple hazard incidents during its lifetime, the expected LCC (C_T) is the aggregate LCCs of construction, maintenance, and repair, as well as the salvage value of the structure:

$$\bar{C}_T = \bar{C}_0 + \bar{C}_M + \bar{C}_R - \bar{V}_S \quad (2\text{-}2)$$

where $\bar{C}_0$ is the expected initial construction cost, $\bar{C}_M$ is the expected total maintenance cost, $\bar{C}_R$ is the expected total hazard-induced cost following hazard events, and $\bar{V}_S$ is the expected salvage value as a function of the hazard-induced damage-state of the system at the end of its service life. In this equation, the negative sign indicates that the salvage value is a benefit in favor of the owner(s). In order to account for the discounted costs in

the analysis, the costs incurred throughout the lifetime of the structure (i.e. $\bar{C}_M$ and $\bar{C}_R$) are considered on a yearly basis. Through the Net Present Value (NPV) formulation, all incurred costs, except for the $\bar{C}_0$, are converted to their equivalent value at the present time. Thus, the NPV for the total LCC of a structure ($\bar{C}_{T,NPV}$) is given by:

$$\bar{C}_{T,NPV} = \bar{C}_0 + \bar{C}_{M,NPV} + \bar{C}_{R,NPV} - \bar{V}_{S,NPV} \tag{2-3}$$

where $\bar{C}_{M,NPV}$ and $\bar{C}_{R,NPV}$ are the NPV of the expected maintenance and hazard-induced LCCs respectively, and $\bar{V}_{S,NPV}$ is the NPV of the expected salvage value of the structure at the end of its lifetime.

2.3.1. Expected Lifecycle Maintenance Cost

Periodical maintenance actions are often performed to maintain the structure in a healthy condition. In this dissertation, the periodical maintenance cost is approximated by a yearly expected constant value of $\bar{C}_m$ throughout the lifetime of the structure. The NPV for this cost incurred at time *t* ($\bar{C}_{m_t,NPV}$) can be written as:

$$\bar{C}_{m_t,NPV} = \gamma^t \times \bar{C}_m \tag{2-4}$$

where γ is the uniform annual discount factor, which can be calculated as $\frac{1}{1+\delta}$, with δ representing the discount rate. While yearly maintenance is performed on the structure, the NPV equivalent of the expected total lifecycle maintenance cost ($\bar{C}_{M,NPV}$) can be derived as follows:

$$\bar{C}_{M,NPV} = \sum_{t=1}^{T_{LC}} \gamma^t \times \bar{C}_m \tag{2-5}$$

where T_{LC} is the service lifetime of the structure.

2.3.2. Expected Hazard-Induced Lifecycle

When a structure is hit by an extreme hazard, it may sustain damage or stay intact. The extent of damage depends on the intensity of the hazard. The induced cost consists of direct losses due to physical damage to the system, injuries and casualties, as well as indirect losses due to the delay in providing services during downtime. Generally, after damages that are induced by hazards, the structure or infrastructure is planned for repair. Repair, downtime, and casualty costs depend on the damage-state of the structure after exposure to the event. It is common that the space of the damage-state of a structure following a hazard is represented by a mutually exclusive and collectively exhaustive set of discrete events. Here, the *n*th damage-state of the structure is represented by DS_n and the associated expected cost due to repair, downtime, and casualty by $\bar{C}_r(DS_n)$. For a single occurrence of a hazard incident, based on the total probability theorem, the expected hazard-induced cost at each time ($\bar{C}_{R,t}$) can be calculated by considering all the damage-states that the structure can experience and their corresponding costs as follows:

$$\bar{C}_{R,t} = \sum_{n=1}^{N_{DS}} \bar{C}_r(DS_n) \times P(DS_n, [t, t+1]) \tag{2-6}$$

where n represents the index for the damage-state of the structure, ranging from the intact condition (n=1) to the most severe state ($n = N_{DS}$) i.e. the collapse of the system (this state is also referred to as complete damage). In addition, the term $P(DS_n, [t, t+1])$ represents the probability that the structure is in damage-state n between time t and t+1.

The expected hazard-induced cost at time *t* when the structure is in damage-state *n* can be expressed as the difference between the expected hazard-induced cost if damage-state *n* is visited within timespan [0 *t*+1], and the expected hazard-induced cost due to damage-state *n* during time period [0 *t*]. Thus, Equation (2-6) can be rewritten as:

$$\bar{C}_{R,t} = \sum_{n=1}^{N_{DS}} \{\bar{C}_r(DS_n) \times P(DS_n, [0, t+1]) - \bar{C}_r(DS_n) \times P(DS_n, [0, t])\} \tag{2-7}$$

In the context of structural reliability, fragility curves are developed to determine the probability that critical engineering demand parameters (EDP) of the structure exceed certain limit-states given a particular hazard intensity (see Figure 2-2). Using this concept, $P(DS_n, [0, t])$ can be derived as the difference between the probabilities of LS_n and LS_{n+1}, which denote the events of exceeding limit-states *n* and *n*+1, respectively:

$$P(DS_n, [0, t]) = P(LS_n, [0, t]) - P(LS_{n+1}, [0, t]) \tag{2-8}$$

The procedure to compute $P(DS_n, [0, t])$ is also graphically depicted in Figure 2-2, where LS_1~LS_4 are limit-states 1~4 and DS_1~DS_4 stand for damage-states 1~4. Using Equation (2-7) and (2-8), Equation (2-6) can be rewritten as:

$$\begin{aligned}\bar{C}_{R,t} = \sum_{n=1}^{N_{DS}} \{&\bar{C}_r(DS_n) \times [P(LS_n, t+1) - P(LS_{n+1}, t+1)] - \bar{C}_r(DS_n) \\ &\times [\, P(LS_n, t) - \, P(LS_{n+1}, t)]\}\end{aligned} \tag{2-9}$$

In order to incorporate the effect of multiple hazard incidents, the term $\bar{C}_r(DS_n)$ in $\bar{C}_r(DS_n) \times [P(LS_n, t+1) - P(LS_{n+1}, t+1)]$ and $\bar{C}_r(DS_n) \times [\, P(LS_n, t) - P(LS_{n+1}, t)]$ should represent the *accumulated* hazard-induced cost due to multiple times of experiencing damage-state *n*, which are caused by multiple occurrences of hazard

events until times t and t+1, respectively. Based on this reasoning, Equation (2-9) should be modified to:

$$\bar{C}_{R,t} = \sum_{n=1}^{N_{DS}} \{\bar{C}_r(DS_n, t+1) \times [P(LS_n, t+1) - P(LS_{n+1}, t+1)] - \bar{C}_r(DS_n, t) \times [P(LS_n, t) - P(LS_{n+1}, t)]\} \quad (2\text{-}10)$$

where $\bar{C}_r(DS_n, t)$ is the expected accumulated hazard-induced cost incurred on the structure, if limit-state n is exceeded between time 0 and t.

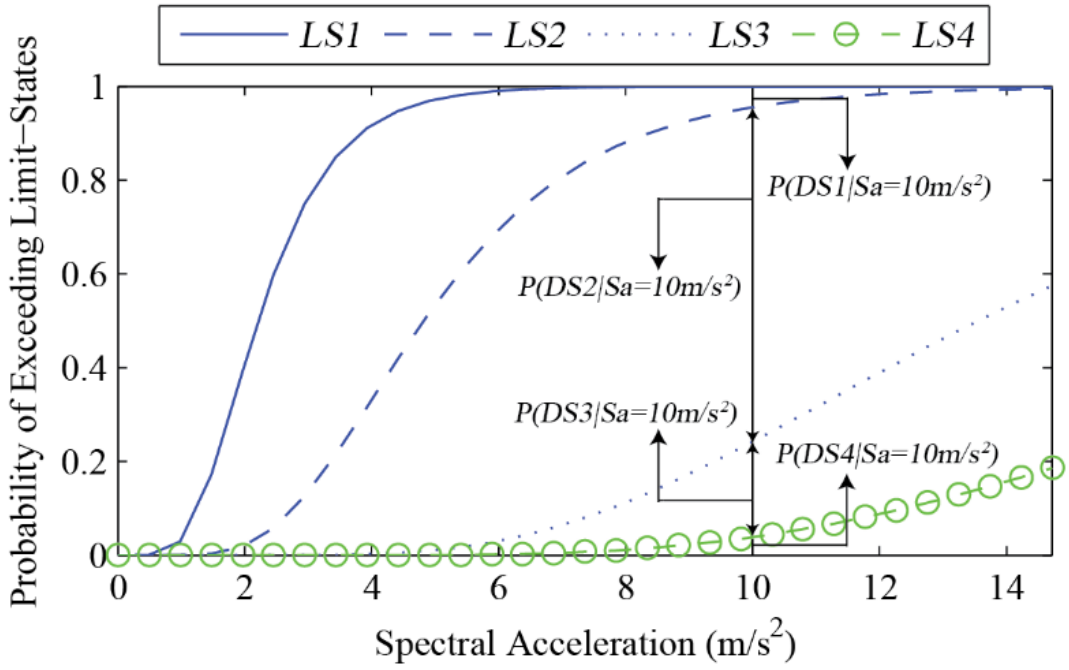

Figure 2-2 Illustration of damage-state probability calculation using exceedance probabilities of limit-states

Having calculated $\bar{C}_{R,t}$ for the entire life-time of the structure (i.e. t=0,…, T_{LC}), the NPV of the expected total LCC of repair ($\bar{C}_{R,NPV}$) follows Equation (2-11):

$$\bar{C}_{R,NPV} = \sum_{t=1}^{T_{LC}} \gamma^t \times \bar{C}_{R,t} \tag{2-11}$$

Substituting Equation (2-10) into Equation (2-11), $\bar{C}_{R,NPV}$ can be rewritten as follows:

$$\begin{aligned} \bar{C}_{R,NPV} = \sum_{t=1}^{T_{LC}} \gamma^t \times \sum_{n=1}^{N_{DS}} \{ & \bar{C}_r(DS_n, t+1) \\ & \times [P(LS_n, t+1) - P(LS_{n+1}, t+1)] - \bar{C}_r(DS_n, t) \\ & \times [\, P(LS_n, t) - \, P(LS_{n+1}, t)]\} \end{aligned} \tag{2-12}$$

A structure may be exposed to multiple hazards during its life-time, and therefore, the chance of exceeding a limit-state in the time period [0, *t*] depends on the number of hazard occurrences. Based on the total probability theorem for the number of hazard events, $\bar{C}_r(DS_n, t) \times [\, P(LS_n, t) - \, P(LS_{n+1}, t)]$ can be expanded and written as:

$$\begin{aligned} & \bar{C}_r(DS_n, t) \times [\, P(LS_n, t) - \, P(LS_{n+1}, t)] \\ & \quad = \sum_{i=0}^{\infty} \bar{C}_r(DS_n, t, i) \times [P(LS_n|i, t) - P(LS_{n+1}|i, t)] \\ & \quad \times P(i, t) \end{aligned} \tag{2-13}$$

where $P(i, t)$ stands for the probability that *i* hazard events occur up to time *t*. Considering hazard scenarios as independent events with the total rate of υ, $P(i, t)$ can be expressed as a Poisson process with the occurrence probability given by:

$$P(i, t) = \frac{(\upsilon \times \mathrm{t})^i e^{-(\upsilon \times \mathrm{t})}}{i!} \tag{2-14}$$

In Equation (2-13), $P(LS_n|i, t)$ denotes the probability of exceeding limit-state *n* resulting from the entire *i* hazard events. $C_r(CS_n, t, i)$ is the cumulative cost of reaching

damage-state n from time 0 to t when i hazard events occur. This term is calculated by summing the expected cost of repair over the entire i hazard events, and can be derived by breaking down the i hazard events into i mutually exclusive and collectively exhaustive scenarios. Thus, Equation (2-13) can be expanded as follows:

$$\begin{aligned}\bar{C}_r(DS_n, t) \times [P(LS_n, t) - P(LS_{n+1}, t)] \\ = \sum_{i=0}^{\infty} \sum_{j=0}^{i} \bar{C}_r\left(DS_n^j\right) \times [P\left(LS_n^j | i, t\right) - P\left(LS_{n+1}^j | i, t\right)] \\ \times P(i, t)\end{aligned} \tag{2-15}$$

where $\bar{C}_r\left(DS_n^j\right)$ is the incurred cost if the structure reaches damage-state n at the jth occurrence of hazard event. $P(LS_n^j | i, t)$ indicates the probability that the structure exceeds limit-state n at the jth hazard incident. Replacing Equation (2-15) into Equation (2-12) and following the same approach for the term $\bar{C}_r(DS_n, t+1) \times [P(LS_n, t+1) - P(LS_{n+1}, t+1)]$ in Equation (2-12), $\bar{C}_{R,NPV}$ can be expressed as:

$$\bar{C}_{R,NPV} = \sum_{t=1}^{T_{LC}} \gamma^t \times \sum_{n=1}^{N_{DS}} \left\{ \sum_{i=0}^{\infty} \sum_{j=0}^{i} \{\bar{C}_r(DS_n^j) \times [P(LS_n^j | i, t+1) - P(LS_{n+1}^j | i, t+1)] \times P(i, t+1)\} - \sum_{i=0}^{\infty} \sum_{j=0}^{i} \{\bar{C}_r(DS_n^j) \times [P(LS_n^j | i, t) - P(LS_{n+1}^j | i, t)] \times P(i, t)\} \right\} \quad (2\text{-}16)$$

When the structure is hit by an extreme event at the *j*-1th hazard occurrence, the event may incur damage or leave the structure intact. If the structure is damaged, based on the damage-state it experiences after such an event, a repair action may be performed to bring back the structure to its original condition. Thus, the duration of the repair action is a function of the structural damage-state following the hazard occurrence. Similar to the assumption made by Jalayer et al. (29), in this paper, the structure is presumed damaged (with the same damage-state), if the next hazard event (i.e. the *j*th occurrence) happens before the repair process is complete. In this case, the damage-state of the structure just before the *j*th hazard event is identical to the damage-state of the structure after the *j*-1th hazard incident. Therefore, the probabilities of exceeding any limit-state right after the *j*th occurrence of hazard event depends on the damage-state of the structure after the *j*-1th hazard incident, and the intensity of hazard at *j*th occurrence represented by *IM*. Consequently, $P(LS_n^j | i, t)$ can be expanded as given in Equation (2-17):

$$P(LS_n^j|i,t) = \sum_{DS_{n'}^{j-1}} \sum_{RP} \sum_{IM} P(LS_n^j|[RP, DS_{n'}^{j-1}], IM, i, t) \times P([RP, DS_{n'}^{j-1}]|IM, i, t) \times P(IM|i,t) \quad (2\text{-}17)$$

where RP indicates the status of the repair action taken on the structure; it takes a value of 1, if the repair action is complete and 0 otherwise. In addition, $DS_{n'}^{j-1}$ denotes the damage-state of the structure after the *j*-1th hazard event. The combination of these two parameters in $[RP, DS_{n'}^{j-1}]$ represents the existing damage-state of the structure when the *j*th hazard scenario takes place. $[RP, DS_{n'}^{j-1}]$ is characterized as follows:

$$[RP, DS_{n'}^{j-1}] = \begin{cases} DS_{n'}^{j-1} & if\ RP = 0 \\ DS_1^{j-1} & if\ RP = 1 \end{cases} \quad (2\text{-}18)$$

where DS_1^{j-1} is the intact damage-state of the structure.

Since $[RP, DS_{n'}^{j-1}]$ is independent of the intensity measure and the repair time is dependent on the damage-state of the structure, the term $P([RP, DS_{n'}^{j-1}]|i,t)$ in Equation (2-17) can be decomposed as follows:

$$P\left(\left[RP, DS_{n'}^{j-1}\right]\middle|IM, i, t\right) = P\left(\left[RP\middle|DS_{n'}^{j-1}\right], i, t\right) \times P(DS_{n'}^{j-1}|i,t) \quad (2\text{-}19)$$

As a particular case of the term $P\left(\left[RP\middle|DS_{n'}^{j-1}\right], i, t\right)$ in Equation (2-19), $P\left(\left[RP = 0\middle|DS_{n'}^{j-1}\right], i, t\right)$ is the probability that the repair action after the *j*-1th hazard occurrence is incomplete, knowing that *i* hazards take place between time 0 and *t*. In order for the repair action to be incomplete, *j*th hazard should take place before there is enough time for repairing damage-state n' due to *j*-1th hazard (and obviously no hazards take

place between *j-1*th and *j*th hazard incidents). Based on Equation (2-17), *j*-2 hazard incidents can take place any time from 0 to *t* preceding *j*-1th hazard event. Again according to this equation, in total, *i* hazard events should occur within timespan $[0\ \ t]$. Thus, *i-j* hazard incidents should take place after the occurrence of the *j*th hazard event until time *t*. These scenarios are graphically shown in Figure 2-3.

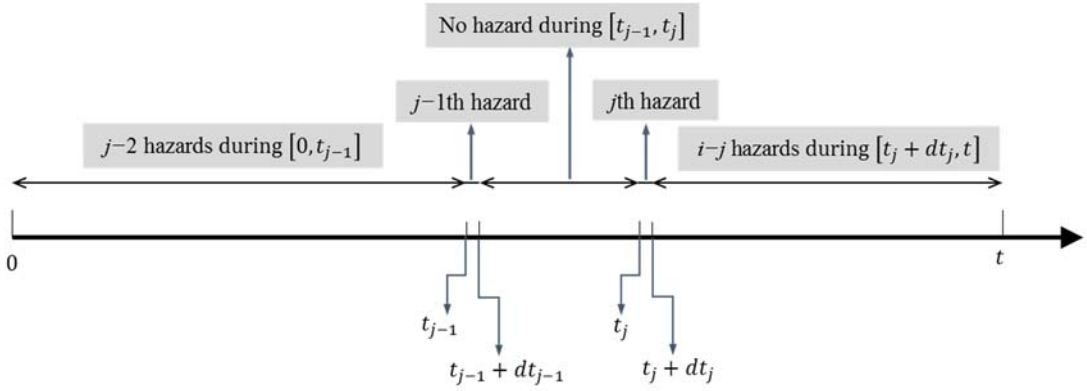

Figure 2-3 Timeline of events for multiple occurrences of hazards, for the calculation of the probabilities of complete/incomplete repairs

Consequently, $P\left([RP = 0|DS_{n'}^{j-1}], i, t\right)$ can be replaced by $P\left(t_j - t_{j-1} < \tau_{n'} | \{j-2, [0\ \ t_{j-1}]\}, \{i-j, [t_j\ \ t]\}\right)$, where t_j and t_{j-1} are the times of *j*-1th and *j*th hazard occurrences, respectively, $\tau_{n'}$ is the required time to repair the structure at damage-state n', $\{j-2, [0\ \ t_{j-1}]\}$ is the event of occurring *j*-2 hazards within $[0\ \ t_{j-1}]$, and $\{i-j, [t_j\ \ t]\}$ is the event of $i-j$ hazards occurring during $[t_j\ \ t]$. Applying Bayes rule, $P\left(t_j - t_{j-1} < \tau_{n'} | \{j-2, [0\ \ t_{j-1}]\}, \{i-j, [t_j\ \ t]\}\right)$ can be expressed as:

$$P\left(t_j - t_{j-1} < \tau_{n'} \middle| \{j-2, [0 \;\; t_{j-1}]\}, \{i-j, [t_j \;\; t]\}\right)$$

$$= \frac{P(t_j - t_{j-1} < \tau_{n'}, \{j-2, [0 \;\; t_{j-1}]\}, \{i-j, [t_j \;\; t]\})}{P(\{j-2, [0 \;\; t_{j-1}]\}, \{i-j, [t_j \;\; t]\})} \tag{2-20}$$

where the term $P(\{j-2, [0 \;\; t_{j-1}]\}, \{i-j, [t_j \;\; t]\})$ is equivalent to $P(i,t)$ as shown in Equation (2-14), since there is no constraint for the occurrence times of t_{j-1} and t_j except that $0 \le t_{j-1} < t_j \le t$. Considering that t_{j-1} and t_j can vary in the timespan of interest, the term $P(t_j - t_{j-1} < \tau_{n'}, \{j-2, [0 \;\; t_{j-1}]\}, \{i-j, [t_j \;\; t]\})$ in Equation (2-20) can be determined using the total probability theorem as follows:

$$P\left(t_j - t_{j-1} < \tau_{n'}, \{j-2, [0 \;\; t_{j-1}]\}, \{i-j, [t_j \;\; t]\}\right)$$

$$= \int_0^t \int_{t_{j-1}}^{\min\{t_{j-1}+\tau_{n'}, t\}} P\left(j-2, [0 \;\; t_{j-1}]\right) \times P\left(0, [t_{j-1} \;\; t_j]\right) \tag{2-21}$$

$$\times P\left(i-j, [t_j \;\; t]\right) \times \upsilon^2 \times dt_j . dt_{j-1}$$

where $P\left(j-2, [0 \;\; t_{j-1}]\right)$, $P\left(0, [t_{j-1} \;\; t_j]\right)$, and $P\left(i-j, [t_j \;\; t]\right)$ are the Poisson probabilities of j-2 hazards occurring in time $[0 \;\; t_{j-1}]$, no hazard happening during $[t_{j-1} \;\; t_j]$, and $i-j$ hazards taking place in $[t_j \;\; t]$, respectively. Also, $\upsilon . dt_{j-1}$and $\upsilon . dt_j$ are the probabilities of j-1th and jth hazards at times t_{j-1} and t_j, respectively.

In addition, $P\left([RP = 1 | DS_{n'}^{j-1}], i, t\right)$ can be calculated as $1 - P\left([RP = 0 | DS_{n'}^{j-1}], i, t\right)$ based on the fact that the considered events are complimentary.

With the analogy provided for Equation (2-8), $P(DS_{n'}^{j-1}|i,t)$ in Equation (2-19) can be computed as the difference between the exceedance probabilities of the two consecutive limit-states $LS_{n'}^{j-1}$ and $LS_{n'+1}^{j-1}$:

$$P\left(DS_{n'}^{j-1}|i,t\right) = P(LS_{n'}^{j-1}|i,t) - P(LS_{n'+1}^{j-1}|i,t) \tag{2-22}$$

In Equation (2-17), $P(IM|i,t)$ represents the probability that intensity measure *IM* occurs, if the *j*th hazard scenario takes place. This event has the following probability (45):

$$P(IM|i,t) = \frac{1}{\upsilon} \times |\Delta\lambda(IM)| \tag{2-23}$$

where υ is the mean annual rate of hazard occurrence, and $\lambda(IM)$ is the mean annual rate of exceeding intensity measure *IM*. For the case of earthquakes, $\lambda(IM)$ can be derived from Probabilistic Seismic Hazard Analysis (PSHA) curves for a region of interest. Substituting Equation (2-19), (2-22) and (2-23) into Equation (2-17), $P(LS_n^j|i,t)$ can be rewritten as:

$$\begin{aligned} P(LS_n^j|i,t) = \sum_{n'=0}^{N_{DS}} \sum_{RP=0,1} \sum_{IM} & P(LS_n^j|[RP, DS_{n'}^{j-1}], IM, i, t) \\ & \times P\left(\left[RP\middle|DS_{n'}^{j-1}\right]\right) \times [P(LS_{n'}^{j-1}|i,t) - P(LS_{n'+1}^{j-1}|i,t)] \times \frac{1}{\upsilon} \\ & \times |\Delta\lambda(IM)| \end{aligned} \tag{2-24}$$

where the two terms $P(LS_{n'}^{j-1}|i,t)$ and $P(LS_{n'+1}^{j-1}|i,t)$ can be derived in a recursive way from Equation (2-24). It is worthy to note that the damage-state of the structure either remains the same or worsens, if two consecutive hazard scenarios occur and there does not exist sufficient repair time after the first hit. This implies that $P(LS_n|[RP =$

$0, DS_{n'}^{j-1}\big], IM, i, t\big)$ is zero for $n' > n$. Furthermore, to solve for $P(LS_n^j|i,t)$, one needs to first input the damage-state probability distribution of the structure before any hazard occurrences (j=0), $P(LS_n^0|i,t), \forall n$. As a prior knowledge about the damage-state of the structure at the beginning of the decision-making period, it is assumed that $P\big(DS_{n'}^0\big)$ is known. Consequently, $P(LS_n^1|i,t)$ is determined as:

$$P(LS_n^1|i,t) = \sum_{n'=0}^{N_{DS}} \sum_{IM} P(LS_n^1|DS_{n'}^0, IM, i, t\big) \times P\big(DS_{n'}^0\big) \times \frac{1}{\upsilon} \times |\Delta\lambda(IM)| \tag{2-25}$$

Assuming that the damage-state of the structure at t=0 (i.e. after the structure is constructed) is known with certainty to be perfect (DS_0^0), Equation (2-25) can be simplified to:

$$P(LS_n^1|i,t) = \sum_{IM} P(LS_n^1|DS_0^0, IM, i, t) \times \frac{1}{\upsilon} \times |\Delta\lambda(IM)| \tag{2-26}$$

where $P(LS_n^1|DCS_0^0, IM, i, t)$ is the conventional fragility model. Knowing the value of $P(LS_n^1|i,t)$, $P(LS_n^j|i,t)$ can be derived through recursive operations.

2.3.3. Expected Lifecycle Salvage Value

The structure, at the end of its lifetime, may have a certain monetary value depending on its damage-state at $t = T_{LC}$. Similar to the case in Equation (2-6) and considering different possibilities for the number of hazard occurrences, $\bar{V}_{S,NPV}$ can be determined based on the total probability theorem for the damage-states that the structure can experience and the number of hazard incidents:

$$\bar{V}_{S,NPV} = \gamma^{T_{LC}} \sum_{i=0}^{\infty} \sum_{n=0}^{N_{DS}} \bar{V}_s(DS_n, [T_{LC}]) \times P(DS_n^i, [T_{LC}], i, T_{LC}) \tag{2-27}$$

where $\bar{V}_s(DS_n, [T_{LC}])$ stands for the salvage value of the structure as a function of its damage-state at time T_{LC}. $P(DS_n^i, [T_{LC}], i, T_{LC})$ also denotes the probability of ending in damage-state *n* at time T_{LC} after the occurrence of the *i*th hazard incident when *i* hazard events occur during [0, T_{LC}]. If the structure is intact after the *i*th hazard occurrence, it will be at the intact condition (*n*=0) at the time T_{LC} as well. Therefore, $P\left(DS_0^i, [T_{LC}]\right) = P\left(DS_0^i | i, T_i\right)$. Thus, Equation (2-27) can be expanded for damage-state 0 as follows:

$$\begin{aligned} \bar{V}_{S,NPV} = \gamma^{T_{LC}} \sum_{i=0}^{\infty} [& \left\{ \sum_{n=1}^{N_{DS}} \left[\bar{V}_s(DS_n, [T_{LC}]) \times P(DS_n^i, [T_{LC}], i, T_{LC}) \right] \right\} \\ & + \bar{V}_s(DS_0, [T_{LC}]) \times P\left(DS_0^i | i, T_i\right) \times P(i, T_{LC})] \end{aligned} \tag{2-28}$$

where $P(i, T_{LC})$ can be computed using Equation (2-14). The probability of being in the intact damage-state, $P\left(DS_0^i | i, T_i\right)$, can be computed by (see Figure 2-2):

$$P\left(DS_0^i | i, T_i\right) = 1 - P(LS_1^i | i, T_i) \tag{2-29}$$

In order for the structure to end up in damage-state *n*, the *i*th hazard event should degrade the damage-state of the structure to *n*, and the required repair action should be incomplete. It should be noted that in such a case, the owner`s decision to sell the structure may change, and he/she may decide to wait for a short time for the completion of the repair process. In this chapter, salvage value is considered assuming that the lifetime of the structure is fixed, however, in further chapters this cost will be excluded due to the aforementioned uncertainty. In this study however, it is assumed that the lifetime of the

structure is fixed. With this assumption, for the structure to experience damage-state *n* at the end of its lifetime, the repair time ($\tau_{n'}$) after the *i*th hazard (T_i) event should exceed the end of the time horizon of the structure ($T_{LC} < T_i + \tau_n$). Therefore, $P(DS_n^i, [T_{LC}])$ can be expressed as follows:

$$P\left(DS_n^i, [T_{LC}], i, T_{LC}\right) = P\left(DS_n^i \middle| i, T_i\right) \times P([T_{LC} < T_i + \tau_n], i, T_{LC}) \quad (2\text{-}30)$$

The term $P\left(DS_n^i \middle| i, T_i\right)$ can be simplified as $P(LS_n^i | i, T_i) - P(LS_{n+1}^i | i, T_i)$ and computed according to Equation (2-24). The event $T_{LC} < T_i + \tau_n$ can be considered as the occurrence of the *i*th hazard event during timespan $[T_{LC} - \tau_n \;\; T_{LC}]$ preceded by *i*-1 hazard incidents. If *i*th hazard occurs at time t'within timespan $[T_{LC} - \tau_n \;\; T_{LC}]$, then *i*-1 preceding hazards should happen during $[0 \;\; t']$ and no hazard should occur in time period $[t' \;\; T_{LC}]$. Thus, applying the total probability theorem for the time of the *i*th hazard incident, i.e. t', with the occurrence probability of $\upsilon . dt'$, $P([T_{LC} < T_i + \tau_n], i, T_{LC})$ in Equation (2-30) can be computed as:

$$P([T_{LC} < T_i + \tau_n], i, T_{LC}) = \int_{T_{LC}-\tau_n}^{T_{LC}} P(i-1, [0 \;\; t']) \times \upsilon \times P(0, [t' \;\; T_{LC}]) . dt' \quad (2\text{-}31)$$

On the contrary, if $T_{LC} > T_i + \tau_n$, there will be sufficient repair time before the lifetime of the structure is over. In this case, the value of the structure at the end of its lifetime is the same as the one for the intact building. This scenario occurs if no hazard event takes place within time period $[T_{LC} - \tau_n \;\; T_{LC}]$. Given the occurrence of *i* hazard events within the time horizon of the building, the *i* hazard incidents must take place

during $[0 \quad T_{LC} - \tau_n]$. Therefore, $P([T_{LC} < T_i + \tau_n], i, T_{LC})$ can be mathematically presented as follows:

$$P([T_{LC} > T_i + \tau_n], i, T_{LC}) = e^{-(\upsilon \times \tau_n)} \times \frac{(\upsilon \times (T_{LC} - \tau_n))^i e^{-(\upsilon \times (T_{LC} - \tau_n))}}{i!} \tag{2-32}$$

Substituting Equation (2-7), and (2-28)-(2-32) into (2-27), the NPV of the expected salvage value is derived as:

$$\begin{aligned} \bar{V}_{S,NPV} = \gamma^{T_{LC}} \sum_{i=0}^{\infty} \Bigg\{ \Bigg[& \sum_{n=1}^{N_{DS}} \bar{V}_s(DS_n, [T_{LC}]) \times [P(LS_n^i | i, T_i) - P(LS_{n+1}^i | i, T_i)] \\ & \times \Big(\int_{T_{LC} - \tau_n}^{T_{LC}} P(i-1, [0 \quad t']) \times \upsilon \times P(0, [t' \quad T_{LC}]) . dt' \Big) \\ & + \bar{V}_s(DS_0, [T_{LC}]) \times [P(LS_n^i | i, T_i) - P(LS_{n+1}^i | i, T_i)] \\ & \times e^{-(\upsilon \times \tau_n)} \times \frac{(\upsilon \times (T_{LC} - \tau_n))^i e^{-(\upsilon \times (T_{LC} - \tau_n))}}{i!} \Bigg] \\ & + \left[\bar{V}_s(DS_0, [T_{LC}]) \times [1 - P(LS_1^i | i, T_i)] \right] \\ & \times \frac{(\upsilon \times T_{LC})^i e^{-(\upsilon \times T_{LC})}}{i!} \Bigg\} \end{aligned} \tag{2-33}$$

2.3.4. Lifecycle Reliability Assessment

As explained before, human casualties and injuries are likely consequences of structural damage. However, estimation of a cost value for such consequences may be debatable and ethically questionable (46,47). As an alternative approach and a common practice in the management of civil structures and infrastructure systems, reliability assessment can be

used for the consideration of life safety criterion. This analysis is a complement to the proposed LCC framework for the definition of optimal design strategies, if casualty and injury losses are not included (which is the case for the first case study in this chapter). In reliability analysis, structural annual rate of collapse should be always above a minimum threshold recommended by the research community and accepted by public decision makers. In past studies, the annual rate of collapse given a hazard occurrence is calculated with the assumption that the structure or infrastructure is in the intact damage-state. However, considering the possibility of multiple hazard occurrences and the required repair time for incurred structural damage, the system may not be in the intact state for next occurrences of the hazard. On this basis, considering *i* hazards occurring during the lifetime of the system, the most critical event for reliability assessment corresponds to the last incident. Consequently, based on the total probability theorem, the mean annual rate of collapse for an expected lifetime of T_{LC}, $\lambda_F^{T_{LC}}$, can be derived through:

$$\lambda_F^{T_{LC}} = \sum_i \lambda(F|i, T_{LC}) \times P(i, T_{LC}|i \geq 1) \tag{2-34}$$

where $P(i, t|i \geq 1)$ is the probability of *i* hazards occurring during time [0 *t*] given that at least one hazard occurs in this time period. According to Bayes rule, this term can be expressed as $\frac{P(i,t)}{P(i\geq 1)}$ with $P(i \geq 1) = 1 - e^{-\upsilon \times t}$ following the exponential function for independent events. The term $\lambda(F|i, T_{LC})$ is the annual rate of collapse for the expected lifetime of T_{LC} if *i* hazard incidents have occurred within time period [0 t). This definition is similar to the formulation provided for the exceedance probability of collapse in Equation (2-24). In order to compute the mean annual rate of exceedance as opposed to

the probability of exceedance, $\frac{1}{\upsilon}$ is removed from the right-hand-side of this equation. Consequently, the mean annual rate of collapse limit-state exceedance can be computed as:

$$\lambda(F|i,T_{LC}) = \sum_{n'=0}^{N_{DS}} \sum_{RP=0,1} \sum_{IM} P(LS_C|[RP, DS_{n'}^i], IM, i, T_{LC}) \times P([RP|DS_{n'}^i]) \times [P(LS_{n'}^i|i,T_{LC}) - P(LS_{n'+1}^i|i,T_{LC})] \times |\Delta\lambda(IM)| \quad (2\text{-}35)$$

where LS_C corresponds to the collapse limit-state. It should be noted that $P(LS_{n'}^i|i,T_{LC})$ is calculated recursively according to Equation (2-24).

2.4. Analytical Framework for Lifecycle Resilience Assessment

During the lifetime of a structure or an infrastructure system in hazard prone regions, the functionality of the system may be impacted by a large number of events. Since resilience index represents functionality performance after hazard occurrences, occurrence of at least one hazard event during the lifetime of the infrastructure should be considered in the formulation of the resilience index. Based on the theorem of total probability for the number of hazard occurrences, the expected risk-based lifecycle resilience index for a service lifetime of T_{LC}, $\overline{RLRI}_{T_{LC}}$, can be presented as:

$$\overline{RLRI}_{T_{LC}} = (\overline{RLRI}_{T_{LC}}|i \geq 1) = \sum_{i=1}^{\infty} (\overline{RLRI}|i, T_{LC}, i \geq 1) \times P(i, T_{LC}|i \geq 1) \quad (2\text{-}36)$$

where $(\overline{RLRI}_{T_{LC}}|i \geq 1)$ is the expected risk-based lifecycle resilience index for a service lifetime of T_{LC} given the assumption that at least one hazard occurs during this lifetime, $(\overline{RLRI}|i, T_{LC})$ is the expected risk-based lifecycle resilience index conditioned on i , $i \geq 1$, hazards occurring during the system service lifetime, and $P(i, T_{LC}|i \geq 1)$ is the probability of this *i* hazards occurring during the lifetime of the system given the assumption of at least one hazard happening in this period. According to Bayes rule, $P(i, T_{LC}|i \geq 1)$ can be expressed as $\frac{P(i,T_{LC},i\geq 1)}{P(i\geq 1)}$. Since at least one hazard occurrence is considered in the formulation of $\overline{RLRI}$ (see Equation (2-36)), the term $P(i, T_{LC}, i \geq 1)$ can be simplified to $P(i, T_{LC})$. Without limiting the generality of the framework, if hazard occurrences are considered independent random events, $P(i, T_{LC})$ can be articulated according to Poisson distribution function as follows:

$$P(i, T_{LC}) = \frac{(\upsilon \times T_{LC})^i e^{-(\upsilon \times T_{LC})}}{i!} \tag{2-37}$$

where υ is the annual rate of hazard occurrences. Following the assumption of independency among hazard occurrences, $P(i \geq 1)$ can be also computed as $1 - e^{-(\upsilon \times T_{LC})}$. Thus, for independent hazards, $P(i, T_{LC}|i \geq 1)$ in Equation (2-36) can be determined as follows:

$$P(i, T_{LC}|i \geq 1) = \frac{(\upsilon \times T_{LC})^i e^{-(\upsilon \times T_{LC})}}{i! \times (1 - e^{-(\upsilon \times T_{LC})})} \tag{2-38}$$

With the same analogy provided for $P(i, T_{LC}, i \geq 1)$ to be simplified to $P(i, T_{LC})$, the term $(\overline{RLRI}|i, T_{LC}, i \geq 1)$ in Equation (2-36) can be also reduced to $(\overline{RLRI}|i, T_{LC})$. In

order to calculate the term $(\overline{RLRI}|i, T_{LC})$, functionality of the system after each of the i hazard incidents should be accounted for. On this basis, $(\overline{RLRI}|i, T_{LC})$ is expressed as:

$$(\overline{RLRI}|i, T_{LC}) = \frac{\sum_{j=1}^{i}(\bar{F}_A^j|i, T_{LC})}{\sum_{j=1}^{i}(FF_A^j|i, T_{LC})} \tag{2-39}$$

where $\bar{F}_A^j$ and FF_A^j are the area under expected functionality curve, and full functionality curve of the system after jth hazard event, respectively. Considering the definition of resilience index, the formulation presented in Equation (2-39) compares the expected functionality of the system during its lifetime with the full functionality of that system in the same period when i hazards occur.

As previously mentioned, functionality of the system after the time of each hazard occurrence is calculated until the end of the duration considered for the control time, i.e. t_h. However, there is a possibility that the restoration process of the system following a hazard is interrupted by the occurrence of a next hazard. Thus, functionality area following any hazard should be calculated from the occurrence time of that hazard to the minimum of 1) the time of next hazard, and 2) sum of the time of the current hazard occurrence and the considered control time. Considering t_j and t_{j+1} as the time of jth and j+1th hazard incidents, $(\overline{RLRI}|i, T_{LC})$ can be expanded as follows:

$$(\overline{RLRI}|i, T_{LC}) = \frac{\sum_{j=1}^{i}\int_{t_j}^{\min(t_{j+1}, t_j+t_h)} \bar{F}(t|i, T_{LC}).\, dt}{\sum_{j=1}^{i} 100\% \times \left(\min\left(t_{j+1}, t_j + t_h\right) - t_j|i, T_{LC}\right)} \tag{2-40}$$

where $\bar{F}(t)$ is the expected functionality of the system at time t. As noted, in Equation (2-40), the upper bound of the integral function in the numerator, which computes the

functionality area between *j*th and *j*+1th hazards, is bounded by $\min(t_{j+1}, t_j + t_h)$. The same upper bound is considered in the denominator of Equation (2-40), where the area corresponding to full functionality of the system between *j*th and *j*+1th hazards is calculated. Figure 2-4 illustrates the calculation of $(\overline{RLRI}|i, T_{LC})$ in Equation (2-40) corresponding to three hazard events occurring at times t_1, t_2, and t_3.

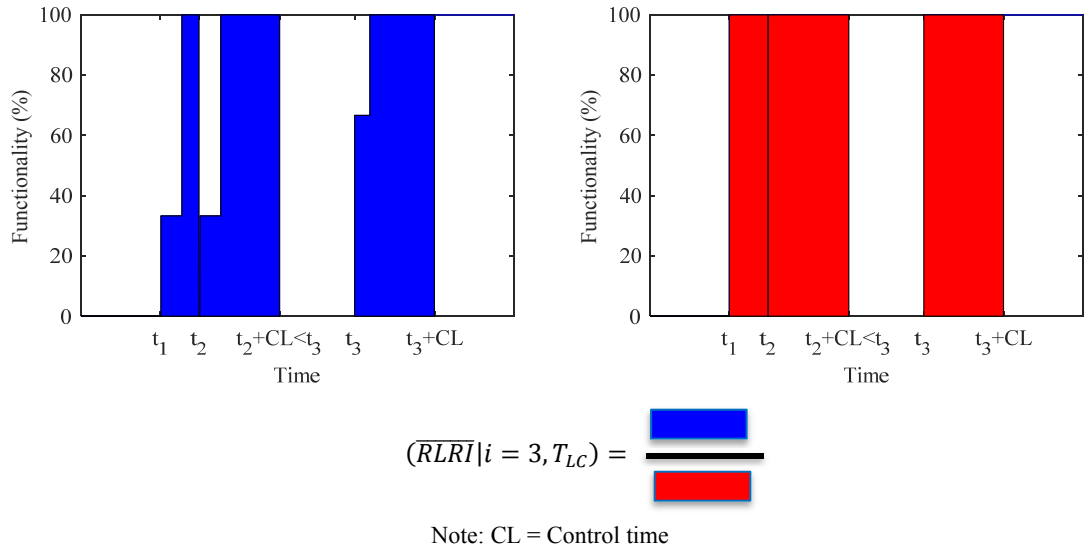

Note: CL = Control time

Figure 2-4 Illustration of the calculation of $(\overline{RLRI}|i, T_{LC})$ corresponding to the occurrence of three hazard events

The functionality curve of the system at each time period $[t_j\ t_{j+1}]$ depends on the damage-state that the structure experiences after the *j*th hazard, among other factors. This factor identifies the initial functionality of the system at time period $[t_j\ t_{j+1}]$. Considering the discrete space of the damage-state possibilities, $(\overline{RLRI}|i, T_{LC})$ in Equation (2-40) can be further expanded to:

$$(\overline{RLRI}|i, T_{LC})$$

$$= \frac{\sum_{j=1}^{i} \sum_{n=1}^{N_{DS}} P\left(DS_n^j | i, T_{LC}\right) \times \int_{t_j}^{\min(t_{j+1}, t_j + t_h)} \bar{F}(t | DS_n^j, i, T_{LC}) \, . \, dt}{\sum_{j=1}^{i} 100\% \times \left(\min\left(t_{j+1}, t_j + t_h\right) - t_j | i, T_{LC}\right)} \quad (2\text{-}41)$$

where $P\left(DS_n^j | i, T_{LC}\right)$ stands for the probability that the system sustains damage-state n due to jth hazard incident, and $\bar{F}(t | DS_n^j, i, T_{LC})$ indicates the expected functionality of the system at time t, where $t_j < t < t_{j+1}$ and the damage-state of the system at time t_j is n. As mentioned in the previous chapter, damage-state 1 and N_{DS} represent the intact and the most severe state of the system, respectively. These damage-states are mutually exclusive and collectively exhaustive. In the rest of this section, the procedures for the calculation of $P\left(DS_n^j | i, T_{LC}\right)$, $\int_{t_j}^{\min(t_{j+1}, t_j + t_h)} \bar{F}(t | DS_n^j, i, T_{LC}) \, . \, dt$, and $100\% \times \left(\min\left(t_{j+1}, t_j + t_h\right) - t_j | i, T_{LC}\right)$ in Equation (2-41) are provided.

2.4.1. Calculating $\boldsymbol{P\left(DS_n^j | i, T_{LC}\right)}$

As explained in Chapter 2, the term $P\left(DS_n^j | i, T_{LC}\right)$ incorporates the potential of damage accumulations due to untreated damages or due to the possibility of incomplete repairs. The procedure for the calculation of this term is elaborated in Section 2.3.2.

2.4.2. Calculating $\boldsymbol{\int_{t_j}^{\min(t_{j+1}, t_j + t_h)} \bar{F}(t | DS_n^j, i, T_{LC}) \, . \, dt}$

As explained previously, the initial functionality of the system at the start of each period $[t_j \; t_{j+1}]$ depends on the damage-state of the system just after the occurrence of the jth

hazard. Generally, after the *j*th hazard incident, system recovers until full functionality is achieved. As explained before, the recovery process may be interrupted by the next hazard, i.e. *j*+1th incident, in which case functionality area should be calculated until the time of *j*+1th hazard. This indicates that the system functionality depends on the inter-arrival times of *j*th and *j*+1th hazards, which are stochastic events. On this basis, $\int_{t_j}^{\min(t_{j+1},t_j+t_h)} \bar{F}(t|DS_n^j, i, T_{LC})\,.\,dt$ can be expanded as:

$$\begin{aligned}\int_{t_j}^{\min(t_{j+1},t_j+t_h)} & \bar{F}\left(t\middle|DS_n^j, i, T_{LC}\right).dt \\ &= \int_{t_j}^{\min(t_{j+1},t_j+t_h)} \bar{F}\left(t\middle|DS_n^j, i, T_{LC}, t_j, t_{j+1}\right) \\ &\times P\left(t_j, t_{j+1}|DS_n^j, i, T_{LC}\right).dt\end{aligned} \tag{2-42}$$

where $P\left(t_j, t_{j+1}\right)$ is the probability that *j*th and *j*+1th hazards occur at t_j and t_{j+1}, respectively. These events are independent of the structural damage-state at the time of *j*th hazard incident; thus, $P\left(t_j, t_{j+1}|DS_n^j, i, T_{LC}\right)$ can be reduced to $P\left(t_j, t_{j+1}|i, T_{LC}\right)$. Using Bayes rule, $P\left(t_j, t_{j+1}|i, T_{LC}\right)$ can be articulated as:

$$P\left(t_j, t_{j+1}|i, T_{LC}\right) = \frac{P\left(t_j, t_{j+1}, i, T_{LC}\right)}{P(i, T_{LC})} \tag{2-43}$$

The following timeline of events determine $P\left(t_j, t_{j+1}, i, T_{LC}\right)$ in Equation (2-43):

- *j*-1 hazards take place during [0 t_{j-1}].
- Two hazards, *j*th and *j*+1th incidents, occur at times t_j and t_{j+1}.
- No hazards take place between times t_j and t_{j+1}.

- *i-j*-1 hazards occur during $[t_{j+1} + dt_{j+1}\ T_{LC}]$.

On this basis, $P(t_j, t_{j+1}, i, T_{LC})$ can be written as:

$$\begin{aligned} P(t_j, t_{j+1}, i, T_{LC}) \\ &= P(j-1, [0\ \ t_j]) \times P(0, [t_j\ \ t_{j+1}]) \\ &\times P(i-j-1, [t_{j+1}\ \ T_{LC}]) \times \upsilon^2 \times dt_j . dt_{j+1} \end{aligned} \tag{2-44}$$

Applying the total probability theorem over the entire space of occurrence times for t_j and t_{j+1}, and inserting Equation (2-44) and Equation (2-43) into Equation (2-42), $\int_{t_j}^{\min(t_{j+1}, t_j + t_h)} \bar{F}(t|DS_n^j, i, T_{LC}) . dt$ can be expressed as:

$$\begin{aligned} &\int_{t_j}^{\min(t_{j+1}, t_j + t_h)} \bar{F}(t|DS_n^j, i, T_{LC}) . dt \\ &= \frac{1}{P(i, T_{LC})} \\ &\times \int_0^{T_{LC}} \int_{t_j}^{T_{LC}} \int_{t_j}^{\min(t_{j+1}, t_j + t_h)} \bar{F}(t|DS_n^j, i, T_{LC}, t_j, t_{j+1}) \\ &\times P(j-1, [0\ \ t_j]) \times P(0, [t_j\ \ t_{j+1}]) \\ &\times P(i-j-1, [t_{j+1}\ \ T_{LC}]) \times \upsilon^2 \times dt . dt_{j+1} . dt_j \end{aligned} \tag{2-45}$$

2.4.3. Calculating $100\% \times (\boldsymbol{min}(\boldsymbol{t_{j+1}}, \boldsymbol{t_j} + \boldsymbol{t_h}) - \boldsymbol{t_j}|\boldsymbol{i}, \boldsymbol{T_{LC}})$

The term $100\% \times (\min(t_{j+1}, t_j + t_h) - t_j|i, T_{LC})$ in the denominator of Equation (2-41) is the expected lifetime functionality area of the system at a fully operational status.

Therefore, this term can be calculated using Equation (2-45), by replacing $\bar{F}\left(t\middle|DS_n^j, i, T_{LC}, t_j, t_{j+1}\right)$ with 100% for all times.

2.5. Case Study 1 for Lifecycle Cost Assessment: Four Story Building

The first case study that is considered for the demonstration of the proposed LCC assessment framework is a four story building structure. The input models and numerical study results for this case study are presented in the following sections.

2.5.1. Input Data for the Case Study

The possibility of multiple earthquake events are considered throughout the lifetime of the case study building. Six retrofit options are considered for the building including: status quo (no retrofit), adding shear walls, adding X-braces, adding chevron braces, retrofitting columns with concrete jackets, and retrofitting columns with FRP wrapping. It is assumed that after retrofitting, the selected retrofit option will be kept throughout the lifetime of the structure, and it will be repaired to its original condition after any damage due to the occurrence of hazard events. The presented framework is applied to determine the optimal retrofit action that results in the least total LCC for the structure.

2.5.1.1. Structural Model and Seismicity of the Region

The case study structure is a three bay, four story moment-resisting concrete frame building described in (48) and (49). An elevation view of the building is shown in Figure 2-5. The frame building was originally designed to insure beam hinging under lateral

seismic loadings. In this frame, each bay is 5m long and each story is 3m high. In addition, the total weight of each story is 702.40 KN except the fourth story that has a weight of 501.29 KN (48). In the frame, the concrete compression strength, reinforcing steel yield strength, and reinforcing steel ultimate strength are 28 N/mm^2, 460 N/mm^2, and 560 N/mm^2, respectively (48). All columns in this structure have the same section, which is displayed in Figure 2-5. On the other hand, beam sections vary with respect to height and position in each story. A detailed description of the beam sections is presented in Table 2-1.

The structure is assumed to be a multi-family residential building located near Sierra Madre fault in southern California. The natural period of the building is 0.615s (49).

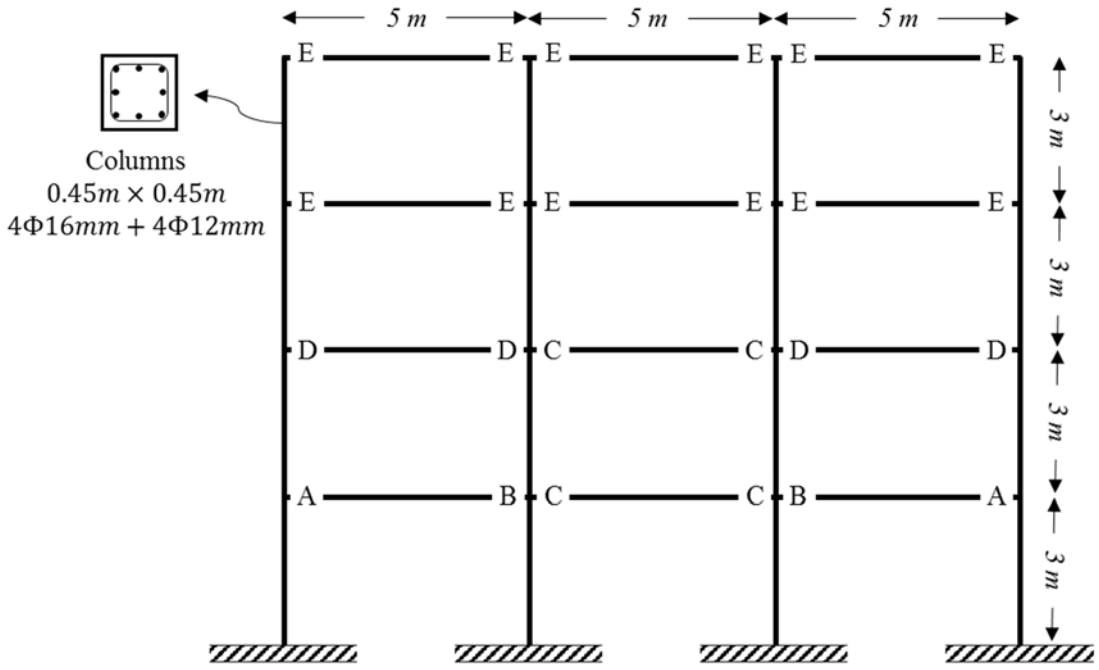

Figure 2-5 Configuration of the case study reinforced concrete moment resisting frame (49)

Table 2-1 Description of the beam sections (49)

Beam Sections	Height (m)	Width (m)	Top Longitudinal Reinforcement	Bottom Longitudinal Reinforcement
Section A	0.6	0.3	$3\Phi16 + 2\Phi12$	$3\Phi12 + 2\Phi10$
Section B	0.6	0.3	$2\Phi10 + 2\Phi16$	$3\Phi10 + 2\Phi10$
Section C	0.6	0.3	$2\Phi16 + 2\Phi12$	$4\Phi10$
Section D	0.6	0.3	$2\Phi16 + 2\Phi12$	$3\Phi12 + 2\Phi10$
Section E	0.6	0.3	$3\Phi12 + 2\Phi10$	$4\Phi10$

Using the Hazard Curve Application provided by USGS (44), the probabilistic seismic hazard curve for the location of the building is derived and plotted in Figure 2-6. It is worthy to mention that a hazard curve presents the annual frequency (rate) of exceeding various ranges of the hazard intensity measure. These curves are region-specific, and are usually developed probabilistically using the historical data for hazards in the region of interest. For the case study bridge in this section, as an appropriate intensity measure, spectral acceleration of the building at the first mode period is considered. Corresponding to this hazard curve, the mean annual rate of earthquake occurrence for the bare frame, υ, is calculated as 0.619.

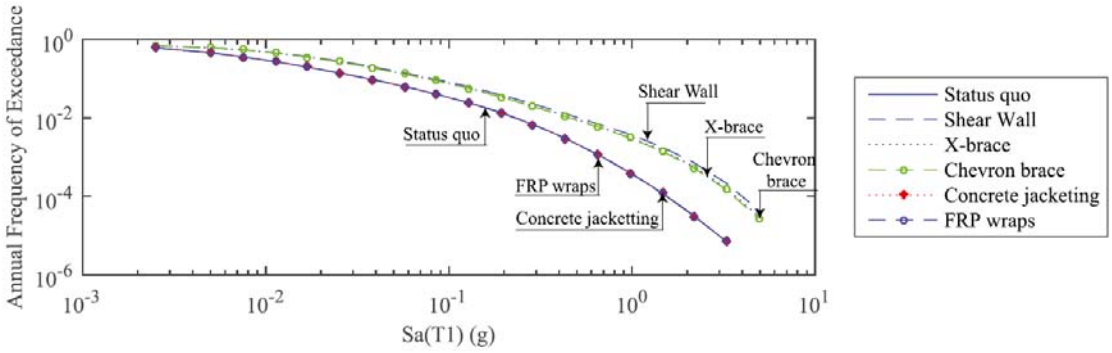

Figure 2-6 Probabilistic seismic hazard curves for the site where the building is located

2.5.1.2. Retrofit Strategies

For enhancing the performance of the case study building, the following six retrofit options are considered for implementation:

Case 1: Status quo: The moment frame will not be retrofitted. The columns and beams will be repaired after any earthquake-induced damages.

Case 2: Shear wall: Shear walls will be added to the middle span of the moment frame at all floors. The thickness of the wall and the concrete compressive strength of these shear walls are 20 cm, and 28 N/mm^2, respectively.

Case 3: X-brace: A set of X-braces will be added to the middle span of the moment frame at all floors. All X-braces are steel double angles with 30 cm length, 15 cm width, and 0.8 cm thickness. The steel material has also a yield stress of 345 N/mm^2.

Case 4: Chevron brace: A set of concentrically chevron braces will be added to the middle span of the moment frame at all floors. The same as X-braces, chevron braces are considered as steel double angles with 30 cm length, 15 cm width, and 0.8 cm thickness. The steel material has also a yield stress of 345 N/mm^2.

Case 5: Concrete jacketing: 80 cm of the top and bottom of all columns of the case study building will be retrofitted with concrete jacketing. For this purpose, the section of the concrete columns are thickened by 10 cm in width and 10 cm in length.

Case 6: FRP wrapping: Tops and bottoms of all columns of the case study building will be wrapped with FRP sheets. While the FRP wrap does not modify the first mode period of the bare frame, the structural response of the frame following this retrofit strategy improves (50). According to the study by Mwafy and Elkholy (50) the ultimate strength, tensile strength, thickness, and modulus of elasticity of the FRP wrap considered for the case study building are 149.5 KN, 1824 N/mm^2, 0.28 mm, and 629.6 KN/mm^2, respectively.

Based on the references provided in Table 2-4 and the configuration of the case study frame building, the first mode period of the structure for the status quo, shear wall, X-brace, chevron brace, concrete jacketing, and FRP wrapping retrofit strategies, is derived as 0.615 s, 0.229 s, 0.279 s, 0.292 s, 0.552 s, and 0.615 s, respectively. In the computation of the expected hazard-induced cost and the expected salvage value for each of the retrofit strategies, the corresponding hazard curve based on the first mode period of that retrofit strategy is utilized (see Figure 2-6).

2.5.1.3. State-Dependent Fragility Curves

Five damage-states are considered for the case study concrete frame, including intact (no damage), light, moderate, irreparable, and near collapse/collapse (49). The drift ratios

corresponding to these damage-states are 0, 0.002, 0.004, 0.01, and 0.018, respectively (51).

The extent of damage after an earthquake event can be estimated using structural fragility curves. However, for the case where a hazard incident occurs while the repair action following the previous hazard event is undergoing, the probability of damage depends on the previous damage-state of the structure. In the context of earthquake engineering, the probability of new damage-states for different levels of hazard intensities can be realized by state-dependent fragility curves (49). For the case study bare frame, Abad et al. (49) used a set of 221 unscaled strong ground motion records to generate damage-state dependent fragility curves. In this regard, first for the intact damage-state, the structure was subjected to the entire set of ground motion records. Based on the sustained drift ratio, the damage-state was identified for the structure, which was then subjected to a randomly selected set of ground motions. Similarly, after that second excitation, the visited drift ratio-based damage-state was monitored and used as the initial state for the next excitation. This procedure was repeated until sufficient data for each damage-state was obtained. Finally, regression analyses were performed on the drift ratios to produce state-dependent fragility curves. For the non-retrofitted as well as retrofitted case study moment-frame structures, the parameters of the lognormal fragility curves are provided in Table 2-2 and Table 2-3. These parameters for the retrofitted state-dependent fragility curves are adopted from several research studies as presented in Table 2-4. In these studies, fragility curves for different damage-states of retrofitted structures are only provided for the intact state. Due to lack of data, in order to derive the parameters of the

state-dependent fragility curves for these retrofit actions, it is assumed that the ratios of the median and standard deviation values for damage-state dependent fragility curves are the same for the non-retrofitted and retrofitted frame buildings. In this regard, the following procedure is applied:

- For each of the retrofit actions and limit-states, the mean and standard deviation values of the fragility curves for concrete frames before and after retrofit are identified.
- Then, the ratios of the means and standard deviations after the retrofit to the corresponding values before the retrofit are multiplied by the mean and standard deviation values of the state-dependent fragility curves of the bare moment-frame.

Table 2-2 Median values for the state-dependent fragility curves for the considered retrofit actions

Initial Damage-state	Exceeded Damage-state	Retrofit Option					
		Status Quo	Shear Wall	X-Brace	Chevron Brace	Concrete Jacketing	FRP Wrapping
Intact	Light	1.03	1.94	2.21	3.36	2.99	2.21
Intact	Moderate	2.25	4.24	4.82	7.34	6.54	4.84
Intact	Irreparable	6.33	11.94	13.56	20.64	18.40	13.61
Intact	Collapse	12.30	23.79	21.83	33.69	35.75	26.44
Light	Moderate	1.98	3.73	4.24	6.46	5.75	4.26
Light	Irreparable	5.78	10.90	12.38	18.85	16.80	12.42
Light	Collapse	11.29	21.84	20.04	30.92	32.81	24.27
Moderate	Irreparable	4.83	9.11	10.35	15.75	14.04	10.38
Moderate	Collapse	9.82	19.00	17.43	26.90	28.54	21.11
Irreparable	Collapse	6.47	12.52	11.48	17.72	18.80	13.91

Table 2-3 Logarithmic standard deviations for the state-dependent fragility curves for the considered retrofit actions

Initial Damage-state	Exceeded Damage-state	Retrofit Option					
		Status Quo	Shear Wall	X-Brace	Chevron Brace	Concrete Jacketing	FRP wrapping
Intact	Light	0.41	0.34	0.43	0.31	0.21	0.21
Intact	Moderate	0.41	0.34	0.43	0.31	0.21	0.21
Intact	Irreparable	0.41	0.35	0.43	0.32	0.53	0.42
Intact	Collapse	0.41	0.35	0.44	0.32	1.05	0.75
Light	Moderate	0.42	0.35	0.44	0.32	0.21	0.21
Light	Irreparable	0.41	0.35	0.43	0.32	0.53	0.42
Light	Collapse	0.41	0.35	0.44	0.32	1.05	0.75
Moderate	Irreparable	0.45	0.38	0.48	0.35	0.58	0.46
Moderate	Collapse	0.44	0.38	0.47	0.35	1.12	0.80
Irreparable	Collapse	0.86	0.74	0.93	0.68	2.20	1.57

These newly produced mean and standard deviation values are then used as the parameters of the retrofitted state-dependent fragility curves (see Table 2-2 and

Table 2-3).

In some retrofit cases, the mean and standard deviation values are only available for some limit-states (in terms of the maximum drift ratio) that are different from the ones used in this study. The required mean and standard deviation values in such cases are linearly interpolated. For the required limit-states with corresponding drift ratios less than the minimum or greater than the maximum available drift ratios, the same mean and standard deviation values corresponding to the minimum and maximum available drift ratios are considered. As shown in Table 2-4, retrofitting with chevron brace results in the largest improvements in the conditional fragility curves except for the collapse damage-state where concrete jacketing provides the most improvement.

Table 2-4 Enhancement ratios of the state-dependent fragility curves for the considered retrofit actions

		Exceeded Damage-states				
		Light	Moderate	Irreparable	Collapse	Adapted from
Retrofit Action	Status Quo	1.00	1.00	1.00	1.00	Abad et al. (49)
	Shear Wall	1.89	1.89	1.89	1.93	Bai (52)
	X-Brace	2.14	2.14	2.14	1.78	Akbari et al. (53)
	Chevron Brace	3.26	3.26	3.26	2.74	Akbari et al. (53)
	Concrete Jacketing	2.91	2.91	2.91	2.91	Mfawy and Elkholy (50)
	FRP wrapping	2.15	2.15	2.15	2.15	Mfawy and Elkholy (50)

2.5.1.4. State-Dependent Repair Times

A key feature of the proposed framework is the consideration of the possibility that the repair action taken after a hazard incident can be incomplete when the next hazard incident hits the structure. As previously explained in the methodology section, the probability that the repair operation is incomplete at the time the next event occurs depends on the required repair time, among others. While repair time may vary for each of the retrofit actions, for illustration purposes in this research, these values are assumed identical for different retrofit actions. Generally, when a structure is damaged by an earthquake, the time to recovery includes (37): 1) a thorough building inspection, T_{ins}, 2) engineering assessment for finance planning and repair consultation, T_{ass}, 3) mobilizing equipment, materials and evacuating the building for repair, T_{mob}, and 4) the repair of the building, T_{rep}. Based on the extent of damage, each of these steps requires a certain amount of time. For each damage-state, the recovery path, and the median and standard deviation of the lognormal distribution models for the involved recovery time components ((37); Table 15.9 in (54)) are provided in Table 2-5. It should be noted that some damage-states have recovery paths

that do not include certain recovery actions. For instance, when the structure is damaged to the extent of collapse, i.e. collapse limit-state is reached, there is no need for inspection and assessment since building collapse is clearly observable.

Table 2-5 The recovery times, and the statistical characteristics for each of the recovery terms ((37); (54))

		Recovery path	Recovery Time Component							
			Median (days)				Dispersion (β)			
			Tins	*Tass*	*Tmob*	*Trep*	*Tins*	*Tass*	*Tmob*	*Trep*
Damage-State	Light	*Tins* + *Trep*	30	-	-	5	0.75	-	-	0.40
	Moderate	*Tins* + *Tass* + *Trep*	30	60	-	30	0.75	0.75	-	0.40
	Irreparable	*Tins* + *Tass* + *Tmob* + *Trep*	30	60	120	120	0.75	0.75	0.75	0.40
	Collapse	*Tmob* + *Trep*	-	-	360	240	-	-	0.75	0.40

2.5.1.5. Cost Terms

The maintenance cost, repair cost and salvage value of the building are assumed to be dependent on the total construction cost of the building. The total construction cost is the sum of the cost of constructing the moment-frame building plus the cost of applying the retrofit action. Following (29), the total construction cost is assumed 91% of the replacement cost. The replacement cost of the residential building is approximated using the data provided in Table 3.7 in (54). The construction cost of the building and the additional cost of each retrofit action are given in Table 2-6. This table also includes references for the unit costs of applying the retrofit actions.

Table 2-6 Costs of construction and retrofit actions implementation, total costs of replacement, and annual maintenance costs for the six retrofit actions

	Unit Cost of Construction	Reference	Retrofit Cost ($)	Cost of Replacement ($)	Annual Maintenance Cost ($/year)
Status Quo	75 ($/ft2)	NIBS, FEMA (54)	-	450000	4091
Shear Wall	55 ($/ft2)	Liel et al. (55)	66000	516000	4691
X-Brace	20000 ($/floor)	Dasse (56)	80000	530000	4818
Chevron Brace	15000 ($/floor)	Authors` judgment	60000	510000	4636
Concrete Jacketing	55 ($/ft2)	Liel et al. (55)	52800	502800	4571
FRP Wrapping	12.5 ($/ft2)	Less (57)	16800	466800	4244

The annual maintenance cost for each building case in Table 4 is assumed 1% of the corresponding total construction cost (29). Hazard-induced cost terms considered in this paper include the direct repair cost, and the indirect loss due to disruption. However, incurred costs due to injuries, casualties and business interruption are not considered in the hazard-induced losses in this case study. Furthermore, the indirect loss of rental income for the owner of the building is disregarded since almost similar rental price should be paid by the tenants during the repair period.

A total of $\$0.82/ft^2$ is considered for the disruption cost which represents the costs of "shifting and transferring" (54). This cost is only applied for the irreparable and collapse damage-states where relocation of the tenants is necessary for the repair of the building.

The direct repair cost is the cost of bringing back the building to its intact condition. This cost includes the induced loss to structural and non-structural components, as well as the contents in the building. The repair cost is a function of the damage-state and the type of the retrofit action. NIBS, FEMA (54) provides repair costs for various

damage-states. The description of the damage-states with regard to the maximum interstory drift ratio is given in Table 5.1 in (54). Comparing the drift ratios corresponding to each damage-state in (54) with the drift ratios considered for the damage-states in this study, the repair costs for the slight, moderate, extensive and complete damage-states in (54) are taken as the costs for light, moderate, irreparable, and collapse limit-states in this study. The cost data for these limit-states are provided in Table 2-7. The repair costs include structural, non-structural and building content costs. The first two terms are provided as the percentage of the building replacement cost, while the latter is given as the percentage of the building contents value. NIBS, FEMA (54) suggests 50% of the building value (i.e. construction cost) as a reasonable estimate for the value of the contents for residential buildings. Furthermore, based on estimates in (54), 50% of the contents after complete damage is retrievable. Thus, the induced cost for different damage-states can be calculated as a function of the building replacement cost given in Table 2-7.

The fourth term of the expected total LCC, i.e. the expected lifecycle salvage value, is also a function of the building condition at the end of its lifetime. In reality, the salvage value depends on many factors such as physical features including the quality and safety of location, and access to public transportation, governmental laws for building restrictions, social features such as population growth or decline, and economic attributes including income levels and new construction techniques (58). However for the purpose of demonstrating the application of the proposed method, the salvage value is assumed to depend only on the damage-state of the building at the end of lifetime and vary linearly for the five damage-states. The maximum considered value is equal to the construction

cost, representing the value of the building for the intact damage-state, while the minimum value is set to zero for the collapse limit-state.

Table 2-7 Repair costs of the building for different damage-states in terms of the percentage of the replacement cost (54)

		Damage-State			
		Light	Moderate	Irreparable	Collapse
Component	Structural	0.3	1.4	6.9	13.8
	Non-Structural Drift Sensitive	0.9	4.3	21.3	42.5
	Non-Structural Acceleration Sensitive	0.8	4.3	13.1	43.7
	Contents	0.5	2.3	11.4	22.8
	Sum	2.5	12.3	52.7	122.8

2.5.2. Numerical Results

The numerical results from implementing the developed framework on the case study building is provided in this section.

2.5.2.1. Probabilities of Exceeding Limit-States and Sustaining Damage-States versus the Number of Hazard Incidents

For the case of status quo retrofit action and performing no repairs following sustained damage-states, the probabilities of exceeding various limit-states versus the number of hazard occurrences are derived using Equation (2-24) and plotted in Figure 2-7-a. As a general trend, when the number of earthquake events increases, the exceedance probabilities increase for all of the limit-states. Since the structure is always in a damage-state equal to or worse than the intact state, the probability of exceeding the intact limit-state is always one. This limit-state is therefore not shown in Figure 2-7-a. As shown in Figure 2-2, the probabilities of reaching each damage-state can be computed based on the

exceedance probabilities of limit-states. These values for the status quo retrofit plan versus the number of hazard incidents are presented in Figure 2-7-b. Results indicate that when no repair is performed on the structure, the probability of staying intact decreases drastically as the number of hazard events increases. The probabilities of being in the light damage-state increases with a decreasing slope. When more than 50 hazard incidents occur, the probability of the light damage-state supersedes the occurrence probability of the intact damage-states. This is expected, as it indicates the vulnerability of the system when no repair is performed as the building experiences more hazard incidents.

Finally, the occurrence probabilities of the last three damage-states, i.e. moderate, irreparable, and collapse, increase monotonically with the number of hazard incidents. This trend is expected since an increase in the number of hazard incidents leads to higher likelihoods of the structure experiencing more severe damage-states due to accumulated damage from past incidents and incomplete repairs.

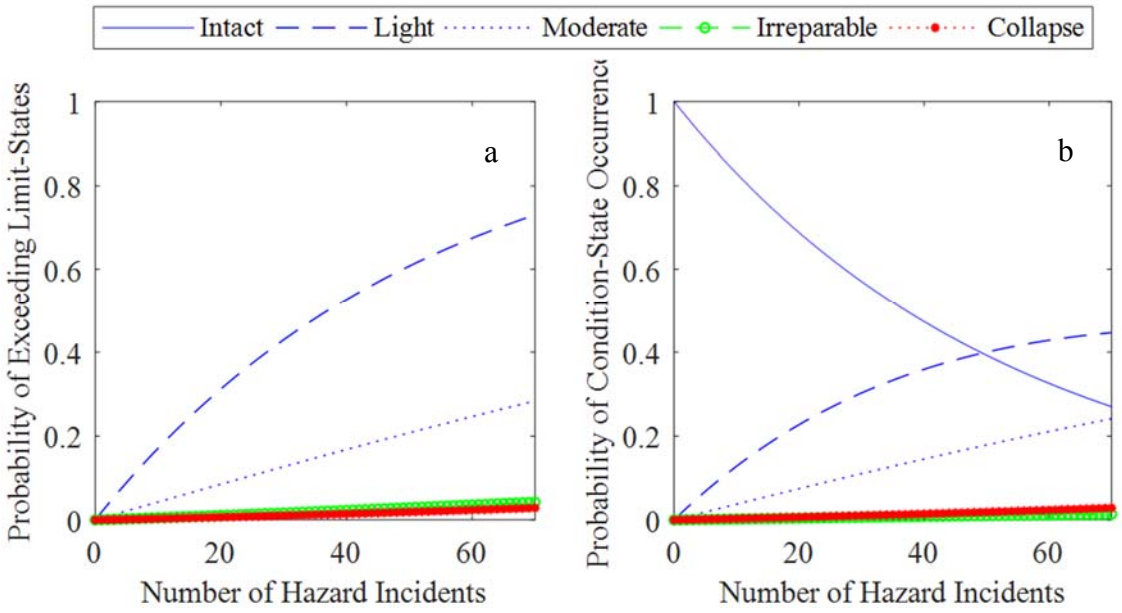

Figure 2-7 Probabilities of a) exceeding limit-states and b) sustaining damage-states for the status quo retrofit plan considering no repair following sustained damages

2.5.2.2. Convergence Analysis

The convergence of the proposed framework for LCC assessment of structures with respect to the number of hazard incidents is investigated in this section. The relative tolerance of 0.002 is considered which corresponds to the absolute tolerance of approximately $100 for 100 years lifetime. When the relative difference of the expected hazard-induced cost from two consecutive steps becomes less than the specified tolerance value, the analysis is considered as converged. Results of convergence analysis for a wide range of lifetimes for the case study building are presented in Figure 2-8. Generally, as the time horizon of the structure increases, the considered number of hazard incidents should increase in order for the framework to converge. This can be justified by the fact that the expected number of hazard incidents following a Poisson process is linearly

proportional to the lifetime, i.e. $E(i|TH) = \upsilon \times TH$. Although, in theory, an infinite number of hazard events should be considered (as required according to Equation (14)), numerical results indicate that convergence will be achieved with a relatively small number of hazard incidents more than the expected number of hazards following Poisson process for the specified lifetime. For this reason, the required number of hazards for convergence is slightly larger for shear wall, X-brace, and Chevron brace retrofit strategies with higher mean annual rates of earthquake occurrences, compared to the rest of the alternatives.

Results of this analysis indicate that a reliable estimation of the LCC of systems requires consideration of the possibility of multiple hazard occurrences throughout the lifetime. This consideration however, is neglected in many existing LCC analysis frameworks.

In the rest of this section, using the proposed framework, the results of various numerical analyses on the case study frame building are presented and discussed.

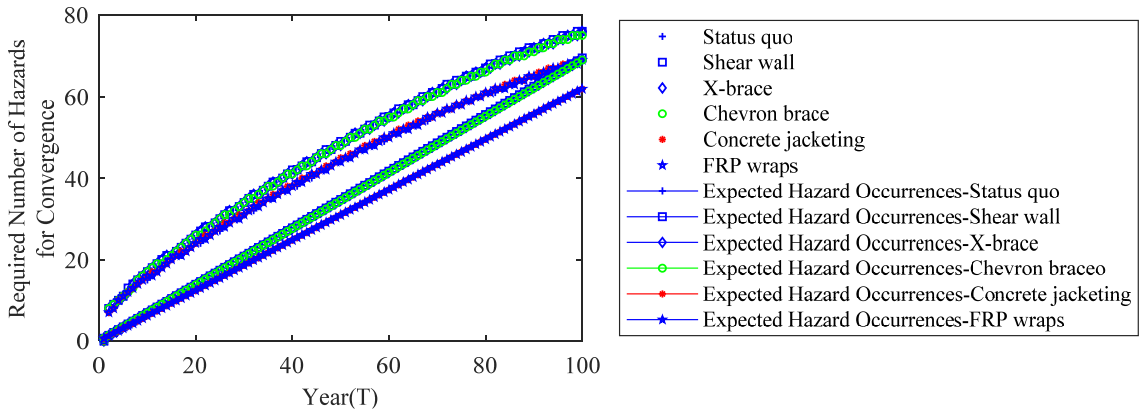

Figure 2-8 Required number of hazard incidents to be considered in the framework for convergence

2.5.2.3. Lifecycle Cost Analysis and Optimal Decision-Making across Predetermined Alternatives

The expected lifecycle maintenance cost, hazard-induced cost, salvage value and total cost for a wide range of lifetimes for the six retrofit options are shown in Figure 2-9-a~d. The discount rate is considered as 5%. It is observed that structures with higher construction costs have higher lifecycle maintenance cost as well. This is expected as the annual maintenance cost is assumed a fraction of the construction cost and the fraction remains the same for all building cases. Results in Figure 2-9-b indicate that the expected lifecycle hazard-induced cost is the highest in the Shear wall and X-brace retrofit plans, whereas status quo stands the third in the ranking. Considering the enhancement ratios in the state-dependent fragility curves provided in Table 2-4, it can be concluded that retrofitting the ductile frame building does not necessarily reduce the likelihood of experiencing damage during earthquakes. A possible reason can be the fact that adding such retrofit systems significantly decreases the structural stiffness and consequently the first mode period.

According to Figure 2-6, these result in a considerable increase in the annual rate of exceeding hazard intensities, which increases the risk of damage due to earthquakes, and thus the expected lifecycle hazard-induced cost. The lifecycle salvage values for different retrofit strategies are shown in Figure 2-9-c. As explained before, the salvage value depends directly on the damage-state of the structure at the end of the lifetime. Here, different retrofit actions are considered to have identical repair times and salvage values. According to Equation (2-33), the building is in the intact damage-state at the end of the horizon, unless there is not sufficient time to repair damage occurred before the end of the time horizon. Since the considered repair times are relatively short, the latter condition is not very likely to be met. As a result, the building is likely to be in the intact damage-state at the end of the lifetime, with nearly identical salvage values for all retrofit actions. As the time horizon increases, the net present of the salvage values decreases exponentially with the rate $\gamma^{T_{LC}}$, where γ is the discount factor with a value less than one. Thus, for sufficiently large values for the time horizon, the salvage value converges to zero, resulting in a small contribution of the salvage value to the overall LCC. The sum of all of the cost components are plotted in Figure 2-9-d.

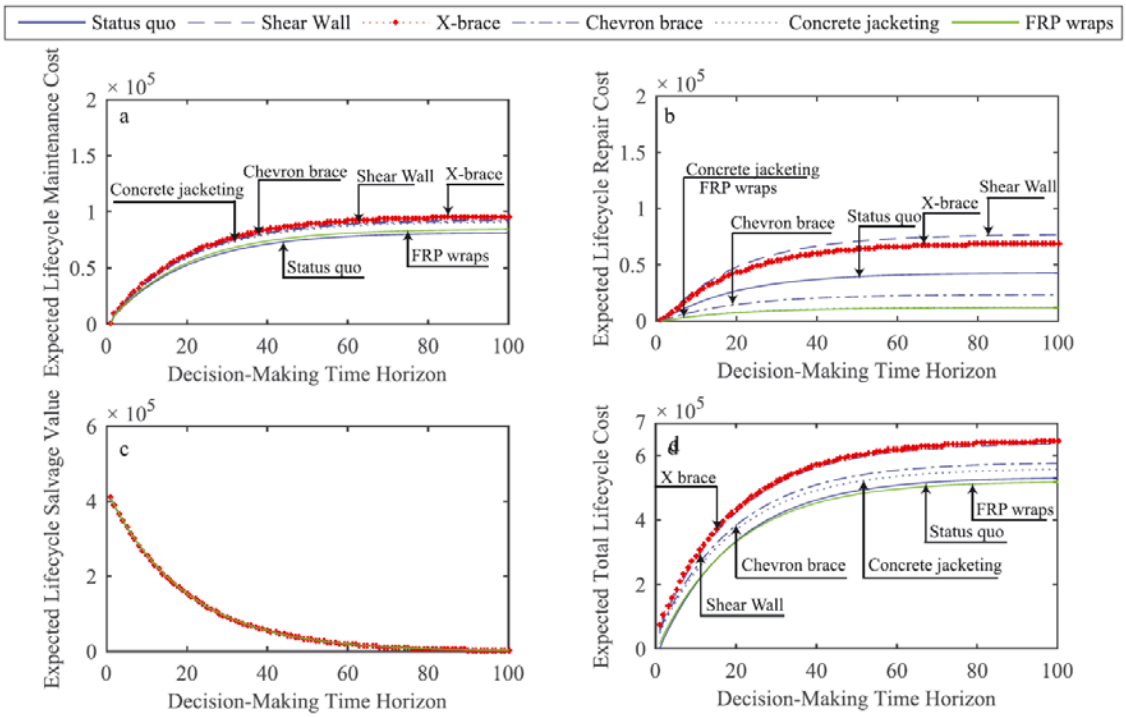

Figure 2-9 The expected lifecycle a) maintenance, b) hazard-induced, c) salvage and d) total costs for different lifetimes for the six retrofit options

For the input parameters described earlier, the FRP wrapping strategy appears to be the optimal retrofit option if the planning horizon is more than 15 years. Finally, it can be observed that the ranking of optimal decisions vary slightly with the lifetime. The variation in the total LCC is also minor among the six retrofit actions. As noted before, in the application of the proposed framework to the case study building, only the direct repair costs and the indirect costs due to disruptions are considered. When other sources of loss such as human injuries and casualties and indirect economic losses are added to these consequences, variation in the LCCs, as well as changes in the ranking of optimal strategies are expected to be more significant than those derived in this study. If these additional loss terms are considered, it is expected that retrofit options with more

enhancement in the fragility curves for severe damage-states will become more attractive alternatives.

2.5.2.4. Variation of Optimal Decisions against Different Repair Times

This section investigates the impact of the total repair time on the expected total LCC and optimal retrofit decision-making across predetermined alternatives. As explained in Section 2.4.5, each of the damage-states has a different restoration path consisting of multiple actions. The total repair time for damage-state j, T_{total}^{j}, is the summation of times required for implementing associated restoration actions; each of these times has a lognormal distribution with parameters provided in Table 2-5. Expected lifecycle hazard-induced cost, salvage value, and total cost of the structure for 0-, 0.5-, and 0.95-percentiles of T_{total}^{j} for the damage-states of the status quo retrofit plan are presented in Figure 2-10. The α-percentile of T_{total}^{j} is denoted by T_{α}^{j} and is determined such that $P\left[T_{total}^{j} \leq T_{\alpha}^{j}\right] = \alpha$. α is called non-exceedance probability. The distribution of T_{total}^{j} and the values of T_{α}^{j} are determined through Monte-Carlo simulations based on Latin Hypercube sampling method. The values of T_{0}^{j}, $T_{0.5}^{j}$, and $T_{0.95}^{j}$ for considered damage-states of the status quo retrofit plan are presented in Table 2-8.

Table 2-8 The 0-, 0.5-, and 0.95-percentiles for the total repair times (in years) of various damage-states of the status quo retrofit plan.

	Damage-state				
	Intact (j=1)	Light (j=2)	Moderate (j=3)	Irreparable (j=4)	Collapse (j=5)
$\boldsymbol{T_{0}^{j}}$	0.0	0.0	0.0	0.0	0.0
$\boldsymbol{T_{0.5}^{j}}$	0.0	0.1	0.3	0.9	1.5
$\boldsymbol{T_{0.95}^{j}}$	0.0	0.3	0.7	1.6	3.3

Results of Figure 2-10 indicate that the total repair time has a noticeable impact on the expected lifecycle hazard-induced and total LCCs of the building, whereas the impact is negligible for the salvage value of the building. As previously explained, this latter effect can be attributed to the low sensitivity of the salvage value to the total repair time. The relative difference between the case of instantaneous repair, T_0^j, and the case of very lengthy repair $T_{0.95}^j$ is about 60% and 7.5% for the expected lifecycle hazard-induced cost and the total LCC, respectively.

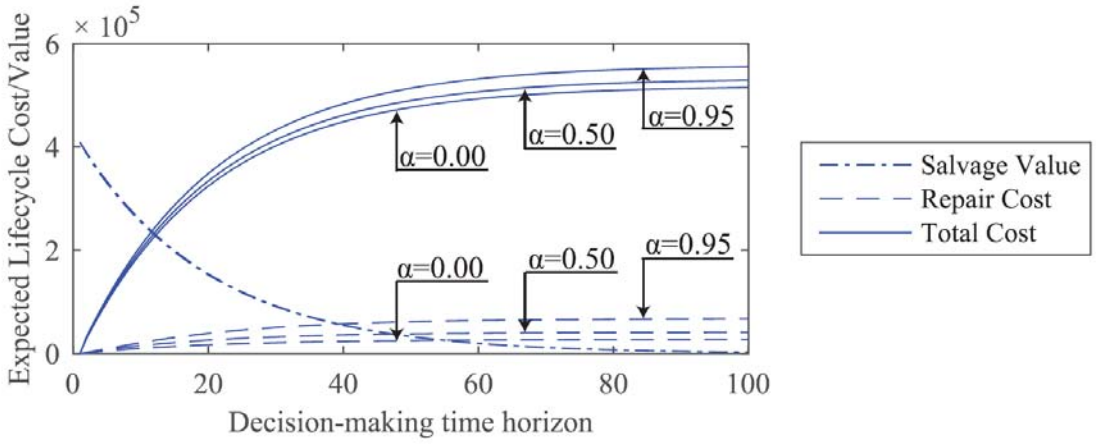

Figure 2-10 Expected lifecycle hazard-induced cost, salvage value, and total LCC for 0-, 0.5-, and 0.95-percentiles of the total repair time

The impact of total repair time on the rankings of retrofit options is investigated in Figure 2-11 where the expected total LCC is determined as a function of lifetime for 0-, 0.5-, and 0.95-percentiles of total repair time. From the results in Figure 2-11-a and Figure 2-11-b, it appears that if the repair time is neglected in the LCC framework, i.e. the case of T_0^j, the status quo option is the optimal action for the first 45 years of planning horizon. As the percentile of the total repair time increases, other retrofit plans become

more attractive. For the case of median values of repair time, $T_{0.5}^{j}$, the status quo is the optimal solution for only the first 15 years, after which the FRP wrapping strategy is the most effective approach. The difference becomes even more significant for $T_{0.95}^{j}$ case where the LCCs of the status quo and FRP wrapping become more apart compared to the cost difference between these two retrofit plans in the T_{0}^{j} and $T_{0.5}^{j}$ cases (see Figure 2-11-c).

It should be noted that in case the damage consequences include indirect economic losses and account for potential injuries and casualties, the impact of the total repair time on the expected repair and total LCCs will be more significant since the cumulative damage costs would be considerably greater. In such cases, retrofit options that provide higher reliability especially for more severe damage-states become more attractive and the contribution of the initial cost to the total LCC decreases. As explained in Section 2.3.4, one way to control such consequences and ensure the safety of buildings is to set a threshold for the annual rate of collapse and evaluate the performance of the retrofit strategies against this limit. The results of this approach is discussed in the next section.

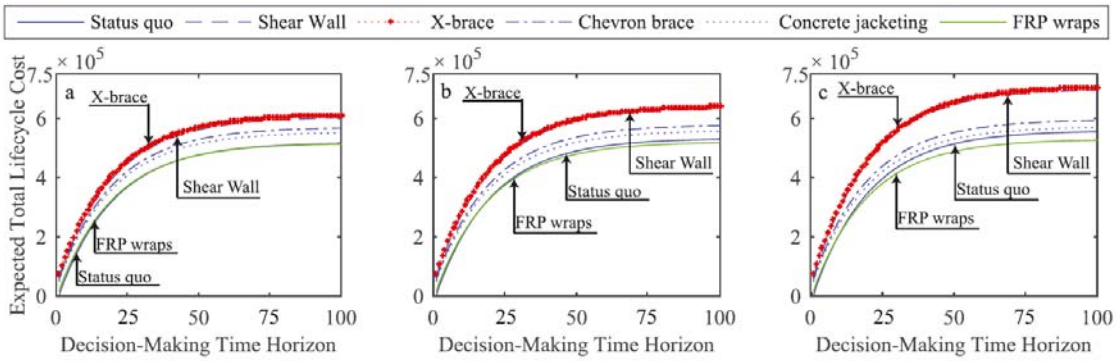

Figure 2-11 Expected total LCC for the six retrofit actions corresponding to a) 0-percentile, b) 0.50-percentile, and c) 0.95-percentile of the total repair time

2.5.2.5. Comparison of the Annual Rate of Collapse with the Allowable Threshold

Acceptable target values for the annual rate of collapse have been defined based on different criteria. For instance, JCSS (59) suggests this value as a function of the severity of collapse consequences and the relative cost of safety. However, an important parameter for the target collapse rate is the collapse risk acceptability of the community. Allen (60) considered this factor in the calculation of the maximum acceptable annual probability of collapse denoted by P_C^{acc}. This relationship which has been used in many studies such as (61) and (62) is as follows:

$$P_C^{acc} = \frac{A}{W\sqrt{n_r}} \times 10^{-5}/_{yr} \tag{2-46}$$

where W is the warning factor, A is the activity factor which defines whether the structure is normal or is intended for activities following the occurrence of a disaster, and n_r is the expected number of people at risk. According to the guidelines provided in (61), for the case study building in this research, $W$and A are taken as 1.0. Furthermore, n_r is

considered as 10^{-4} based on recommendations in FEMA 227 (63). The assumptions for selecting these parameters are that the case study building is intended for normal activities (i.e. not for activities following a disaster); the nature of structural collapse under seismic excitations is sudden without previous warnings; and the building is rehabilitated. Substituting these values into Equation (2-46), P_F^{acc} is derived as 10^{-3}. The calculated annual probability of collapse can then be transformed into the acceptable mean annual rate of collapse, λ_F^{acc}, through Equation (2-47), where at least one occurrence of collapse is of interest in a year:

$$P_F^{acc} = 1 - e^{-\lambda_F^{acc} \times 1} \tag{2-47}$$

Using P_F^{acc} value of 10^{-3}, λ_F^{acc} is calculated as 10^{-3}.

As explained in Section 2.3.4, annual rate of collapse may not be constant due to the possibility of the structure to be in different damage-states originated from multiple hazard occurrences. Following Equation (2-34), for the case study building $\bar{\lambda}_F^{T_{LC}}$ is computed for the status quo retrofit plan for expected lifetimes ranging from 0 to 100 years and from 0 to 0.99 probabilities of non-exceedance for the total repair time; the results for each damage-state are presented in Figure 2-12-a~e. In performance-based structural design, these annual rates of reaching different damage-states can be used to ensure that multiple objectives involving a set of damage-states are satisfied. As expected, the annual rates of reaching damage-states decreases with the severity of the damage-states, but increases with the probability of non-exceedance of total repair time or equivalently the duration of the repair time, and the time passed since the first retrofit. Focusing on the annual rate of collapse in Figure 2-12-e, the maximum threshold of 10^{-3}

is shown with a dashed line. If the impact of repair time in LCC analysis is disregarded i.e. the case of T_0^j, the annual rate of collapse for the case study frame building is less than the maximum allowable value for the entire lifetimes. This observation implies that the status quo retrofit option is a safe alternative. However if the total repair time is considered, the annual collapse rate exceeds the maximum allowable level of 10^{-3} for non-exceedance probabilities larger than 0.5 for the total repair time. This indicates that there is 50% chance that the structure is not safe. In addition if the median value of the repair time is considered, the status quo retrofit plan is not safe for periods shorter than eight years. Therefore, this option should not be selected as the optimal plan despite the fact that it yields one of the least total LCCs as shown in Figure 2-9-d.

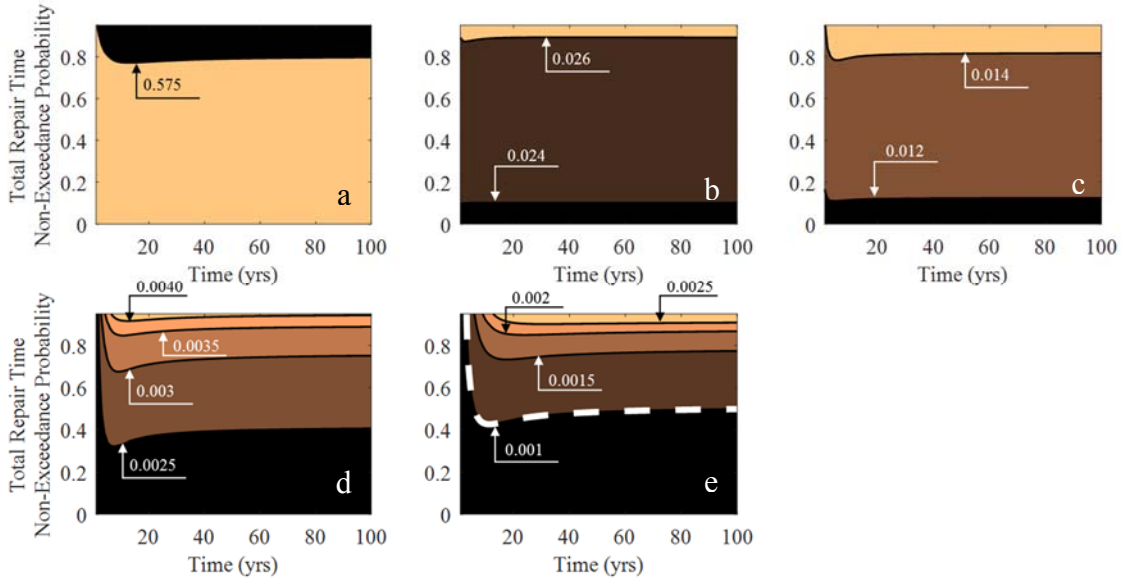

Figure 2-12 Mean annual rate of occurrence for a) intact, b) moderate, c) irreparable, d) severe, and e) collapse damage-states as a function of lifetime and different non-exceedance probabilities of repair time

2.6. Case Study 2 for Lifecycle Cost Assessment: Five Span Concrete Bridge

To further demonstrate the capabilities and various practical applications of the developed LCC assessment framework, a five span reinforced concrete bridge is considered as the second case study in this section. To reduce the runtime and complexity of the problem, the salvage value is excluded from LCC analysis. In addition, as demonstrated in Section 2.4 this term is not a significant contributor to the total LCCs in the context of optimal decision-making across predetermined hazard-mitigation strategies. In the following sections, the input models and numerical results for the case study bridge are presented.

2.6.1. Input Data for the Case Study

The bridge under study is a realistic three lane, five span reinforced concrete (RC) box girder bridge used and analyzed by (51) (see Figure 2-13). The length of the bridge is 239.1 m, and the foundation system under each pier is a group of 40 piles, which are mainly subjected to local scour (51,64). More details about the case study bridge can be found in (51).

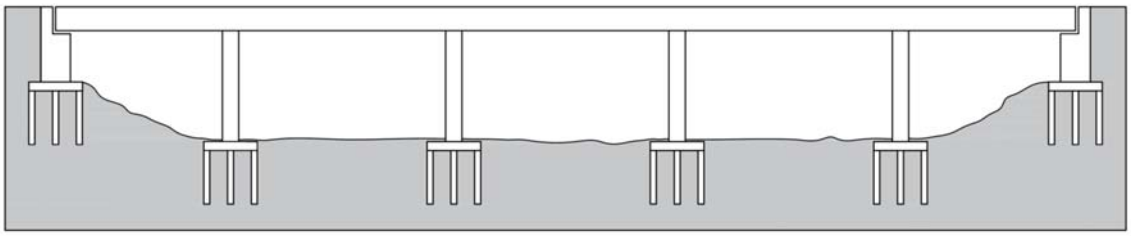

Figure 2-13 Elevation view of the case study bridge (51,65)

2.6.1.1. Hazard-Mitigation Alternatives

Bridges are vital members of transportation networks as the safety and serviceability of these structures have high implications for economic prosperity at regional and national levels. In seismic regions, the performance of bridges throughout their lifetime can be significantly degraded by multiple occurrences of earthquakes. As an example, Figure 2-14 shows the historic major earthquakes near the city of Sacramento, California, in the past 40 years with magnitude greater than 6 (66). As seen, there are a number of historic earthquakes that have occurred within a very short time.

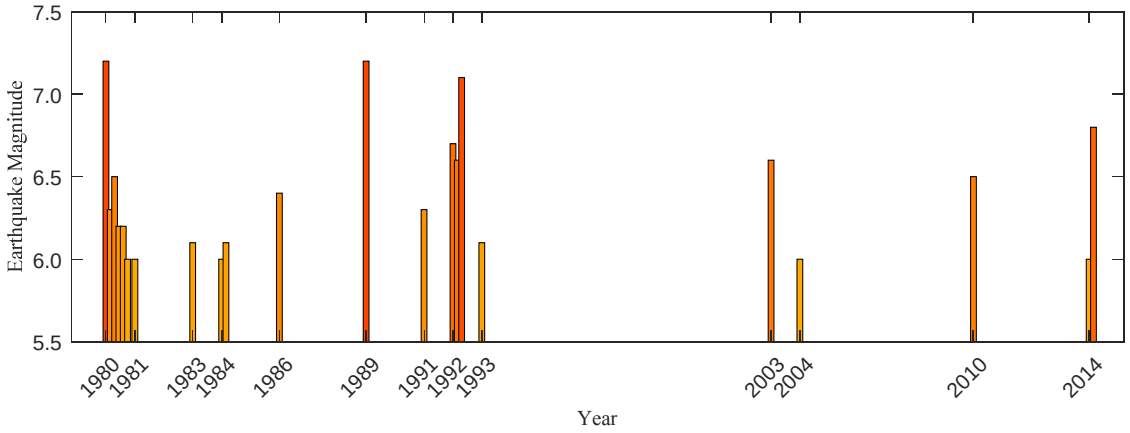

Figure 2-14 Historic major earthquakes near Sacramento in the past 40 years with magnitude greater than 6 (66)

As noted earlier in this chapter, the incurred losses may considerably increase if earthquakes occur within a short period of time from previous events. This is due to the fact that short occurrence intervals may leave insufficient time for the repair of seismic-induced damages from prior hazards, and that existing damage in bridges increases their fragility to future seismic events. Fast but costly repair techniques may reduce such structural vulnerabilities and consequently disruptions in transportation services; however, application of these repair techniques increases the repair costs of damages for the responsible agency. On the other hand, performing repair actions for all extents of seismic-induced damages reduces the safety risk on bridges arising from future earthquakes; however, implementation of these extensive repairs increases the disruption in traffic and subsequent economic losses. Thus, it is important to optimally manage the extent and speed of repair actions after earthquake occurrences.

For the lifetime of the infrastructure, two plans for the extent of repair actions and three strategies for the speed of repair actions are evaluated. The two plans for the extent of repairs include 1) performing repair actions for all extents of seismic-induced damages, and 2) conducting repairs for all extents of seismic-induced damage, except for the slight damage-state. Notably, adopted from Furtado and Alipour (67), the bridge can be left untreated to provide full service to users when it sustains slight damage-state. However, this increases the likelihood of experiencing more severe damage-states due to future earthquakes, which require more costly repairs and more disruption in transportation services. Moreover, three repair speeds of slow, average and fast are considered and evaluated for the case study bridge. Following (68), it is considered that the required repair times will reduce by 15% when the physical cost of repairs increases by 15%; this case represents fast repairs in this study. On the other hand, for slow repairs, the agency can spend 20% less for repair actions at the cost of 15% increase in the duration of repairs.

2.6.1.2. Seismic Hazard Curves

For the purpose of comparison between the identified optimal decisions, two locations are assumed for the case study bridge system; city of Sacramento, California, with moderate chance of high-intensity earthquakes and city of Sierra Madre, California, with high chance of high-intensity earthquakes. Following Prasad and Banerjee (51), and Kelly (69), class C is assigned to the site of the case study bridge. Considering this site class, seismic hazard curves are generated for the cities of Sacramento and Sierra Madre using an online application developed by USGS (44) (see Figure 2-15). In line with the available data on

damage-state dependent fragility curves for the case study bridge, peak ground acceleration (PGA) is selected as the intensity measure for these hazard curves. The curves present the annual rate of PGA exceedance given various possibilities of PGA occurring in the region. According to the generated hazard curves, the annual rate of earthquake occurrence for the cities of Sacramento and Sierra Madre are derived as 0.3700 and 0.3704, respectively.

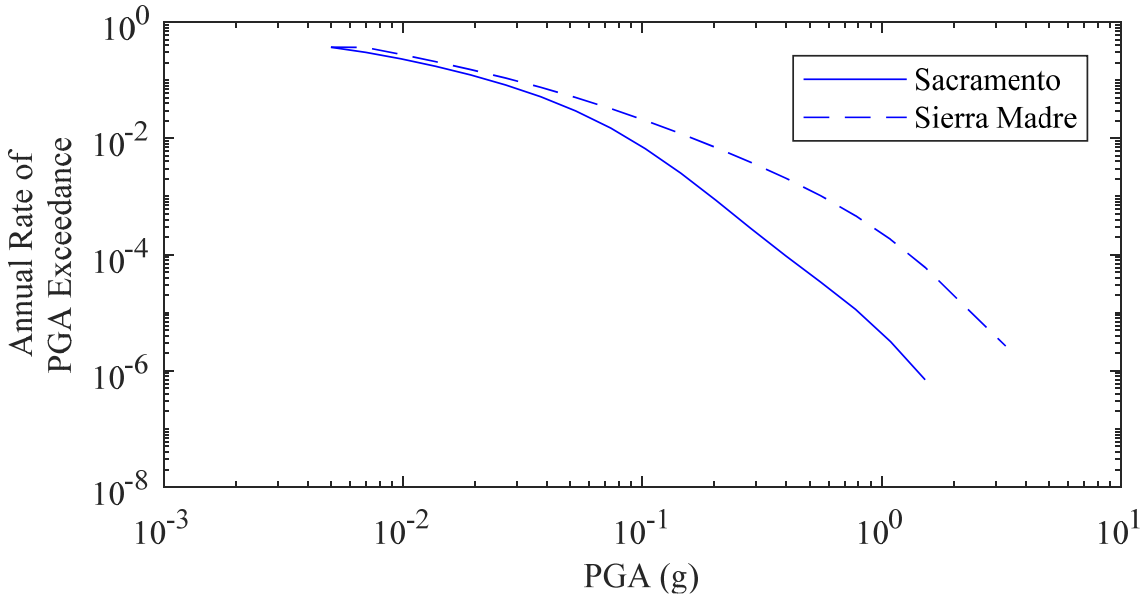

Figure 2-15 Hazard curves for two cities in California: Sacramento and Sierra Madre (44)

2.6.1.3. Damage-state Dependent Fragility Curves

Five earthquake-induced damage-states that are consistent with NIBS, FEMA (54) definitions are considered here; these include intact (no damage), slight, moderate, extensive, and complete (collapse) damage-states. Prasad and Banerjee (51) suggested equivalent displacement ductility thresholds for the case study bridge columns as 2.25,

2.90, 4.60, and 5.0, for damage-states slight, moderate, extensive, and complete, respectively. The median values for the lognormal cumulative distribution functions of the fragility curves for these damage-states are determined by Prasad and Banerjee (51) and are given in Table 2-9. A logarithmic standard deviation of 0.5 is considered for all fragility curves (70).

Table 2-9 Median values of PGA (g) for the lognormal cumulative distribution functions of the fragility curves for the case of initial intact seismic damage-state (70)

Damage-state			
slight	Moderate	Extensive	Complete
0.73	0.90	1.27	1.44

The above set of fragility curves represent the case where the bridge at the time of the earthquake occurrence is in the intact seismic damage-state. For other damage-states, due to lack of available data and for the purpose of demonstration of the proposed method, it is assumed that the ratio of the median of the fragility curves when the initial condition of the bridge is intact, to the median of the fragility curves when the bridge is initially in other than the intact state follows the values given in Table 2-10. These ratios have a reasonable agreement with the ones reported by Raghunandan et al. (71) for building structures, as such reliable data are currently not available for bridges.

The damage-state dependent fragility curves for the case study bridge are shown in Figure 2-16.

Table 2-10 The ratios of the median of the fragility curves when the initial condition of the bridge is intact, to the median of the fragility curves when the bridge is initially in other than the intact state

				Initial damage-state					
				Slight			Moderate		Extensive
				Limit-state in fragility curve					
				Moderate	Extensive	Complete	Extensive	Complete	Complete
Initial damage-state	Intact	Limit-state in fragility curve	Moderate	1.25	-	-	-	-	-
			Extensive	-	1.25	-	1.5	-	-
			Complete	-	-	1.25	-	1.5	2

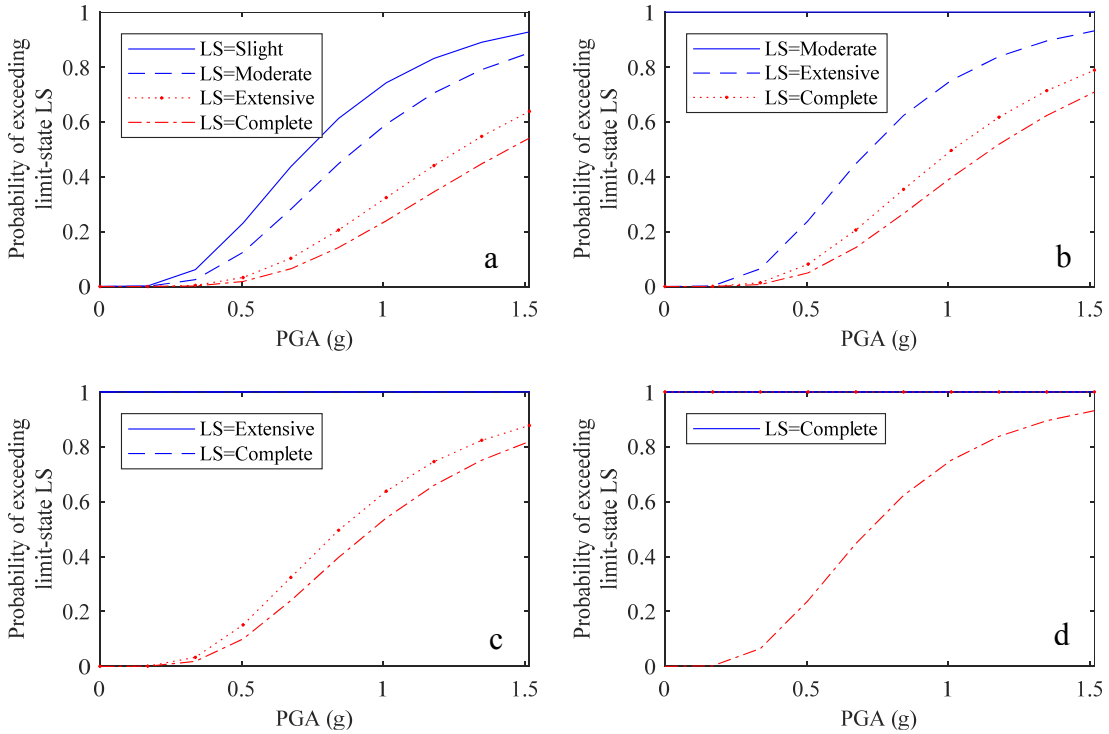

Figure 2-16 Damage-state dependent fragility curves when the bridge is at a) intact b) slight c) moderate and d) extensive damage-states

2.6.1.4. State Dependent Repair Times

Generally, the more severe a damage-state, the more time required for repairing the damage and improving the structural condition of the bridge to its original state. For each

seismic damage-state, the set of tasks that constitute the recovery path along with the corresponding probabilistic models for required times are provided in Table 2-11. In this Table, T_{ins} stands for the time required for inspection and estimation, $T_{d\&c}$ is the required time for preparing a repair plan, bidding and contracting, T_{mob} is the time required for the mobilization of resources (i.e. materials and crews) and T_{rep} is the required time for repair.

Table 2-11 Seismic damage-dependent recovery path and the statistical information for the required time for each task of the recovery paths

		Recovery Path	Recovery Time (Days)							
			Lognormal Mean (days)				Lognormal Standard Deviation (days)			
			Tins	*Tmob*	*Td&c*	*Trep*	*Tins*	*Tmob*	*Td&c*	*Trep*
Damage-state	Light	$T_{ins} + T_{d\&c} + T_{rep}$	4	-	30	0.6	3.6	-	27.4	0.6
	Moderate	$T_{mob} + T_{ins} + T_{d\&c} + T_{rep}$	4	45	40	2.5	3.6	41.0	36.5	2.7
	Extensive	$T_{mob} + T_{ins} + T_{d\&c} + T_{rep}$	4	45	50	75	3.6	41.0	45.6	42
	Complete	$T_{mob} + T_{ins} + T_{d\&c} + T_{rep}$	4	45	60	230	3.6	41.0	54.7	110
Used References			R1	R2	R2 and R3	R4	R2 and R5	R2 and R5	R2 and R5	R4

Note: R1=Gordin (72), R2=Author`s judgment, R3=Shinozuka et al. (73), R4=NIBS, FEMA (54), R5=Burton et al. (37)

2.6.1.5. Cost Terms

As reported by Yilmaz et al. (25), according to Caltrans construction statistics, the average physical cost of replacement of box girder bridges becomes \$1949/m^2 for 2017. This cost is used for the replacement cost of the studied bridge. The annual discount rate, δ, is considered as 5% for all years. As noted previously, following each hazard occurrence, depending on the induced damage, a set of direct and indirect user and agency costs are

incurred on the community. Accurate prediction of these costs results in reliable LCC analysis for the case study system. Other research studies, e.g. Fereshtehnejad et al. (65), have also evaluated a comprehensive list of user and agency costs for the repair of infrastructural defects as a function of the extent of system deficiencies. This has led to objective and reliable performance assessment of those infrastructure systems. As mentioned in Section 2.3.4, some may argue against the incorporation of injury and casualty losses in terms of costs. However, for objective evaluation of all consequences, in this section and the rest of the chapters of this dissertation, these costs are considered for hazard-induced LCC calculations. On this basis, the following set of costs is considered for the case study bridge in this section: direct costs of repairing the damage and human casualties, and indirect costs of delay time, vehicle operation, and excess gas emission on users, damage to the environment, and economic losses. These costs are summed to yield the overall cost for each damage-state, i.e. $\bar{C}_r\left(DS_n^j\right)$ in Equation (2-16). In the following sections, these costs are presented and discussed.

2.6.1.5.1. Agency Repair Costs

Agency-incurred repair costs are incurred following the occurrence of each of the seismic-induced damage-states. These values, according to NIBS, FEMA (54), are estimated as 0.03, 0.08, 0.25, and 1.00 times the replacement cost for slight, moderate, extensive, and complete damage-states, respectively. Furthermore, according to Caltrans (74), there are two cost terms that should be added to the total repair costs; these include mobilization and contingency costs, which are estimated as 10% and 20% of the bridge repair cost,

respectively (74). Contingency cost covers unpredicted costs that may arise during inspection and mobilization and also from unforeseen costs due to design changes (72,74).

2.6.1.5.2. User Costs of Imposed Delay, Vehicle Operation and Excess Emission

For performing repair actions on highway bridges, partial or complete closure of bridges are often required for the safety of workers in work zones. As a result of such disruptions in the traffic flow, user costs will incur due to delays imposed on passengers, extra operation of vehicles, and excess gas emission of hydrocarbons, carbon monoxide, and nitrogen oxide (75). These costs, denoted by $C_U(CS_n)$, are included in the damage-state dependent hazard-induced costs for the case study bridge as follows:

$$C_U(DS_n) = \min(\tau_n, 1/\upsilon_1) \times (t_{ij}^{D/R} - t_{ij}^{O}) \times [(AADT - AADTT) \times \rho_C + AADTT \times \rho_T] \quad (2\text{-}48)$$

where $\min(\tau_n, 1/\upsilon_1)$ is the expected time of traffic interruption as a result of repairing seismic-induced damages to the case study bridge. According to Equation (2-16), the expected hazard-induced costs are considered independent of the times of hazard occurrences and are added together for entire potential times that hazards take place. For this reason, the expected time of traffic interruption is the minimum of the required repair time for damage-state *n* and the expected time difference between earthquake occurrences. This assumption is released in Chapter 4 of this dissertation. In Equation (2-48), $AADT$ and $AADTT$ are the annual average daily traffic and annual average daily truck traffic of path *ij* that the bridge is part of, τ_n is the recovery time for damage-state *n* (see Table 2-11), and t_{ij}^{O} is the original time for passing path *ij* using the main bridge with no

partial/complete closure or speed reduction. According to Bocchini and Frangopol (42), t_{ij}^{O} can be computed by:

$$t_{ij}^{O} = t_{ij}^{F} \times \left[1 + \alpha(\frac{f_{ij}}{f_{ij}^{c}})^{\beta}\right] \tag{2-49}$$

In this equation, t_{ij}^{F} is the time required to pass through path *ij* at free flow speed, and can be estimated by the length and speed limit of the path. f_{ij} represents the traffic flow in the highway segment *ij*, and is equal to the *AADT* of the main bridge. f_{ij}^{c} stands for the critical flow (maximum flow capacity) of the bridge, and α and β are model parameters considered as 0.15 and 4, respectively (42). In Equation (2-48), $t_{ij}^{D/R}$ is the time delay for users that drive through the detour or for the portion of the traffic that passes the bridge with the reduced speed limit, all as a result of repair actions that are conducted on the bridge. Assuming that the traffic flow on the detour is low compared to the traffic flow on the main path, $t_{ij}^{D/R}$ can be calculated by the following formulation from Bocchini and Frangopol (42):

$$t_{ij}^{D/R} = t_{ij}^{F/R} \times \left[1 + \alpha(\frac{f_{ij}}{f_{ij}^{c}})^{\beta}\right] + \sum_{b \epsilon ij} s_{b,ij} \times t_{b,ij}^{d} \times \left[1 + \alpha(\frac{s_{b,ij} \cdot f_{ij}}{f_{b,ij}^{c}})^{\beta}\right] \tag{2-50}$$

where $t_{ij}^{F/R}$ is the time required to pass through path *ij* with a reduced speed limit on the main road due to repair activities. $f_{b,ij}^{c}$ stands for the critical flow (maximum flow capacity) of the path of interest together with detour *b* that joins points *i* and *j*. In addition, $s_{b,ij}$ is the fraction of traffic from point *i* to *j* that passes through detour *b*, and $t_{b,ij}^{d}$ is the time required to move form point *i* to *j* through detour *b* at free flow speed. In Equation

(2-48), ρ_C and ρ_T are the user costs of imposed delay, vehicle operation and excess emission due to the incurred delay for using detours or speed reductions for unit car and unit truck, respectively. After updating unit user costs specified in ODOT (76), ρ_C and ρ_T are found as \$22.88/hour and \$58.83/hour for year 2017, respectively. In addition, for the calculation of user costs, the following assumptions and considerations are made:

- The bridge connects two points *i* and *j* in the city of Sacramento with a distance of 16.1 km (10 mi).
- For the three lane case study bridge, the maximum flow capacity of the bridge required for the calculation of d_{ij}^n is considered as 1750 vehicles/hour/lane (77).
- The *AADT* of 154000/2 for the three lane Capital City highway (78), which crosses the American River in the Sacramento County, is considered for the three lane case study bridge.
- Trucks contribute 9.6% to the *AADT* of the bridge (78).
- The speed limit of 60 mph is considered for the highway road that the case study bridge is located on.
- In case of a partial closure of the bridge due to repair activities, the posted reduced speed limit on the bridge is considered as 50 mph (following recommendations by Caltrans (79)). This speed limit is also considered for the detour road parallel to the main highway.
- An extra time of five minutes is added to the trip from point *i* to *j*, if passengers use the detour to reach their destination point *j* (Bocchini and Frangopol (42)).

- The maximum flow capacity of the detour is considered half the maximum flow capacity of the highway that the bridge is located on (Bocchini and Frangopol (42)).
- Similar to Furtado and Alipour (67), complete, extensive, moderate, and slight damage-states are assumed to degrade the functionality of the bridge by 100%, 100%, 66.7%, and 33.3%, respectively. The latter two cases correspond to the closure of two and one lane of the bridge for inspection and repair activities, respectively.

2.6.1.5.3. Cost of Economic Losses

Businesses especially those nearby the bridge will be affected by the interruption in traffic due to partial/complete bridge closure. Accurate identification of this cost requires transportation system and economic analyses, which is not in the scope of this study. Instead, twice the user cost of imposed delay, vehicle operation and excess emission is considered for the cost of economic losses. This factor is chosen here based on a study by Klisen and Mill (80) for economic impacts of hazard-induced damage to transportation systems.

2.6.1.5.4. Cost of Human Casualties

Human casualties including injuries and deaths are potential consequences of damage to bridges. Casualty rate defined as the ratio of casualties to the total number of people at risk can be used to estimate human losses. According to NIBS, FEMA (54), the casualty rate for continuous bridges when collapse damage-state is experienced is 17%, 20%, 37%, and 7% for casualty severity levels of 1 to 4, respectively. The severity levels in NIBS,

FEMA (54) are similar to minor, moderate, severe, and fatal casualty levels in Porter et al. (81) where the corresponding cost values are provided. After updating, the casualty costs per person are derived as \$8500, \$68000, \$833000, and \$4421200, respectively, for severity levels of 1 to 4. Due to lack of data, NIBS, FEMA (54) does not provide casualty rates for slight, moderate and extensive damage-states for bridge structures. These values are assumed proportional to those for building structures, for which such information is presented in NIBS, FEMA (54). Table 2-12 shows casualty rates for various damage-states and severity levels considered in this study.

Table 2-12 Casualty rates for various damage-states and severity levels considered in this study (adopted from NIBS, FEMA (54))

	Intact	Slight	Moderate	Extensive	Complete
Severity Level 1	0.00%	0.20%	1.00%	4.00%	17.00%
Severity Level 2	0.00%	0.00%	1.11%	3.70%	20.00%
Severity Level 3	0.00%	0.00%	0.00%	0.70%	37.00%
Severity Level 4	0.00%	0.00%	0.00%	0.70%	7.00%

Based on the length and *AADT* of the bridge and considering the average of 1.42 passengers per vehicle on the Capital City highway (82), it is estimated that on average 75.7 people will be at risk due to potential damage to the bridge at the time of an earthquake occurrence. Thus, the cost of human casualties for each condition-state, $C_H(DS_n)$, is determined by:

$$C_H(DS_n) = \sum_{i=1}^{4} C_{SL_i} \times CR_n^{SL_i} \times NPAR \tag{2-51}$$

where C_{SL_i} denotes the cost of human casualty for severity level i, $CR_n^{SL_i}$ stands for the casualty rate for severity level i and damage-state n, and $NPAR$ is the total number of people at risk.

2.6.1.5.5. Cost of Environmental Damage

Traffic delays due to partial/complete closure of the bridge increase air pollution, consumption of energy, and the possibility of global warming (83,84). This cost can be quantified as follows:

$$C_E(DS_n) = C_{Env} \times \min(\tau_n, 1/\upsilon_1) \times AADT \times \left[l_{ij} \times En_{V_{ij}} + \sum_{b \epsilon ij} s_{b,ij} \times l_{b,ij} \times En_{V_{b,ij}} - l_{ij} \times En_{V_{ij}^O} \right] \quad (2\text{-}52)$$

where l_{ij} and $l_{b,ij}$ are the length of the path ij through the main highway and detour b, respectively. $En_{V_{ij}^O}$, $En_{V_{b,ij}}$, and $En_{V_{ij}}$ denote the unit value of carbon dioxide emission at speeds V_{ij}^O, V_{ij}, and $V_{b,ij}$, which are the average velocity of vehicles traveling from point i to j passing through: the main highway before interruption by partial/complete road closure, the main highway after interruption by partial/complete road closure, and detour b, respectively. Based on Equation (2-50), V_{ij}^O, V_{ij}, and $V_{b,ij}$ can be derived as $\frac{l_{ij}}{t_{ij}^F \times \left[1+\alpha(\frac{f_{ij}}{f_{ij}^c})^\beta\right]}$, $\frac{l_{ij}}{t_{ij}^F \times \left[1+\alpha(\frac{(1-s_{b,ij}) \times f_{ij}}{f_{ij}^c})^\beta\right]}$, and $\frac{l_{b,ij}}{t_{b,ij}^d \times \left[1+\alpha(\frac{s_{b,ij} \cdot f_{ij}}{f_{b,ij}^c})^\beta\right]}$, respectively. For the example bridge settings, the corresponding $En_{V_{ij}^O}$, $En_{V_{b,ij}}$, and $En_{V_{ij}}$ are extracted from Gallivan et al. (85). Finally, C_{Env} stands for the unit cost of environmental damage, for which Kendall

et al. (86) derived a value of $26 per ton of carbon dioxide emission for year 2003. After updating this cost to year 2017, $35.61 is considered for C_{Env} in this research.

2.6.2. Numerical Results

To determine the optimal repair policy, the proposed framework is applied to the case study bridge in the two considered locations; Sacramento and Sierra Madre in California. Like the building case study in Section 2.4, discount rate of 5% is considered for LCC calculations.

Figure 2-17-a shows the expected LCC of earthquakes for various lifetimes, considering that the bridge is located in Sacramento. The LCCs are calculated for the six repair plans that are explained in Section 2.5.1.1. Since these repair plans do not change the total lifecycle maintenance costs of the bridge, optimal decision-making across predetermined design or retrofit alternatives can be made solely based on the expected earthquake-induced LCCs. As shown, the expected earthquake-induced LCCs for time horizons from 1 to 75 years are less if no repair action is conducted for slight damages. This shows reducing disruptions in the passing traffic is more cost-effective than conducting costly and time-consuming repairs in order to slightly improve the reliability of the bridge against future hazards. Results show investing on fast repair technologies reduces the expected LCC of earthquakes by almost 10%, despite the higher costs of implementing these methods.

To investigate the impact of dependencies between damages from consecutive hazards, earthquake-induced LCCs are also calculated when these dependencies are

overlooked. This is equivalent to considering instant repairs, which is a common assumption in many of the existing LCC frameworks. Results of this analysis, presented in Figure 2-17-b, shows that the optimal repair policy is identical to the case where damage-dependencies are considered in the analysis, however, the LCC values are considerably underestimated. As an example, for 75 years for the service lifetime of the bridge, the expected budget for the repair of seismic-induced damages following the optimal strategy is underestimated by 20%. This can adversely impact the allocation of the repair budget for the lifetime of the bridge.

Furthermore, when damage-dependencies are disregarded, the benefit of fast repairs in reducing the likelihood of damage accumulations are overlooked. For this reason, one may expect to see higher LCCs for repair plans that are conducted with faster speeds, considering that faster repairs incur more cost on the agency. However, Figure 2-17-b shows that performing repair plans with a faster speed of execution is still optimal. The reason can be attributed to the fact that faster repairs are less time-consuming, and thus incur less user cost of DVE, and economic and environmental losses. The amount of reduction in these costs is more than the increase in the agency cost of implementing fast repairs, considering that the traffic demand on the bridge is relatively high. Therefore, performing faster repairs are optimal even in the case where damage-dependencies are disregarded.

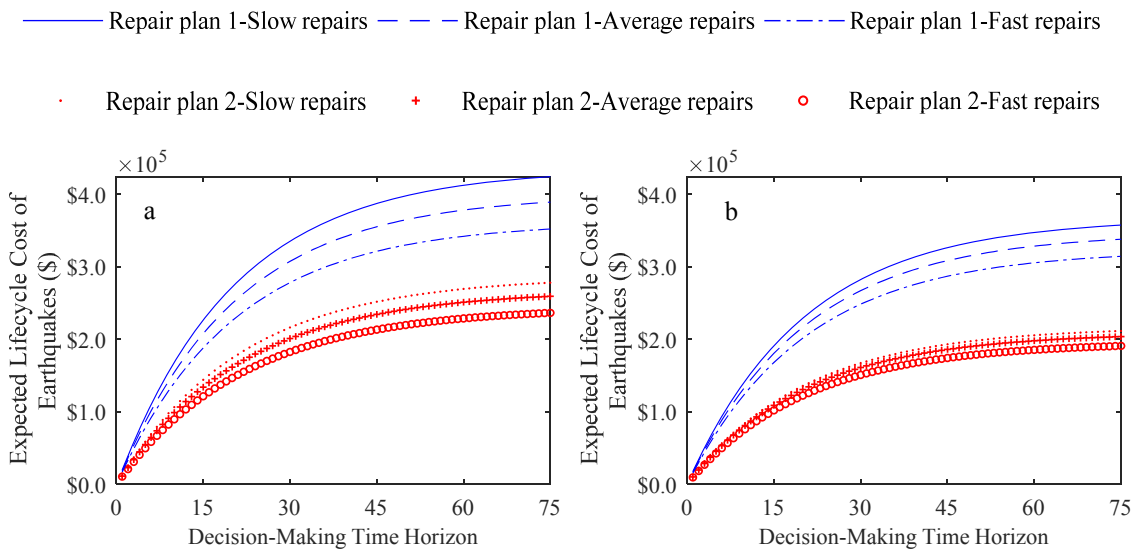

Note: Repair plan 1: Performing repairs for all extents of damages. Repair plan 2: Performing repair actions for all extents of damages, except for the slight damage-state.

Figure 2-17 Expected LCC of earthquakes for various lifetimes in Sacramento, a) considering dependencies b) ignoring dependencies among damages from consecutive hazards

Similar trends are observed when the bridge is located in Sierra Madre with higher seismicity (see Figure 2-18). Furthermore, due to the higher seismicity of the region, the expected LCC of earthquakes is larger compared to the case where the bridge is located in Sacramento with a lower seismicity. In addition, it can be seen that repairing all extents of damage with fast repairs result in expected LCC values that are very close to those of the optimal strategy. This is expected due to the high seismicity of the region, which increases the likelihood of severe damage-states especially when the structure is at a damaged state. As Figure 2-18-b shows, this finding cannot be made if damage-dependencies are ignored.

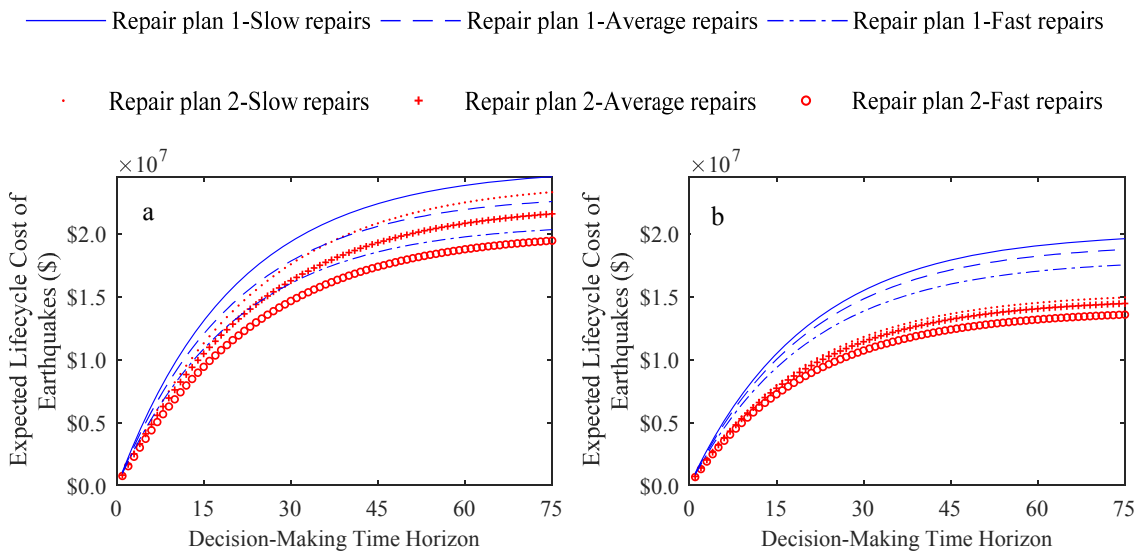

Note: Repair plan 1: Performing repairs for all extents of damages. Repair plan 2: Performing repair actions for all extents of damages, except for the slight damage-state.

Figure 2-18 Expected LCC of earthquakes for various lifetimes in Sierra Madre, a) considering dependencies b) ignoring dependencies among damages from consecutive hazards

2.7. Case Study for Lifecycle Resilience Assessment: Five Span Concrete Bridge

The case study in this chapter is the realistic five span RC bridge that is introduced in Section 2.6.

2.7.1. Input Data for the Case Study

Similar to that section, the following six repair alternatives are considered:

1) Repair plan 1 with slow repairs: Performing repairs for all extents of damage, considering a slow speed for conducting repairs.
2) Repair plan 1 with average repairs: Performing repairs for all extents of damage, considering an average speed for conducting repairs.

3) Repair plan 1 with fast repairs: Performing repairs for all extents of damage, considering a fast speed for conducting repairs.
4) Repair plan 2 with slow repairs: Performing repairs for all extents of damage, except for the slight damage-state, considering a slow speed for conducting repairs.
5) Repair plan 2 with average repairs: Performing repairs for all extents of damage, except for the slight damage-state, considering an average speed for conducting repairs.
6) Repair plan 2 with fast repairs: Performing repairs for all extents of damage, except for the slight damage-state, considering a fast speed for conducting repairs.

In addition, the same two locations are considered for the case study bridge: city of Sacramento, California with moderate chance of high-intensity earthquakes and city of Sierra Madre, California with high chance of high-intensity earthquakes. The required information for hazard curves of these two regions, the damage-state dependent fragility curves, and state dependent repair times are provided in Sections 2.5.1.2~4, respectively. In the following sections, the required data for the functionality assessment of the bridge in various damage-states are presented.

2.7.2. Functionality Recovery Functions

Expected functionality recovery curves for the four seismic-induced damage-states are shown in Figure 2-19. The curves are stepwise functions generated based on the mean values of recovery paths for the repair of the damage-states presented in Table 2-11. It is

worthy to mention that stepwise recovery functions for bridge systems have been suggested by others, such as those in (14,38). At any time of the recovery process, certain number of lanes are open to traffic, while the rest are closed due to reduction in the load carrying capacity of the bridge or for repair processes. As explained in the previous chapter, adopted from (67), when a bridge sustains complete and extensive damage-states, it will be fully closed during the entire time of repair. If moderate damage-state is sustained, the functionality of the bridge will be reduced by almost 66.67% (i.e. only one lane will be open). However, until the end of the initial inspection to identify the extent of this damage, the bridge will be fully closed for the safety of passengers. For slight damage-state, due to the space required for inspection and then repair activities, one lane is considered to be closed until the end of the repair process. As explained before, agencies may decide not to perform repair actions following the slight damage-state. In this case, for the slight damage-state, the bridge is considered fully operational after the inspection time. While this strategy reduces the disruption to the passing traffic, vulnerability of the bridge against future earthquakes increases. Optimality of this scenario is also evaluated in this chapter.

In addition to the repair paths presented in Table 1-10, in order for a bridge to be fully operational after conducting necessary repairs, a post-repair inspection and authorities' approval are needed. This prolongs the functionality recovery time, as compared with the total repair time (see Table 2-13). Based on consultations with bridge engineers at Ohio Department of Transportation, the post-repair inspection of bridges may take from a few days to few weeks depending on the extent of the repair action. On this

basis, 10% of the total required repair time of each damage-state is considered as an approximation for the sum of the post-inspection and approval time in the functionality recovery functions.

Finally, following the recommendation in (41), the control time is considered as the largest of the functionality recovery times, which is associated with the complete damage-state. This value is shown in Figure 2-19.

Table 2-13 Functionality recovery paths for seismic-induced damages, and their corresponding required times

		Recovery Path for full functionality	Mean Recovery Time				
			Tins	*Tmob*	*Td&c*	*Trep*	*Ti&a*
Damage-state	Slight	$T_{ins} + T_{d\&c} + T_{rep} + T_{i\&a}$	4	30	30	0.6	6.5
	Moderate	$T_{mob} + T_{ins} + T_{d\&c} + T_{rep} + T_{i\&a}$	4	45	40	2.5	9.3
	Extensive	$T_{mob} + T_{ins} + T_{d\&c} + T_{rep} + T_{i\&a}$	4	45	50	75	17.4
	Complete	$T_{mob} + T_{ins} + T_{d\&c} + T_{rep} + T_{i\&a}$	4	45	60	230	34.0
Used References			R1	R2	R2 and R3	R4	R2 and R5

Note: *Tins*=Inspection time, *Tmob*=Mobilization time, *Td&c*=Design and contracting time, *Trep*=Repair time, *Ti&a*=Post-repair inspection and approval time.

Note: R1=(72), R2=Author`s judgment, R3=(73), R4=NIBS, FEMA (54), R5=Expert elicitation

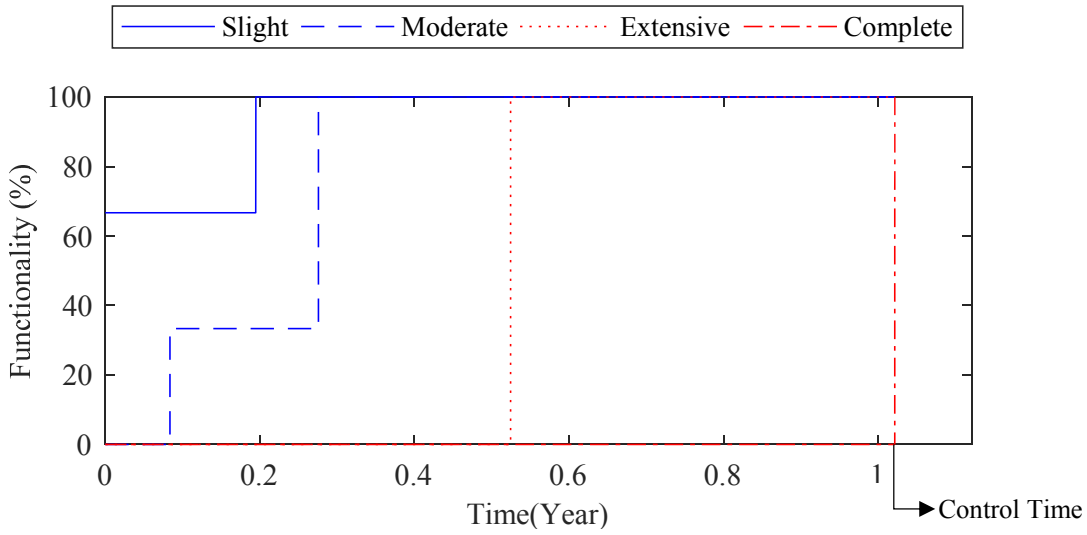

Figure 2-19 Functionality recovery curves for slight, moderate, extensive, and complete damage-states

2.7.3. Numerical Results

In this section, the application of the developed risk-based resilience index framework to the case study bridges is presented in detail.

2.7.3.1. Scenario-Based Resilience Assessment

The significance of considering couplings between damages from consecutive hazards for the estimation of resilience index is demonstrated by a hypothetical scenario of two consecutive earthquakes presented in Table 2-14 and Figure 2-20. It is assumed that the case study bridge, which is initially at its intact state, experiences two earthquakes that are six months a part. The first earthquake induces a PGA of 1.2 g, while the second one shakes the region with half of the intensity of the first earthquake, i.e. 0.6 g. Probability mass functions of damage-states slight to complete as well as the expected damage-states

following the first and the second earthquakes are provided in Table 2-14. Evidently, the expected damage-state of the bridge followed by the second earthquake is more severe when dependencies among damages induced by consecutive earthquakes are considered. This can be explained as follows. After the first earthquake, the likelihood of severe damage-states extensive and complete become as high as 46% (see Table 2-14). These damage-states require more time than the time difference between the first and second earthquakes in the considered scenario. Consequently, there is a considerable chance that the bridge is in those damage-states at the time of the second earthquake. This results in a more severe expected damage-state and thus less functionality following the impact of the second earthquake compared to the case where the bridge is considered to be in the intact state right before the second earthquake when damage-dependencies are disregarded.

The above finding can be also confirmed by comparing the functionality area plotted in Figure 2-20-a for the case of considering damage-dependencies, with that displayed in Figure 2-20-b for the case of disregarding damage-dependencies. According to these figures, the functionality area followed by the second earthquake is smaller for the former case than the latter one. This also indicates a lower serviceable state for the bridge when damage-dependencies are taken into consideration.

The results in Table 2-14 also show that the expected resilience index of the case study bridge for the considered scenario of two consecutive earthquakes is computed as 53.45%. However, neglecting dependencies among damages from consecutive hazards results in 41% overestimation of the resilience index for the system. This significant error

could lead to misleading post-hazard management plans for the recovery of the system, which can drastically impact the community.

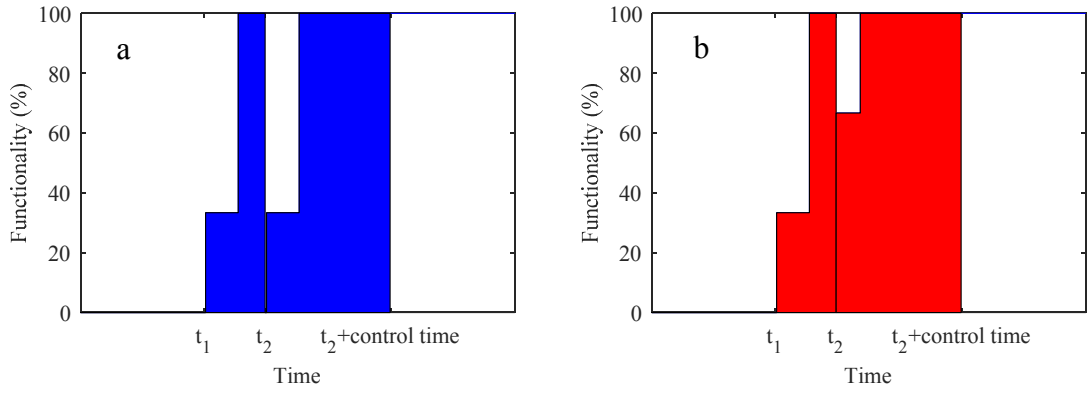

Figure 2-20 Functionality area for the expected damage-state at the time of the second earthquake a) considering, b) neglecting the dependency between the damage incurred by the first earthquake on the damage as a result of the second earthquake

Table 2-14 Risk-based resilience index and probability distributions of damage-states for a scenario of two consecutive earthquakes, a) considering, b) neglecting the dependency between damages incurred by the first earthquake on the damage as a result of the second earthquake

	First Hazard: PGA=1.2g					Expected DS After First Hazard	Second Hazard: PGA=0.6g					Expected DS After Second Hazard	Expected Resilience Index (%)
	DS1	DS2	DS3	DS4	DS5		DS1	DS2	DS3	DS4	DS5		
Considering Dependency	0.16	0.12	0.26	0.10	0.36	moderate	0.42	0.09	0.09	0.02	0.38	moderate	53.45
Neglecting Dependency	0.16	0.12	0.26	0.10	0.36	moderate	0.65	0.14	0.14	0.03	0.04	slight	75.44

Note: DS=Damage-State, DS1=Intact, DS2=Slight, DS3=Moderate, DS4=Extensive, DS5=Complete

2.7.3.2. Lifecycle Resilience Index and Optimal Decision-Making across Predetermined Alternatives

Figure 2-21 presents $\overline{RLRI}$ values for the case study bridge in Sacramento and Sierra Madre for the six considered repair alternatives. It is observed that $\overline{RLRI}$ values are above 98.8%. The reason for such high values can be attributed to the fact that the bridge is seismically designed and therefore can perform well against potential earthquakes. Similar high values are also reported in other studies such as (35,36) for the resilience index of other systems. Yet, it is important to further enhance the lifetime resilience of infrastructure systems, since small disruptions in the serviceability of these systems may incur considerable adverse consequences to communities. As can be seen in Figure 2-21, $\overline{RLRI}$s increase first and then decrease or remain relatively constant. One reason for lower $\overline{RLRI}$s for very short lifetimes is that there is a higher chance that the system will not be recovered by the end of its lifetime. Moreover, damage-state dependencies, which make the system more vulnerable to future earthquakes, cause the system resilience to reduce gradually as the expected service lifetime of the system increases. The extent of reduction in resilience converges to negligible values when repairs are performed on all extents of hazard-induced damages, whereas it remains significant for the case where repairs are not conducted for slight damages.

As seen in Figure 2-21-a, since the bridge is seismically designed, under a moderate risk of high-intensity earthquakes, the lifetime expected serviceability interruptions when all damage-states are repaired is higher than that for the case where slight damages are not repaired. That is why repair plan 2 leads to higher $\overline{RLRI}$ values

than repair plan 1 for all lifetimes. Thus, from a serviceability viewpoint, agencies may decide to leave slight seismic-induced damages untreated. However, when this bridge is located in a region with high risk of high-intensity earthquakes, the potential of moderate and severe damages increases (see Figure 2-21-b). Consequently, for service lifetimes above 35 years, conducting repair plan 1 for seismic-induced damages results in higher $\overline{RLRI}$ values compared to repair plan 2. On this basis, the agency is recommended to conduct repair on all seismic-induced damage-states to attain the maximum expected resiliency of the system when a lifetime more than 35 years is considered for the bridge.

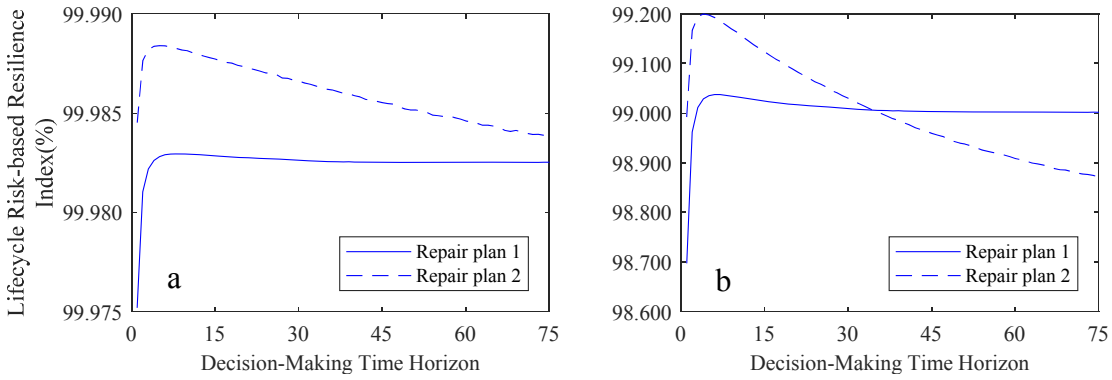

Figure 2-21 Expected lifecycle risk-based resilience index for two repair plans, when the case study bridge is located in a) Sacramento b) Sierra Madre

2.7.3.3. Significance of Incorporating Damage-Dependencies in Lifecycle Resilience Index Assessment

Figure 2-22 demonstrates the significance of considering damage-state dependencies between consecutive hazards for the estimation of the lifecycle resilience index. As shown

in Figure 2-22-a and Figure 2-22-b, ignoring the couplings between damages from consecutive hazards results in an overestimation of $\overline{RLRI}$ values. This error increases as the considered structural lifetime increases with larger errors for repair plan 2. This can be attributed to the fact that the likelihood of incomplete repairs and/or untreated seismic damages lead to the potential of damage accumulations, which reduce the functionality and thus the resilience of the bridge against future hazards. This reduction, which is more significant for repair plan 2 where repairs are not conducted for slight damages, is not captured if damage-dependencies are disregarded.

In addition, for the city of Sierra Madre with a higher chance of high-intensity earthquakes, these effects are more significant. As the results show, ignoring dependencies among damages from subsequent earthquakes falsely identifies the strategy where slight damages are not repaired as the optimal option for any service lifetime. As a result of this decision, the $\overline{RLRI}$ of the bridge reduces from 99.0018 to 98.8712. This reduction in the resilience index of the bridge may have large adverse consequences on the community.

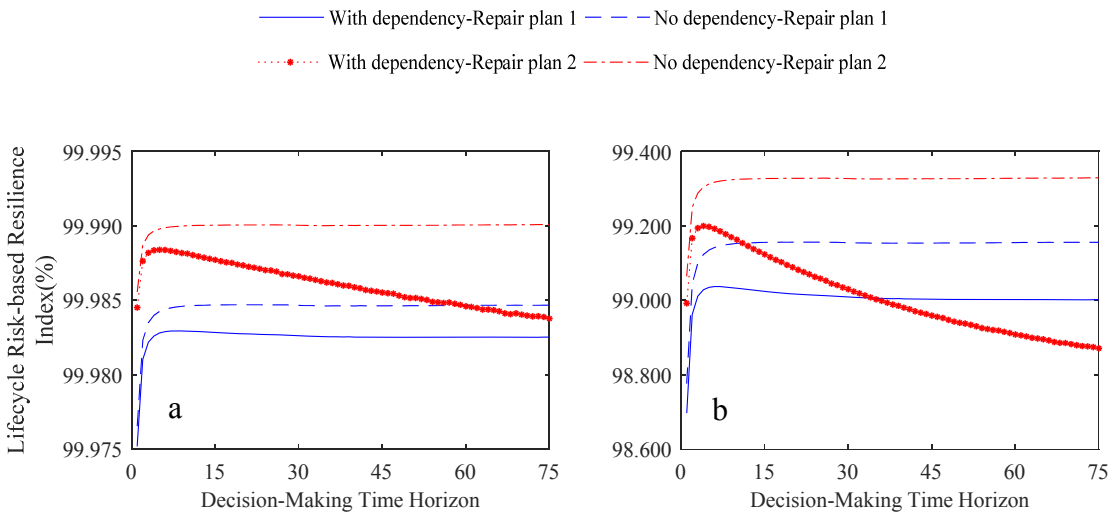

Note: Repair plan 1: Performing repairs for all extents of damages. Repair plan 2: Performing repair actions for all extents of damages, except for the slight damage-state.

Figure 2-22 Lifecycle risk-based resilience index for two repair plans considering and ignoring dependencies between damages from subsequent earthquakes, when the case study bridge is located in a) Sacramento b) Sierra Madre

2.7.3.4. Optimal Decision-Making across Predetermined Alternatives using the Proposed Resilience Index and Lifecycle Cost of Alternatives

The combined measurements of the proposed $\overline{RLRI}$ and the expected LCC of various repair alternatives on the agency can assist in selecting the best repair decision among predetermined alternatives for structures and infrastructure systems. This feature is demonstrated in Figure 2-23 and Figure 2-24. The expected total LCC of repair for the case study bridge is calculated according to the method proposed in Section 2.3.2, considering only the agency cost of repairs. As explained in Section 2.5.1.1, according to (43), the duration of repairs increases or decreases by 20% if the agency spends 15% less

or more for repair activities, respectively. On this basis, for each repair plan, three levels of working speed is considered for repair activities: slow, average and fast repairs. The costs and durations of these alternatives are 85% and 120%, 100% and 100%, and 115% and 80% of the mean cost and duration of repair actions, respectively.

The $\overline{RLRI}$ and the expected LCC of these alternatives are computed for a wide range of structural lifetime horizons and shown in Figure 2-23-a and Figure 2-23-b, respectively. Looking at the considered repair plans, the resilience index increases as repairs are conducted faster. This is expected, since the recovery process becomes less time-consuming and the full functionality of the bridge is attained more quickly. Just considering resilience index for decision-making across predetermined alternatives, i.e. assuming that the agency has no budget limitations, if the case study bridge is located in Sacramento, performing repair work plan 2 with fast repairs results in the highest expected lifetime functionality among all alternatives. When the bridge is in Sierra Madre that has a higher seismicity, repair work plan 2 with fast repairs and repair work plan 1 with fast repairs are the optimal alternatives for lifetimes less than or equal to 35 years and more than 35 years, respectively.

Figure 2-23 shows when repairs are performed for all damage-states, i.e. repair plan 1, the expected LCCs increase as the repair actions become more costly. For repair plan 1, this finding indicates that conducting fast repairs may not significantly reduce the likelihood of sustaining severe damage-states, which are costly to repair. When slight damage-states are not repaired, i.e. repair plan 2, LCCs become significantly less compared to those calculated for repair plan 1. This may indicate that the repair cost of

slight damage-state contributes significantly to the lifecycle repair costs of the bridge. This is expected since the bridge is designed according to seismic guidelines, which limits the vulnerability of the bridge in experiencing severe seismic-induced damages.

Additionally, repair plan 2 incurs the least expected LCCs on the agency. This is favorable for the agency, however, this work plan leads to the least $\overline{RLRI}$s for many service lifetimes, which makes this work plan unfavorable for users. Therefore, the agency is recommended to consider both the LCC and the resilience of the system for optimal decision-making among predetermined repair alternatives.

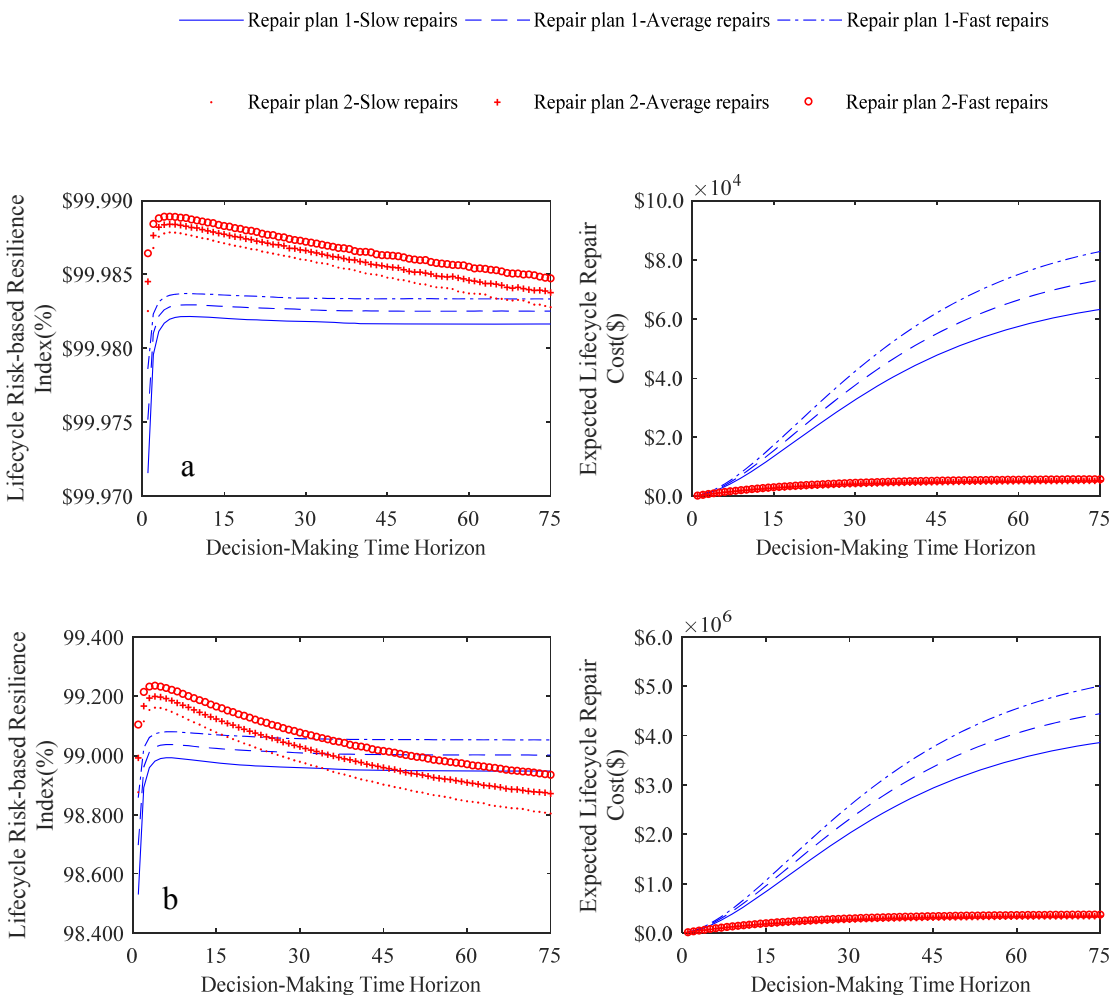

Note: Repair plan 1: Performing repairs for all extents of damages. Repair plan 2: Performing repair actions for all extents of damages, except for the slight damage-state.

Figure 2-23 Lifecycle risk-based resilience index and expected LCC of repair for six repair alternatives, for the case study bridge located in a) Sacramento b) Sierra Madre

Next, an example is provided for an optimal decision-making across predetermined repair alternatives considering both $\overline{RLRI}$ and LCCs of repairs on the agency. Figure 2-24-a and Figure 2-24-b illustrate two scenarios of decision-making across predetermined repair alternatives corresponding to 20 and 75 years of expected

lifetimes, when the bridge is located in the city of Sierra Madre. These results are extracted from Figure 2-23-b. For 20 years of lifetime, all alternatives of repair plan 1, together with repair plan 2 with slow repairs can be removed from the list of optimal repair policies, since repair plan 2 with average repairs not only is less costly for the agency, but also results in higher resilience for the system. Considering the two remaining strategies, i.e. repair plan 2 with average and fast repairs, the agency may decide to consider a slightly higher value for its repair budget and implement fast repairs for potential seismic-induced damages to achieve higher resilience for the bridge system.

For 75 years of service lifetime, only repair plan 2 with slow repairs can be removed from the list of optimal strategies. Then, the agency can make the final decision based on its budget limitation. For instance, for $1 million of expected LCC of repairs for 75 years lifetime, the agency may decide to implement repair plan 2 with fast repairs for seismic-induced damages. This repair policy results in $\overline{RLRI}$ of 98.95%. The decision could be changed to repair plan 1 with fast repairs, if the available budget increases to $5 million. In this case, a higher $\overline{RLRI}$ of 99.05% is attained.

Finally, it is worth noting that a comparison between the optimal alternatives that are recognized following the lifecycle resilience index framework with those determined according to the proposed total LCC framework, presented in Section 2.6, shows that the same repair plan is optimal in both frameworks, when the bridge is located in the region with a moderate chance of high-intensity earthquakes. That is both frameworks recommend avoiding repairs for slight damages. However, when the bridge is in the region with more likelihood for high intensity earthquakes and the expected lifetime of the bridge

is more than 35 years, the two frameworks identify different extents of repair as the optimal alternative; i.e. the LCC framework still suggests to avoid repairs on slight damages, while the resilience index framework recommends to conduct repairs on all extents of damages. This indicates that repair plans inducing maximum functionality do not necessarily lead to minimum expected lifecycle hazard-induced costs. The latter focuses only on the serviceability performance of the system, while the former incorporates a comprehensive list of consequences objectively through the unified metric of cost.

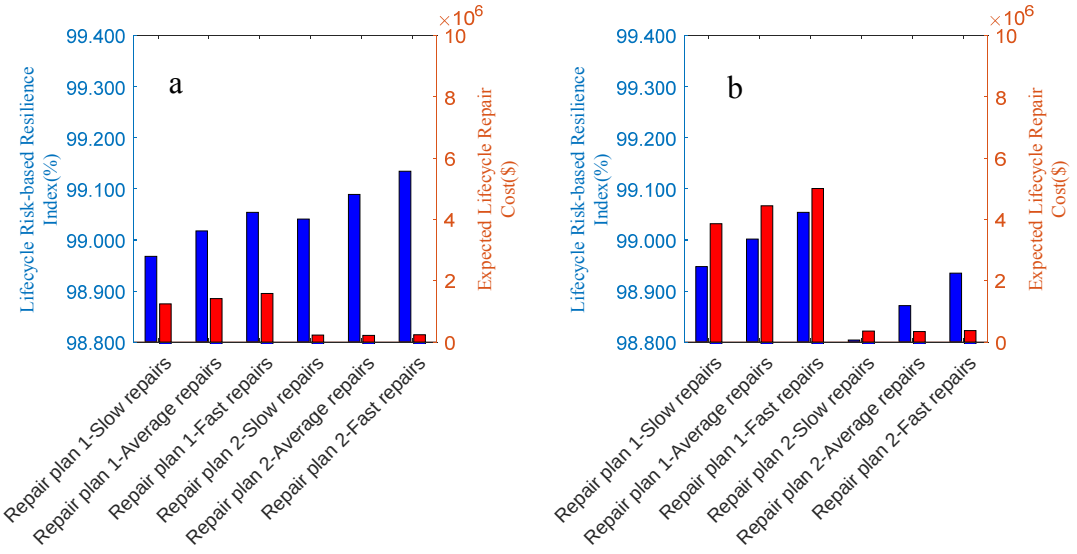

Note: Repair plan 1: Performing repairs for all extents of damages. Repair plan 2: Performing repair actions for all extents of damages, except for the slight damage-state.

Figure 2-24 Two scenarios of decision-making across predetermined repair plans corresponding to a) 20, and b) 75 years of expected lifetimes, when the bridge is located in the city of Sierra Madre

2.8. Concluding Remarks

This chapter first proposed a framework for LCC assessment of individual structures and infrastructure systems exposed to multiple occurrences of a hazard type in their lifetime. The cost elements include the initial construction cost, annual maintenance cost, the hazard-induced costs considering the potential for the occurrence of multiple hazard incidents, and the salvage value of the system. The proposed framework requires as input hazard curve, state-dependent fragility curves, maintenance, hazard-induced and retrofit implementation costs, and expected repair times. The framework uses the total probability theorem to compute the risk cost associated with each of the system damage-states considering a wide range of possibilities for the number of hazard events that the structure may experience during a given lifetime. The system damage-state following the occurrence of hazard incidents is derived as a function of the intensity of the event and the existing condition of the structure at the time of the incident. This was achieved by expressing the existing condition of the structure or infrastructure based on the damage-state of the system induced by the previous event and whether the required repair is finished by the time of the next event. The probability of each structural damage-state was found for each number of hazard incident occurrences, starting from zero occurrence to infinity (i.e. a very large number). The recursive function developed in Section 2.3 was utilized to derive probabilities for the damage-states at jth hazard occurrence based on probabilities for the damage-states at j-1th hazard occurrence. This approach provides a comprehensive and accurate yet computationally efficient method for LCC analysis of

systems considering the impact of repair time and multiple occurrences of a hazard type during lifetimes.

The proposed framework was first demonstrated for seismic retrofit decision-making of a moment-frame building among predetermined alternatives. Using the proposed method, LCCs were evaluated for six retrofit strategies considering the possibility of multiple earthquake occurrences throughout the lifetime of the structure. Analysis results indicated that the repair time has a considerable impact on the total LCC of the structure; however, these effects are not the same for all retrofit plans. In fact, the ranking of retrofit plans in terms of their cost-effectiveness changed for different percentiles of the total repair time of involved damage-states. In addition, the rankings were also affected by the lifetime. With respect to the safety evaluation of retrofit plans when injury and death costs are preferred to be disregarded form LCC analysis, results showed that neglecting repair time may lead to identification of status quo strategy as safe, while with a large probability of about 50%, this hypothesis was found to be incorrect when repair times were considered. This is due to neglecting plausible accumulated damage from incomplete repairs of damage from prior hazard incidents. Furthermore, the convergence analysis of the framework showed that the computational cost of the lifecycle analysis of the system is limited even for a small error tolerance. In general, the proposed framework provides a practical tool for optimal retrofit decision-making across predetermined alternatives for structural systems when multiple incidents of a hazard type may expose the system to various levels of damage.

In a second case study, the proposed LCC framework was applied to a realistic bridge system to identify the optimal speed and extent of repairs following earthquake-induced damages. Results showed that not performing repairs for slight damages result in less incurred expected earthquake-induced LCCs compared to the case where all extents of earthquake-induced damages are repaired. Furthermore, investing on fast repair technologies was found to decrease the expected lifecycle earthquake costs despite the higher costs of implementing these methods. Finally, results demonstrated that the agency may end up mismanaging its budget due to the underestimation of the expected lifecycle repair costs when the impact of dependencies between damages from subsequent earthquakes are overlooked. These findings show the ability of the proposed framework in assisting agencies to arrive at optimal risk-informed decisions for management of their systems.

In addition, in this chapter, the formulation of the resilience index, which is a common performance measure for disaster recovery assessment, is enhanced probabilistically to accurately account for the possibility of multiple hazard occurrences and the potential for damage-accumulation in the lifetime of individual structures or infrastructure systems. Unlike existing resilience indexes, the developed index, called Risk-based Lifecycle Resilience Index (RLRI), stochastically incorporates the following factors in the resilience index formulation:

- The inter-arrival time between hazard occurrences, which can be less than the considered control time in the resilience index formulation.

- The possibility of the accumulation of damage at the time of hazard occurrences due to incomplete repairs or untreated damages from previous hazards.

These factors are incorporated using the theorem of total probability, conditional probability chain rule at multiple levels, Bayes rule, and the foregoing recursive function for damage-state transition probabilities, and time-variant reward functions for system recovery at different damage-states.

The realistic multi-span RC bridge is selected for the implementation of the proposed framework. The significance of incorporating couplings between damages from consecutive hazards in resilience assessment is demonstrated through a hypothetical scenario of two consecutive earthquakes for the case study bridge. It is shown that neglecting such dependencies overlooks damage propagation and results in 40% overestimation of the resilience index, which can be misleading for in-advance management of post hazard recovery of infrastructure systems.

The developed RLRI is then evaluated for two repair plans concerning the extent of repairs for earthquake-induced damages. Results show that for a region with a moderate chance of high-intensity earthquakes, avoiding repairs for slight damages and subsequent reduced traffic disruptions result in higher lifecycle functionality for the bridge. However, when the bridge is located in a region with a more chance of high-intensity earthquakes, for service lifetimes more than 35 years, the agency is recommended to conduct repairs for all extents of damages.

If dependencies between damages from subsequent hazards are ignored, not only the lifecycle resilience of the bridge is overestimated, but also an improper repair plan is

indicated as the optimal policy for all considered service lifetimes of the bridge. This false identification of the optimal action reduces the resilience of the bridge, which may impose adverse consequences on the community.

Finally, considering a wide range of service lifetimes for the case study bridge, expected RLRIs and LCCs are calculated for multiple repair alternatives with various extents and working speeds of repair actions. As a result, considering limitation on agency's budget and a designated lifetime for the case study bridge, optimal repair plans that lead to the highest expected RLRI values are identified.

The proposed resilience index in this chapter accurately captures the serviceability vulnerability of individual structures or infrastructure systems exposed to multiple occurrences of a hazard type. As shown in this chapter, the developed index can be particularly useful for risk-informed decision-making across predetermined alternatives when the functionality performance of systems is the priority.

Chapter 3: Risk-Based Lifecycle Cost Analysis Considering Multiple Types of Hazards

3.1. Summary

Structures and Infrastructure systems, especially those in hazard-prone regions, may face multiple occurrences of multiple types of hazards during their lifetime. The type and intensity of the hazards and the impacts on systems can vary from one event to another. In the presence of the potential for multiple types of damages induced by diverse hazard types, an important factor that has yet to be properly addressed in natural hazard loss estimation frameworks is that a damage induced by a prior event, if not repaired by the time of the next event, may aggravate the extent of the same or other types of damage that the system experiences during future potential hazards.

This chapter extends the LCC framework presented for multiple occurrences of one hazard type in Chapter 2 to multiple occurrences of multiple types of hazards that may occur at any time and order during the lifetime of a structure or an infrastructure system. In this approach, the damage-state space is extended to a multi-dimensional space of mutually exclusive and collectively exhaustive damage-states. Based on the proposed LCC analysis method in this chapter, optimal decision-making can be made across predetermined design or retrofit alternatives.

This framework is demonstrated for the realistic case study bridge used in previous chapters. This time the bridge, which is assumed to cross over a river, is exposed to not only earthquake hazards, but also to flood incidents. Four retrofit alternatives are considered for the bridge. According to the proposed LCC framework, ranking of these retrofit plans are identified for various service lifetimes. In addition, results show the significance of considering different damage types induced by multiple types of hazards, and repair time variations for LCC analysis of structures and infrastructure systems.

3.2. Introduction

In some regions, structures and infrastructure systems are exposed to multiple types of hazards with the potential of each hazard type occurring multiple times during the service lifetime of the system. For example, in a seismic region, an arterial highway bridge built on a river with high water discharge is prone to experience multiple occurrences of earthquakes and floods. These hazards may induce different types of damage once they occur.

As noted in previous chapters, an incurred damage, if not fully repaired before the next hazard event occurs, may aggravate the extent of induced damage during future potential hazards. Thus, damage could accumulate and degrade the condition of a structure or an infrastructure at a faster rate, if repair actions are incomplete by the time of next hazard incidents. Moreover, as demonstrated through results in preceding chapters, repair time may vary from a short period to a long time depending on many factors including the extent of damage, type of repair or retrofit strategy, the agency's response time to plan for

post-hazard inspections and repairs, and socio-economic factors. In the presence of multiple types and occurrences of hazards, this highlights the need to consider variations in repair times and account for effects of residual damage of different types from prior events in the hazard performance assessment of structures and infrastructure systems.

Looking at the LCC performance assessment of infrastructure systems subjected to multiple types of hazards, many studies disregarded potential dependencies among damage conditions induced by various hazard types. For instance, in the frameworks proposed by (27,28), total LCC of an infrastructure exposed to multiple types of hazards was derived as the sum of independently-computed LCC of individual hazard events. As discussed in Chapter 2, Jalayer et al. (29) attempted to address such dependencies for multiple hazard types in a framework that requires simulating all possible scenarios for the order of hazard events of various types and intensities. According to the theorem of total probability, in order for the risk evaluation to be complete, all possible combinations of these ordered-event scenarios must be evaluated for the LCC analysis; this requirement makes the strategy significantly time-consuming considering that the required number of combinations of hazard order and intensities can be extremely large. In addition, in that framework, modeling each hazard scenario requires extensive static pushover and nonlinear dynamic analyses, thus further increasing the computational demand of the framework. There are also a number of assumptions in the framework that may not accurately represent the performance of actual systems (30). These assumptions are elaborated in Chapter 2.

In Chapter 2, a probabilistic framework is developed for the calculation of the expected lifecycle hazard risk costs; the framework addresses some of the above issues by incorporating dependencies of the hazard performance of a structure or an infrastructure during the next extreme event to existing conditions arrived at as a result of untreated or incomplete repair of damage from prior events. However, the framework could handle only one type of hazard e.g. only earthquakes. This chapter extends the framework by addressing the remaining issues and releasing the assumption of one hazard type throughout the service life of the system. The proposed framework computes the expected lifecycle risk costs that are caused by multiple types and occurrences of hazards, with the following new contributions:

- Probabilistically taking into consideration the impact of damages of different types induced by various types of prior hazards on the increased vulnerability of systems against future potential hazards for lifecycle cost assessments.
- Developing a time-efficient risk analysis procedure for the computation of the lifecycle risk costs for systems exposed to multiple types of hazards. This feature is achieved by developing a dynamic programming procedure, similar to the one developed in Chapter 2, for calculating the expected damage-state probabilities at each hazard occurrence. In this approach, the damage-state space is extended to a multi-dimensional space of mutually exclusive and collectively exhaustive damage-states to facilitate the calculation of joint probabilities containing damage-states of different types.

The proposed method is demonstrated for the calculation of the expected LCC of the realistic case study bridge in the previous chapter. The expected total LCC is used for the identification of optimal retrofit plans for the bridge for a wide range of lifetimes. While this study focuses on LCC assessment of single structures and infrastructure systems, the proposed framework can be extended in future to estimate the LCC of network systems, considering correlations between individual systems. Such correlations could be significant in the performance of infrastructure networks (87).

In the rest of this chapter, in Section 3.3 the proposed framework is presented in detail. Section 3.4 provides the required data for the application of the proposed LCC analysis framework for the case study bridge, in addition to those presented in previous chapters. In Section 3.5, a numerical analysis is performed to investigate the convergence of the framework, and LCC analysis results are provided for a set of retrofit options for various lifetimes. Moreover, the various advantages offered by the proposed framework are explained in this section. Finally, in Section 3.6, concluding remarks are presented.

3.3. Lifecycle Cost Analysis Framework

As explained and demonstrated in the previous chapter, salvage value is an uncertain term and is not usually a significant contributor to the total LCCs in the context of optimal decision-making among predetermined hazard-mitigation strategies. Therefore, the expected total LCC, $\bar{C}_T$, in the service lifetime of a structure or an infrastructure system typically includes the expected initial construction or retrofit cost, $\bar{C}_0$, expected lifecycle maintenance cost, $\bar{C}_M$, and the expected cost incurred on users, agencies, the economy,

and environment as a result of damages induced by extreme hazards that occur in the lifetime of these systems, $\bar{C}_R$. As explained in Chapter 2, for the purpose of comparison and to account for the discounted values of these costs incurred in different years, Net Present Value (NPV) of the costs are considered in the LCC formulation presented as follows:

$$\bar{C}_{T,NPV} = \bar{C}_0 + \bar{C}_{M,NPV} + \bar{C}_{R,NPV} \tag{3-1}$$

where $\bar{C}_{T,NPV}$, $\bar{C}_{M,NPV}$, and $\bar{C}_{M,NPV}$ are the discounted NPV of the $\bar{C}_T$, $\bar{C}_M$, and $\bar{C}_R$ cost terms, respectively. It is often practical to perform periodical maintenance actions on structures and infrastructure systems to keep them functioning in a healthy condition. On annual basis, $\bar{C}_{M,NPV}$ can be represented as follows:

$$\bar{C}_{M,NPV} = \sum_{t=1}^{T_{LC}} \gamma^t \times \bar{C}_{m,t} \tag{3-2}$$

where $\bar{C}_{m,t}$ is the expected maintenance cost at year *t*, T_{LC} is the expected service lifetime of the system, and γ is the annual discount factor equal to $\frac{1}{1+\delta}$, with δ as the discount rate.

In the lifetime of a structure or an infrastructure, the system may experience multiple types of hazards. In addition, each of these hazard types may occur several times within the service life of the system. After each such incidents, the system may experience damage or stay intact. Different types of damage may be incurred by diverse hazard types. The space of damage possibilities for each damage type can be broken into a set of discrete mutually exclusive and collectively exhaustive damage-states. Each damage-state is followed by consequences that are typically expressed in cost terms. These costs comprise agency cost of repairing the system, user costs such as the delay cost associated with the

reduced serviceability of the system during the repair process, impacts on the economy and related environmental costs. In addition, injuries and casualties are potential consequences of damage to structures or infrastructure systems that can be directly included in the cost associated with each damage-state. In this chapter, sum of the foregoing costs is referred to as the hazard-induced cost.

Similar to $\bar{C}_{M,NPV}$, in order to account for the discounted hazard-induced costs that are likely to incur at different times in future, NPV of the expected lifecycle hazard-induced cost can also be split into yearly expected hazard-induced costs as follows:

$$\bar{C}_{R,NPV} = \sum_{t=1}^{T_{LC}} \gamma^t \times \bar{C}_{R,t} \tag{3-3}$$

where $\bar{C}_{R,t}$ is the expected hazard-induced cost incurred at year *t*, which are considered as the expected lump sum of hazard-induced costs incurred during $[t, t+1]$. $\bar{C}_{R,t}$ can be further expanded and expressed as a function of the damage-states that the system may experience after hazards taking place at year *t*, i.e. during $[t, t+1]$. Applying the total probability theorem, $\bar{C}_{R,t}$ is given by:

$$\bar{C}_{R,t} = \sum_{n=1}^{N_{DS}} \bar{C}_r(DS_n) \times P(DS_n, [t, t+1]) \tag{3-4}$$

where N_{DS} is the total number of damage-states, $\bar{C}_r(DS_n)$ is the expected hazard-induced cost when the system experiences damage-state *n,* DS_n, and $P(DS_n, [t, t+1])$ is the probability of the structure sustaining damage-state *n* between time *t* and *t*+1. The term $\bar{C}_r(DS_n) \times P(DS_n, [t, t+1])$ in Equation (3-4) is also called the risk cost of being at damage-state *n*. The right hand side of Equation (3-4) can be articulated as the difference

between the accumulated risk cost of experiencing damage-state *n* from time 0 to *t*+1 and the accumulated risk cost of experiencing the same damage-state from time 0 to *t*. Thus, Equation (3-4) is modified as:

$$\bar{C}_{R,t} = \sum_{n=1}^{N_{DS}} \{\bar{C}_r(DS_n) \times P(DS_n, [0, t+1]) - \bar{C}_r(DS_n) \times P(DS_n, [0, t]\} \quad (3\text{-}5)$$

Theoretically, any number of hazard events of different types may occur within a period of time. If *i* hazard incidents occur in that period, at each occurrence, the system may experience a damage-state with a particular hazard-induced cost. Therefore, if *i* incidents occur, the accumulated hazard-induced costs as a result of sustaining damage-state *n* is the sum of the expected hazard-induced costs of damage-state *n* times the probability of sustaining that damage-state after each of such *i* hazard events. Consequently, for each damage-state *n*, by applying the theorem of total probability over the total number of hazard incidents *i*, the accumulated risk cost within period [0 *t*] can be calculated according to Equation (3-6).

$$\bar{C}_r(DS_n) \times P(DS_n, [0, t]) = \sum_{i=0}^{\infty} P(i, t) \times \sum_{j=0}^{i} \bar{C}_r(DS_n) \times P\left(DS_n^j | i, t\right) \quad (3\text{-}6)$$

where $P(i, t)$ is the probability that *i* hazards occur during [0 *t*], and $P\left(DS_n^j | i, t\right)$ is the probability that damage-state *n* is experienced by the system at *j*th hazard incident if *i* hazards take place during [0 *t*]. Noticeably, it is through this term, $P\left(DS_n^j | i, t\right)$, that the likelihood of incomplete repairs and consequently accumulation of damage are accounted for. This term is elaborated in the rest of this section. In theory, infinite number of hazard events should be incorporated in Equation (3-6). However, the stopping criterion for this

analysis can be considered as the condition where the relative difference in the total hazard risk costs during [0 t], i.e. $\bar{C}_r(DS_n) \times P(DS_n, [0,t])$, between two consecutive steps of the number of hazards becomes less than a tolerance value. As demonstrated in Section 3.5.1, higher number of events should be considered for convergence as the considered duration and the rate of hazards' occurrences increase. As explained before, the system may be exposed to multiple occurrences of multiple types of hazards. Assuming that these events occur independently, $P(i,t)$ can be calculated following a Poisson distribution function given by:

$$P(i,t) = \frac{(\sum_{h=1}^{N_H} \upsilon_h \times \mathrm{t})^i e^{-(\sum_{h=1}^{N_H} \upsilon_h \times \mathrm{t})}}{i!} \tag{3-7}$$

where υ_h stands for the occurrence rate of hazard type h, and N_H represents the total number of hazard types that may hit the system throughout its lifetime.

As noted in Chapter 2, as a common practice in structural reliability, fragility curves are provided to express the probability of exceeding critical structural limits as a function of the intensity of a hazard (30,88,89). These limit-states are used to quantify structural damage-states (90). Limit-states vary depending on the damage type that a system may experience. For instance for the case study bridge system that is exposed to both earthquakes and floods, limit-states for earthquake hazard are usually available in terms of displacement ductility of piers, while the limit-states for flooding hazard are often available in terms of scour depth (i.e. the height of eroded soil on foundations and piles). Given that these two types of hazards cause different types of damage, the limit-state of the bridge system under study is defined as a 1×2 vector where the first and second

elements of the vector represent the seismic and flooding related limit-states respectively. In general when N_H hazard events can potentially cause *M* damage types in a system, the dimension of the vector of limit-state is $1\times M$. It should be noted that associated with each limit-state, a damage-state is considered in this research. Thus, the vector of damage-state has identical dimensions as the vector of limit-state. On this basis, when the structure is exposed to more than one type of damage, the term DS_n presented in Equations (3-4) to (3-6) represents the vector of the system's damage-states. Additionally, the number of damage types is not necessarily equal to the total number of hazard types.

In order to calculate the risk cost from Equation (3-6), $P\left(DS_n^j|i,t\right)$ that indicates the probability of experiencing the damage-state vector *n* should be derived as a function of the probability of exceeding limit-states defined for the structure. Let's consider the case study bridge under two hazard types of earthquakes and floods. As elaborated later in Section 3.4, displacement ductility thresholds for columns are considered to define intact, minor, moderate, major, and collapse damage as 1 to 5 seismic damage-states, respectively. In addition, scour depths of 0, 0.6 m, 1.5 m, and 3.0 m are used to define damage-states 1 to 4 for the flooding hazard. The probability that any limit-state *k* is exceeded involves the probability of events where any other less severe limit-state is exceeded, as well. On the other hand, the probability that those less severe limit-states are exceeded entails probability of events that may or may not exceed limit-state *k*. Therefore for one type of damage and two consecutive limit-states, $P(LS_k \cap LS_{k+1}) = P(LS_{k+1})$, where $P(LS_k)$ is the probability of limit-state *k* being exceeded. The probability of being

at damage-state k, $P(DS_k)$, is defined as the probability of being only at a state between limit-states k and $k+1$ as follows:

$$P(DS_k) = P(LS_k) - P(LS_{k+1}) \tag{3-8}$$

Next, the probability of the joint damage-state of the two damage types for displacement ductility (n_1) and scour depth (n_2), $P\left(DS_{[n_1,n_2]}\right)$, can be expressed as the probability of being only at a state between limit-states $[n_1, n_2]$ and the neighbor limit-states of $[n_1+1, n_2]$, $[n_1, n_2+1]$ and $[n_1+1, n_2+1]$. Since $P\left(LS_{[n_1,n_2]}\right) \cap P\left(LS_{[n_1+i_1,n_2+i_2]}\right) = P\left(LS_{[n_1+i_1,n_2+i_2]}\right)\ \forall\, i_1, i_2 \in \{0,1\}$, $P\left(DS_{[n_1,n_2]}\right)$ can be determined as:

$$P\left(DS_{[n_1,n_2]}\right) = P(LS_{[n_1,n_2]}) - \bigcup_{\substack{i_1,i_2\in\{0,1\} \\ (i_1,i_2)\neq(0,0)}} P(LS_{[n_1+i_1,n_2+i_2]}) \tag{3-9}$$

where $\bigcup_{\substack{i_1,i_2\in\{0,1\} \\ (i_1,i_2)\neq(0,0)}} P(LS_{[n_1+i_1,n_2+i_2]})$ is the union of the probability of the events of $P\left(LS_{[n_1,n_2+1]}\right)$, $P\left(LS_{[n_1+1,n_2]}\right)$, and $P\left(LS_{[n_1+1,n_2+1]}\right)$. It is clear that the intersection of any combination of these probability terms is $P\left(LS_{[n_1+1,n_2+1]}\right)$, since this probability indicates the exceedance probability of limit-states for both damage types with indexes equal to or one larger than all other events. In other words, this event corresponds to limit-states that are equal to or one level worse than all other limit-states in the union term. Thus, Equation (3-9) can be expanded as follows:

$$P\left(DS_{[n_1,n_2]}\right) = P\left(LS_{[n_1,n_2]}\right) - P\left(LS_{[n_1,n_2+1]} \cup LS_{[n_1+1,n_2]} \cup LS_{[n_1+1,n_2+1]}\right)$$
$$= P\left(LS_{[n_1,n_2]}\right) - P\left(LS_{[n_1,n_2+1]}\right) - P\left(LS_{[n_1+1,n_2]}\right) \quad (3\text{-}10)$$
$$+ P\left(LS_{[n_1+1,n_2+1]}\right)$$

Generalizing Equation (3-9) to *M* different damage types, the probability of being at damage-state $[n_1, \dots, n_M]$, becomes:

$$P\left(DS_{[n_1,\dots,n_M]}\right) = P(LS_{[n_1,\dots,n_M]}) - \bigcup_{\substack{i_1,\dots,i_M \in \{0,1\} \\ (i_1,\dots,i_M) \neq (0,\dots,0)}} P(LS_{[n_1+i_1,\dots,n_M+i_M]}) \quad (3\text{-}11)$$

The union terms can be expanded based on the principle of inclusion and exclusion (91), where based on the foregoing explanations, the intersection of any events can be calculated as follows:

$$P\left(LS_{[n_1+i_1,\dots,n_M+i_M]} \cap \dots \cap LS_{[n_1+z_1,\dots,n_M+z_M]}\right)$$
$$= P\left(LS_{[n_1+\max(i_1,\dots,z_1),\dots,n_M+\max(i_M,\dots,z_M)]}\right) \quad (3\text{-}12)$$

Based on Equation (3-11), $P\left(DS_n^j | i,t\right)$ in Equation (3-6) can be determined in terms of probabilities of exceeding limit-states as follows:

$$P\left(DS^j_{[n_1,\dots,n_M]} | i,t\right)$$
$$= P(LS^j_{[n_1,\dots,n_M]} | i,t) - \bigcup_{\substack{i_1,\dots,i_M \in \{0,1\} \\ (i_1,\dots,i_M) \neq (0,\dots,0)}} P(LS^j_{[n_1+i_1,\dots,n_M+i_M]} | i,t) \quad (3\text{-}13)$$

In general, the state of a structure or an infrastructure after the occurrence of a hazard incident depends on several factors including the type and intensity of the hazard as well as the response of the system to the hazard; the latter depends on the damage-state of the system right before the occurrence of the hazard. As a common practice, if a hazard

induces damage in the system, repair is performed to bring the system back to the original state. The duration of the repair process vary with the level of damage in the system. If another hazard event occurs before the repair is complete, the overall extent of damage is expected to be higher compared to the case where the structure is in its original intact state. Therefore, in addition to the previously mentioned factors, the state of the system after each hazard depends on the repair status of the system following previous hazards. If the repair process of a damage type is incomplete at the time of a hazard incident, it is assumed that the damage-state of the system remains the same as its condition just before the start of the repair action. Applying the rules of conditional probabilities, $P\left(LS^{j}_{[n_1,\dots,n_M]}|i,t\right)$ in Equation (3-14) can be derived as:

$$\begin{aligned} P\left(LS^{j}_{[n_1,\dots,n_M]}|i,t\right) &= P(LS^{j}_{[n_1,\dots,n_M]}|[RP, DS^{j-1}], HT, IM, i, t) \\ &\times P([RP|DS^{j-1}, HT, IM, i, t]) \times P(DS^{j-1}|HT, IM, i, t) \\ &\times P(HT|IM, i, t) \times P(IM|i, t) \end{aligned} \tag{3-14}$$

where RP is the repair status, DS^{j-1} is the damage-state of the system just after the previous hazard, HT is the hazard type, and IM is the intensity measure of hazard type HT. It is obvious that repair status just before the time of *j*th hazard occurrence is independent of the intensity of this hazard. In addition, the sustained damage-state just after *j*-1th hazard is independent of the hazard type and intensity at *j*th incident. Finally, no dependencies are considered among hazard types, and the type and intensity of each

hazard with respect to time and order of occurrence. On this basis, according to the theorem of total probability, Equation (3-14) can be written as:

$$P\left(LS^{j}_{[n_1,\dots,n_M]}|i,t\right)$$

$$= \sum_{n'_1=1}^{N'_1} \dots \sum_{n'_M=1}^{N'_M} \sum_{h=1}^{N_H} \sum_{RP} \sum_{IM_h} P(LS^{j}_{[n_1,\dots,n_M]} \left|\left[RP_{[n'_1,\dots,n'_M]}, DS^{j-1}_{[n'_1,\dots,n'_M]}\right], HT_h, IM_h, i, t\right) \tag{3-15}$$

$$\times P\left(\left[RP_{[n'_1,\dots,n'_M]}\middle|DS^{j-1}_{[n'_1,\dots,n'_M]}, HT_h, i, t\right]\right) \times P(DS^{j-1}_{[n'_1,\dots,n'_M]}|i,t) \times P(HT_h)$$

$$\times P(IM_h)$$

where N'_M is the total number of damage-states for damage type *M* that the structure may sustain right after *j*-1th hazard, N_H is the total number of hazard types that may hit the system, $RP_{[n'_1,\dots,n'_M]}$ is the repair status (either complete or incomplete) for each of the *M* damage types, HT_h is hazard of type *h*, and IM_h is the intensity measure of hazard type *h*. Noticeably, $[n'_1, \dots, n'_M]$ and $[n_1, \dots, n_M]$ are the vector of damage-state sustained by the system after *j*-1th hazard, and the vector of the limit-state that is exceeded after *j*th hazard, respectively.

In Equation (3-15), $\left[RP_{[n'_1,\dots,n'_M]}, DS^{j-1}_{[n'_1,\dots,n'_M]}\right]$ represents the damage-state of the system at *j*th hazard incident given the damage-state after *j*-1th hazard event, $DS^{j-1}_{[n'_1,\dots,n'_M]}$, and the repair status for each of the *M* damage types, $RP_{[n'_1,\dots,n'_M]}$. The repair of each damage type is either complete (1) or incomplete (0). Thus, $RP_{[n'_1,\dots,n'_M]}$ is a 1×*M* vector with values of zero or one. If the repair action of any damage type is complete at the time of *j*th hazard incident, the damage-state corresponding to that damage type is one (original

condition). Otherwise, the state of the system is the same as its damage-state right after *j*-1th hazard. As a result, $\left[RP_{[n'_1,\dots,n'_M]}, DS^{j-1}_{[n'_1,\dots,n'_M]}\right]$ identifies the state of the system just before the occurrence of *j*th hazard event. In Equation (3-15), $P\left(LS^{j}_{[n_1,\dots,n_M]} \middle| \left[RP_{[n'_1,\dots,n'_M]}, DS^{j-1}_{[n'_1,\dots,n'_M]}\right], HT_h, IM_h, i, t\right)$ is the probability of exceeding limit-state $[n_1, \dots, n_M]$ at *j*th incident given the damage-state of the system in terms of $\left[RP_{[n'_1,\dots,n'_M]}, DS^{j-1}_{[n'_1,\dots,n'_M]}\right]$, the occurrence of hazard type *h*, intensity of the hazard type *h*, and *i* hazards taking place during time period [0 *t*]. As discussed previously, this probability can be derived from fragility curves. Since the damage-state at the time of *j*th hazard can be different from the intact damage-state, the fragility curves need to be available for all damage-state possibilities. Henceforth, such curves are called damage-state dependent fragility curves. An example of such scenario is the case study bridge system that is exposed to earthquakes and floods. As explained before, floods erode the soil around bridge foundations and piles. When an earthquake occurs, more damage is incurred in the bridge due to the loss of soil support compared to the situation where no scour is present. On the contrary, the earthquake-induced damage does not influence the level of scour depth that the flood hazard incurs.

$P(DS^{j-1}_{[n'_1,\dots,n'_M]}|i,t)$ in Equation (3-15) can be derived in terms of exceedance probability terms using Equation (3-13) by substituting index *j* with *j*-1; each term in this equation is then calculated recursively using Equation (3-15). In other words, in order to compute $P\left(LS^{j}_{[n_1,\dots,n_M]}|i,t\right)$ for *j*th hazard occurrence, $P\left(LS^{j-1}_{[n_1,\dots,n_M]}|i,t\right)$ associated with *j*-1th hazard event should be available. For this purpose, a dynamic programming scheme

is proposed. In the first step, based on prior knowledge about the damage-state of the system before the occurrence of any hazard, $P\left(DS^{0}_{[n'_1,\dots,n'_M]}|i,t\right)$ is known and used as input to solve for $P\left(LS^{1}_{[n_1,\dots,n_M]}|i,t\right)$ for all combinations of limit-states. Second, this information forms the required input for the computation of $P\left(LS^{2}_{[n_1,\dots,n_M]}|i,t\right)$ for each limit-state. This procedure is then continued until $P\left(LS^{j-1}_{[n_1,\dots,n_M]}|i,t\right)$ is calculated. Finally, these values are used to solve for $P\left(LS^{j}_{[n_1,\dots,n_M]}|i,t\right)$. This proposed recursive function is the key for the computational efficiency of the lifecycle hazard-induced cost assessment of structures and infrastructure systems subject to multiple occurrences of multiple types of hazards.

In Equation (3-15), the term $P(HT_h)$ is the probability that the structure is impacted by hazard type *h* at *j*th hazard occurrence. Since hazard events are considered independent with occurrence rates of υ_h, $P(HT_h)$ can be written as:

$$P(HT_h) = \frac{\upsilon_h}{\sum_{h'=1}^{N_H} \upsilon_{h'}} \tag{3-16}$$

The probability of a certain intensity of hazard type *h*, $P(IM_h)$ in Equation (3-15), can also be found from hazard curves. These curves are usually expressed in terms of the annual rate of hazard exceedance versus an intensity measure of hazard type *h*. On this basis, $P(IM_h)$ can be derived as (92):

$$P(IM_h) = \frac{1}{\upsilon_h} \times |\Delta\lambda(IM_h)| \tag{3-17}$$

where $\lambda(IM_h)$ is the annual exceedance rate of intensity measure *IM* of hazard type *h*.

Finally, the term $P\left(\left[RP_{[n_1',\dots,n_M']}\middle|DS^{j-1}_{[n_1',\dots,n_M']},HT_h,i,t\right]\right)$ in Equation (3-15) is the probability that the system is in repair status $RP_{[n_1',\dots,n_M']}$ at the time of *j*th hazard, if the damage-state of the system after *j*-1th incident is $[n_1',\dots,n_M']$ and hazard type *h* occurs at *j*th hazard event when *i* hazards have taken place during period [0 *t*]. As explained before, $RP_{[n_1',\dots,n_M']}$ takes values of one or zero for each damage type and indicates whether the system is recovered from this damage type that was present after *j*-1th hazard. For the case where two damage types exist, the repair status at each hazard occurrence has four combinations: $RP_{[n_1',n_2']}=[0,0]$, $RP_{[n_1',n_2']}=[1,0]$, $RP_{[n_1',n_2']}=[0,1]$ and $RP_{[n_1',n_2']}=[1,1]$. As a particular case, $P\left(\left[RP_{[n_1',n_2']}=[0,0]\middle|DS^{j-1}_{[n_1',n_2']},HT_h,i,t\right]\right)$ in Equation (3-15) will be elaborated. Representing the probability that there is not enough time for repairing the two damage types in the system caused by previous hazards, this term can be computed by incorporating the entire events of incomplete repairs for both damage types. Assuming that the repair process of the two damage types are independent, $P\left(\left[RP_{[n_1',n_2']}=[0,0]\middle|DS^{j-1}_{[n_1',n_2']},HT_h,i,t\right]\right)$ can be written as $P\left(\left[RP_{n_1'}=0\middle|DS^{j-1}_{n_1'},HT_h,i,t\right]\right)\times P\left(\left[RP_{n_2'}=0\middle|DS^{j-1}_{n_2'},HT_h,i,t\right]\right)$.

In the following, the formulations presented in Chapter 2 for calculating the probability of incomplete repair for one type of hazard is extended for a multi-hazard type case. In this case, a system subjected to two hazard types (type 1 and type 2) is considered where each hazard induces a particular type of damage. If the *j*th hazard incident is of type 1, $P\left(\left[RP_{n_1'}=0\middle|DS^{j-1}_{n_1'},HT_1,i,t\right]\right)$ can be determined as follows. Unlike the case

explained in Chapter 2 where only one type of hazard existed, it is not known with certainty what type of hazard has occurred before the *j*th hazard incident. This information is necessary because for calculating the probability of incomplete repair for damage type 1 at *j*th hazard incident, one needs to know the time difference between the occurrences of the hazard type 1 happening at *j*th incident and the last time before *j*th occurrence that this type of hazard took place. The following solution is thus proposed to account for such uncertainty. First, following Bayes rule, $P\left(\left[RP_{n_1'}=0\middle|DS_{n_1'}^{j-1},HT_1,i,t\right]\right)$ can be expressed as:

$$P\left(RP_{n_1'}=0|DS_{n_1'}^{j-1},HT_1,i,t\right)=\frac{P\left(RP_{n_1'}=0,HT_1,i,t|DS_{n_1'}^{j-1}\right)}{P\left(HT_1,i,t|DS_{n_1'}^{j-1}\right)} \tag{3-18}$$

If j_1 out of j events occurring at or before the *j*th incident are of type 1 (and thus $j-j_1$ events are of type 2), Equation (3-18) will be modified to:

$$P\left(RP_{n_1'}=0|DS_{n_1'}^{j-1},HT_1,i,t,j_1\right)=\frac{P\left(RP_{n_1'}=0,HT_1,i,t,j_1|DS_{n_1'}^{j-1}\right)}{P\left(HT_1,i,t,j_1|DS_{n_1'}^{j-1}\right)} \tag{3-19}$$

The timeline of events for the calculation of $P\left(RP_{n_1'}=0,HT_1,i,t|DS_{n_1'}^{j-1},j_1\right)$ is given in Figure 3-1. In this timeline:

- j_1-2 hazards of type 1 occur during timespan [0 t_{j_1-1}], where t_{j_1-1} is the time that j_1-1th hazard takes place.
- No hazard of type 1 happens during $\left[t_{j_1-1}\ \ t_j\right]$, where $t_j=t_{j_1}$.
- The time difference between the two hazards of type 1 occurring at t_{j_1-1} and t_j should not exceed $\tau_{n_1'}$.

- $j - j_1$ hazards of type 2 occur during timespan [0 t_j].
- $i - j$ hazards (either of type 1 or 2) happen during [t_j t].

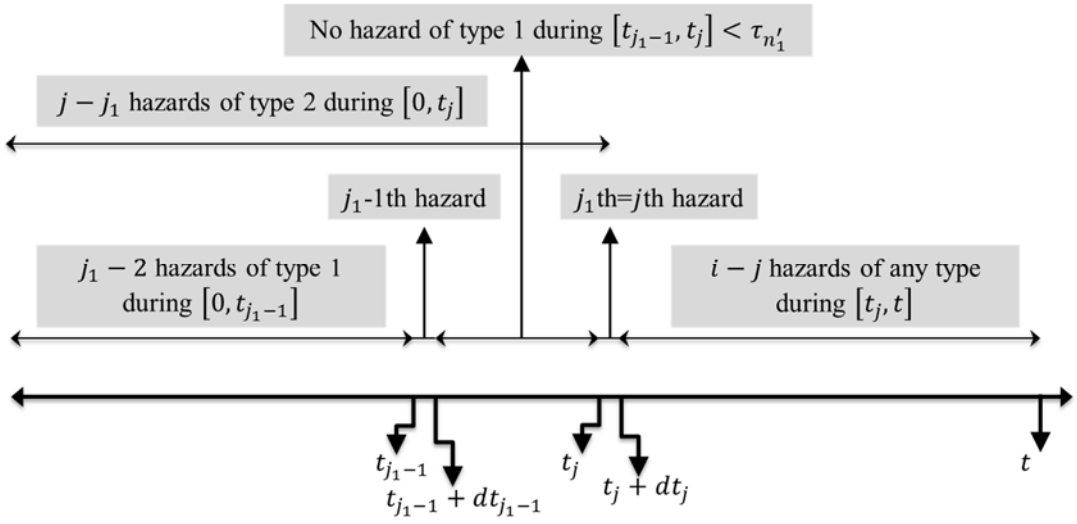

Figure 3-1 Timeline of events for multiple hazard occurrences of two types, for the calculation of the probabilities of the incomplete repair of damage type 1

In Equation (3-19), $P\left(RP_{n_1'} = 0, HT_1, i, t, j_1 | DS_{n_1'}^{j-1}\right)$ can be derived as:

$$P\left(RP_{n_1'} = 0, HT_1, i, t, j_1 | DS_{n_1'}^{j-1}\right)$$

$$= \int_0^t \int_{t_{j_1-1}}^{\min\{t_{j_1-1}+\tau_{n_1'}, t\}} P_1\left(j_1 - 2, \left[0 \;\; t_{j_1-1}\right]\right) \times P_1\left(0, \left[t_{j_1-1} \;\; t_{j_1}\right]\right) \times P_2\left(j - j_1, \left[0 \;\; t_{j_1}\right]\right) \times P_U\left(i - j, \left[t_{j_1} \;\; t\right]\right) \times \upsilon_1^2 \times dt_{j_1} . dt_{j_1-1} \quad (3\text{-}20)$$

where subscripts 1 and 2 in $P_1(\cdot)$ and $P_2(\cdot)$ indicate that these Poisson probabilities should be calculated with the rate of occurrence of υ_1 and υ_2, respectively. Subscript U on the other hand indicates that the Poisson probability should be computed considering the union of both hazards; that is $\upsilon_U = \upsilon_1 + \upsilon_2$.

The term $P\left(HT_1, i, t, j_1 | DS_{n_1'}^{j-1}\right)$ in the denominator of Equation (3-19) is different from $P(i,t)$ which can be calculated according to Equation (3-7). The difference is due to the presence of HT_1 in the multi hazard type case; this term enforces the occurrence of hazard type 1, among other types, at *j*th incident. In addition, it should be noted that if the initial damage-state of the system associated with damage type 1 is intact and no hazard of type 1 occurs before the *j*th hazard (which is of type 1), the damage-state of the system related to damage type 1 will be also intact at *j*th hazard event. In other words, if $j_1 = 1$, then $P\left(RP_{n_1'} = 0, HT_1, i, t, j_1 | DS_{n_1'}^{j-1}\right)$ is zero. Consequently, at least one hazard of type 1 should exist before the *j*th hazard incident, in order to compute the probability of the incomplete repair following Equations (3-18) and (3-19); that is, $j_1 \geq 2$ in Equation (3-19). Thus, $P\left(HT_1, i, t, j_1 | DS_{n_1'}^{j-1}\right)$ should be calculated considering that $j_1 \geq 2$. Therefore, $P\left(HT_1, i, t, j_1 | DS_{n_1'}^{j-1}\right)$ can be determined in the same way as the term $P\left(RP_{n_1'} = 0, HT_1, i, t, j_1 | DS_{n_1'}^{j-1}\right)$ but without the constraint for the time of $j_1 - 1$ and j_1th hazards. Consequently, $P\left(HT_1, i, t, j_1 | DS_{n_1'}^{j-1}\right)$ is determined as follows:

$$P\left(HT_1, i, t, j_1 | DS_{n_1'}^{j-1}\right)$$

$$= \int_0^t \int_{t_{j_1-1}}^t P_1\left(j_1 - 2, [0 \;\; t_{j_1-1}]\right) \times P_1\left(0, [t_{j_1-1} \;\; t_{j_1}]\right) \times P_2\left(j - j_1, [0 \;\; t_{j_1}]\right) \times P_U\left(i - j, [t_{j_1} \;\; t]\right) \times \upsilon_1^2 \times dt_{j_1} . dt_{j_1-1} \tag{3-21}$$

Next, to account for all these possibilities of j_1 values, based on the theory of total probability, $P\left(RP_{n_1'} = 0 | DS_{n_1'}^{j-1}, HT_1, i, t, j_1\right)$ can be decomposed as:

$$P\left(RP_{n_1'} = 0 | DS_{n_1'}^{j-1}, HT_1, i, t, j_1\right)$$

$$= \sum_{j_1=2}^{j} P\left(RP_{n_1'} = 0 | DS_{n_1'}^{j-1}, HT_1, i, t, j_1\right) \times P(j_1 \; out \; of \; j) \tag{3-22}$$

where $P\left(RP_{n_1'} = 0 | DS_{n_1'}^{j-1}, HT_1, i, t, j_1\right)$ is calculated using Equations (3-18), (3-19) and (3-20). For the two hazard type case, $P(j_1 \; out \; of \; j)$ can be calculated according to the binomial distribution:

$$P(j_1 \; out \; of \; j) = \binom{j}{j_1} \times P(HT_1)^{j_1} \times P(HT_2)^{j-j_1} \tag{3-23}$$

where $P(HT_1)$ and $P(HT_2)$ are calculated using Equation (3-16).

As explained before, the extent of damage induced by hazards may depend on more than one type of damage sustained by the system. Therefore, it is imperative to evaluate the status of repair for all types of damage that impact the induced damage during the next hazard event. As a result for the case of two hazard types, when the *j*th hazard

incident is of type 1, the probability of incomplete repair for damage type 2, $P\left(RP_{n_2'}=0|DS_{n_2'}^{j-1},HT_1,i,t\right)$, should be also calculated. This term can be computed in a similar way as $P\left(RP_{n_1'}=0|DS_{n_1'}^{j-1},HT_1,i,t\right)$. When j_1 out of j hazards occurring at or before the *j*th incident are of type 1, according to Equation (3-19), $P\left(RP_{n_2'}=0|DS_{n_2'}^{j-1},HT_1,i,t\right)$ can be expressed as:

$$P\left(RP_{n_2'}=0|DS_{n_2'}^{j-1},HT_1,i,t,j_1\right)=\frac{P\left(RP_{n_2'}=0,HT_1,i,t,j_1|DS_{n_2'}^{j-1}\right)}{P\left(HT_1,i,t,j_1|DS_{n_2'}^{j-1}\right)} \tag{3-24}$$

Note that following the assumption of independency of repair processes for different damage types, the repair status of damage type 2 right before *j*th hazard event depends only on the condition of the system corresponding to damage type 2 after *j*-1th hazard, $DS_{n_2'}^{j-1}$. Following the timeline of events presented in Figure 3-2, $P\left(RP_{n_2'}=0,HT_1,i,t,j_1|DS_{n_2'}^{j-1}\right)$ can be determined as:

$$\begin{aligned}P\left(RP_{n_2'}=0,HT_1,i,t,j_1|DS_{n_2'}^{j-1}\right)&\\ =\int_0^t\int_{t_{j_2}}^{\min\{t_{j_2}+\tau_{n_2'},t\}}&P_1\left(j_1-1,\left[0\ \ t_{j_1}\right]\right)\\ \times P_2\left(j-j_1-1,\left[0\ \ t_{j_2}\right]\right)&\times P_2\left(0,\left[t_{j_2}\ \ t_{j_1}\right]\right)\\ \times P_U\left(i-j,\left[t_{j_1}\ \ t\right]\right)&\times\upsilon_1\times\upsilon_2\times dt_{j_1}.dt_{j_2}\end{aligned} \tag{3-25}$$

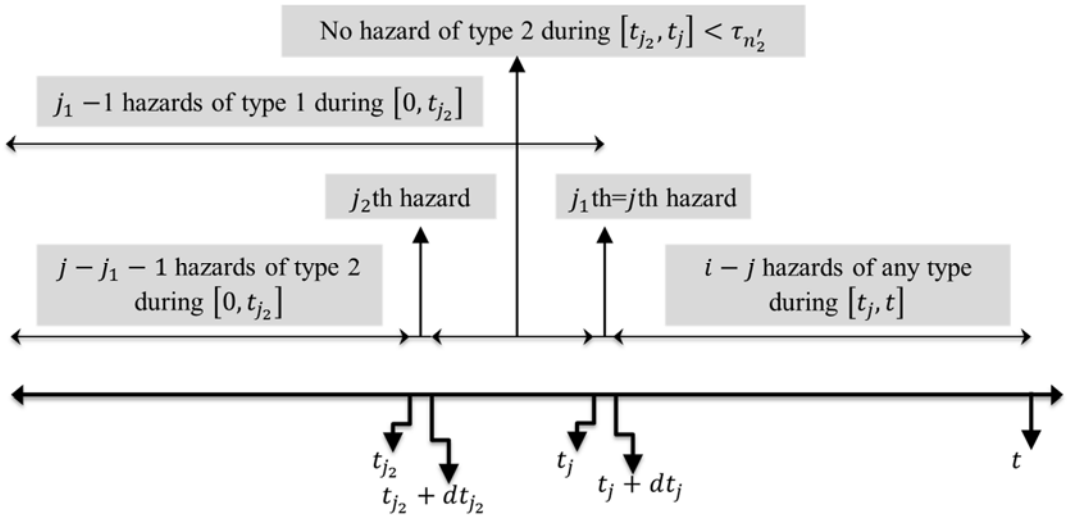

Figure 3-2 Timeline of events for multiple hazard occurrences of two types, for the calculation of the probabilities of the incomplete repair of damage type 2

Further, since the term $P\left(HT_1, i, t, j_1 | DS_{n_2'}^{j-1}\right)$ in Equation (3-24) is independent of the damage-state of the system after j-1th hazard, it can be calculated using Equation (3-21). Similar to Equation (3-22), to account for all possibilities of j_1 values, the binomial distribution function can be applied. Analogous to the reasoning provided for the lower bound of j_1 when computing probability of incomplete repair for damage type 1, the upper bound for the binomial function is j-1; since $j_1 = j$ is equivalent to no damage of type 2 happening before jth incident, there would be no damage of type 2 at j-1th hazard to repair, i.e. $P\left(RP_{n_2'} = 0, HT_1, i, t, j_1 | DS_{n_2'}^{j-1}\right) = 0$ if $j_1 = j$. Thus, $P\left(RP_{n_2'} = 0, HT_1, i, t, j_1 | DS_{n_2'}^{j-1}\right)$ can be calculated as follows:

$$P\left(RP_{n_2'}=0|DS_{n_1'}^{j-1},HT_1,i,t,j_1\right)$$

$$=\sum_{j_1=1}^{j-1}P\left(RP_{n_2'}=0|DS_{n_2'}^{j-1},HT_1,i,t,j_1\right) \quad (3\text{-}26)$$

$$\times P(j_1\ out\ of\ j)$$

where $P(j_1\ out\ of\ j)$ can be determined using Equation (3-23). Now considering the independency of repair processes for the two damage types, $P\left(\left[RP_{[n_1',n_2']}=[0,0]\right]DS_{[n_1',n_2']}^{j-1},HT_h,i,t\right]\right)$ that describes the joint probability of incomplete repairs is derived by combining Equations (3-21) and (3-25) as follows:

$$P\left(\left[RP_{[n_1',n_2']}=[0,0]\right]DS_{[n_1',n_2']}^{j-1},HT_h,i,t\right]\right)$$

$$=\sum_{j_1=2}^{j-1}P\left(RP_{n_1'}=0|DS_{n_1'}^{j-1},HT_1,i,t,j_1\right) \quad (3\text{-}27)$$

$$\times P\left(RP_{n_2'}=0|DS_{n_2'}^{j-1},HT_1,i,t,j_1\right)\times P(j_1\ out\ of\ j)$$

For other cases where the complete repair status of a damage type is involved, the complement of the probability of incomplete repair should be used in Equation (3-27) instead of the probability of incomplete repair status for that damage type. This procedure can be generalized to calculate the joint probability of repair status for *M* different damage types.

Having calculated all the terms that are present on the right hand side of Equation (3-15), the transition probabilities of exceeding any limit-state $[n_1,\dots,n_M]$ from any damage-state $[n_1',\dots,n_M']$ can be determined. These values vary for the timespan *t*, total number of hazard incidents within this timespan, and the *j*th hazard incident at which the

transition probabilities are calculated. The computed transition probabilities are then used to calculate the total hazard-induced LCC for the system. A flowchart illustrating the proposed framework and procedures for LCC assessment of a structure or an infrastructure subjected to two types of hazards is presented in Figure 3-3.

In the next section, the case study system, as well as the required data for the implementation of the proposed LCC analysis framework for this case study are presented.

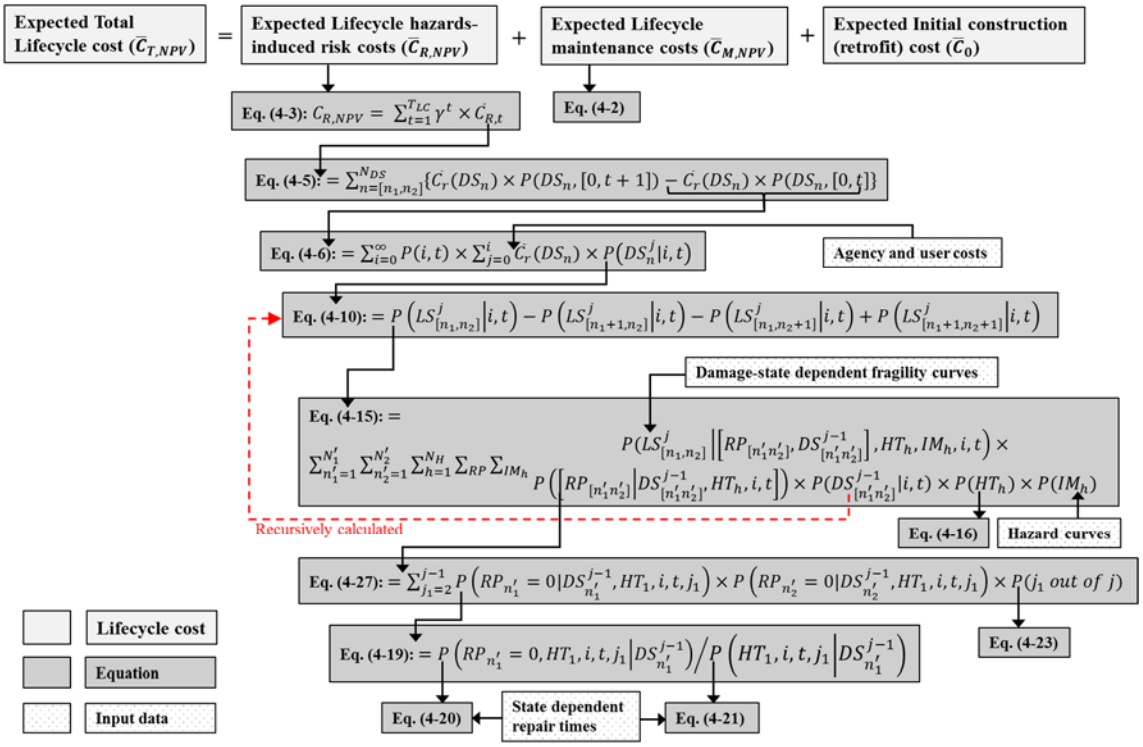

Figure 3-3 Flowchart of the proposed framework for LCC assessment of a strucure or an infrastructure systems subjected to two types of hazards

3.4. Case Study: Five Span Concrete Bridge

The proposed LCC framework is implemented for the realistic five span RC bridge that is introduced in Section 2.5. This time the bridge, which is assumed to cross over a river, is exposed to not only earthquake hazards, but also to flood incidents (see Figure 3-4). Additionally in this chapter, the bridge is considered to be located in Sacramento, California.

Combinations of retrofit alternatives including no retrofit, applying CFRP wrapping, and performing scour countermeasures are considered here. Through comparison of such alternatives, the proposed LCC framework identifies the least costly option for various lifetimes during which the bridge is expected to serve. The system is initially in the intact damage-state, and later may experience earthquakes of any intensities and flooding events of various discharge rates according to their corresponding probabilistic hazard models for the area. The repair process for any seismic induced damage starts following each earthquake event. For the case of flood hazard, the scour countermeasure, if implemented, will be applied at the start of lifetime. For retrofit alternatives where no scour countermeasures are performed initially, scour depth accumulates as the number of flood events increases.

The required information for the seismic hazard curve corresponding to the location of the bridge, the state dependent repair times for the repair of earthquake-induced damages, and seismic damage-state dependent cost terms are provided in Sections 2.5.1.2, 2.5.1.4, and 2.5.1.5, respectively. In the following, the required data for the flood hazard curve of the river that passes under the bridge, the damage-state dependent fragility curves

for the combinations of earthquake- and scour damage-states, and the implementation cost for the considered retrofit alternatives are presented.

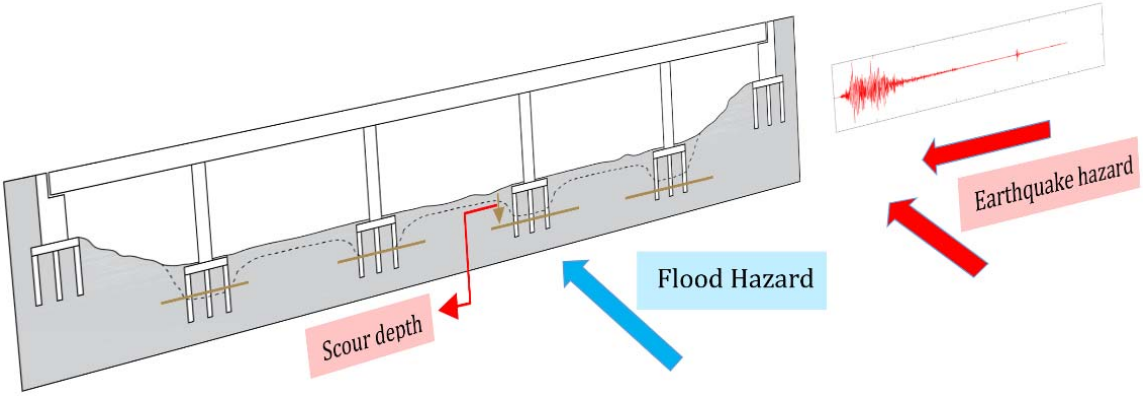

Figure 3-4 Schematics of the case study bridge and the hazard types that this bridge is exposed to

3.4.1. Flood Hazard Curve

The case study bridge is assumed to be located in the city of Sacramento, California, over the American river. Using the historic flood data of the county of Sacramento, Prasad and Banerjee (51) generated the flood hazard curve shown in Figure 3-5. The annual rate of occurrence of the flood hazard, based on this curve, is 1.01.

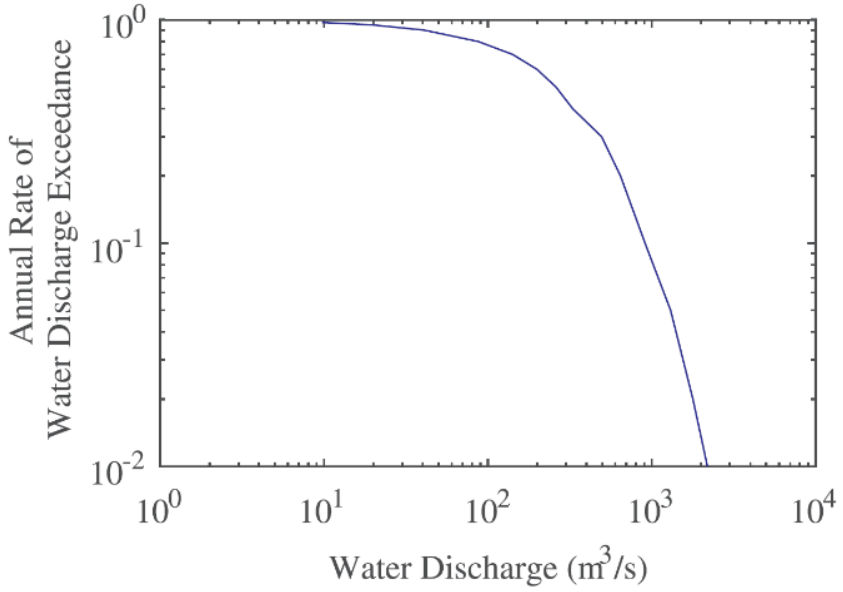

Figure 3-5 Flood hazard curve for the river that passes under the case study bridge in Sacramento (51)

3.4.2. Damage-State Dependent Fragility Curves

The five earthquake-induced damage-states considered for the bridge are described in Section 2.5.1.3. The second type of damage for the case study bridge in this chapter is scour, which is associated with flood hazard. Four limit-states are considered for this damage type: 0 m, 0.6 m, 1.5 m, and 3.0 m scour depth. As mentioned before, the extent of seismic-induced damage predicted by the fragility curves depends on the scour depth in addition to the intensity of the seismic event. The median values for the lognormal cumulative distribution functions of the fragility curves for these damage-states are determined by Prasad and Banerjee (51) and are given in Table 3-1. These values are for the non-retrofitted case study bridge, where the bridge is initially in the intact seismic

condition. A logarithmic standard deviation of 0.5 is considered for all fragility curves (70).

Table 3-1 Median values of PGA (g) for the lognormal cumulative distribution functions of the fragility curves for the case of initial intact seismic damage-state considering various scour depths (70)

		Damage-state			
		Minor	Moderate	Extensive	Complete
Scour Depth (m)	0.00	0.73	0.90	1.27	1.44
	0.60	0.56	0.78	1.28	1.34
	1.50	0.51	0.72	1.13	1.28
	3.00	0.50	0.71	1.09	1.13

Since the bridge is located on a river in the city of Sacramento with a "Mediterranean" weather (93), the marine environment can be considered for the deterioration performance of the piers. A major source of deterioration for bridge piers in this environment is corrosion in steel rebar due to chloride penetration (18,94). In this environment, application of steel jacketing alone, as a retrofit action, is an inefficient strategy, since exposed steel elements are extremely vulnerable to corrosion (95). Thus, application of FRP wraps that are more durable against corrosion are considered in this research. Two of the most commonly used FRP actions are carbon fiber reinforced polymer (CFRP), and glass fiber reinforced polymer (GFRP) (96). Comparing CFRPs and GFRPs, GFRPs have shown weaker performance, in terms of strength, stiffness and ductility, under extreme environments such as dry-wet and freeze-thaw conditions (97). For these reasons, wrapping the whole piers of the case study bridge with CFRP is evaluated as one of the retrofit alternative in this study.

Retrofitting bridge piers using CFRP wrapping will enhance the capacity of the bridge against seismic excitations and will consequently increase the median of the fragility curves. For retrofitting all piers of multi-span RC bridges with steel jackets, Shinozuka et al. (98) quantified the percentage increase in median fragility curves, *EP*, that can be achieved by this retrofit action as follows:

$$EP = 11.8 \times e^{0.53n_i'} \times 100\% \quad \forall n_i' \in \{2, \dots, 5\} \tag{3-28}$$

where n_i' is the limit-state index for the seismic fragility curve of interest (2~5 represent minor, moderate, extensive, and complete limit-states).

For FRP wrapping, due to lack of data for the amount of improvement in the median of fragility curves provided by this retrofit action for the case study concrete bridge, the results of the analysis conducted by Billah et al. (99) are employed. In this study, CFRP wrapping and steel jacketing are evaluated as two retrofit options for a seismically deficient concrete bridge bent. The comparison of fragility curves associated with these two retrofit actions under a set of far field ground motions indicates that the median of fragility curves, in terms of PGA, for slight, moderate, extensive and complete limit-states for the system retrofitted with FRP wrapping is 1.17, 1.16, 1.31, and 1.31 times those as a result of enhancing with steel jacketing. These values are multiplied, respectively, by the *EP* values derived from Equation (3-28) to give the percentage increase in median fragility curves achieved by retrofitting all piers with CFRP wraps compared to the status quo of the bridge.

The above set of fragility curves for unretrofitted and retrofitted bridges represent the case where the structure at the time of the earthquake occurrence is in the intact seismic

damage-state. As elaborated in Chapter 2, for other damage-states, the ratios provided in Table 2-10 are used to arrive at the median of the associated fragility curves. Furthermore, these ratios are considered the same for all scour depths and retrofit strategies. As an example, considering Table 3-1 and Table 2-10, the lognormal median PGA of the fragility curve for the major limit-state when the existing seismic damage-state of the bridge is moderate and the scour depth is 0.6 m is equal to 0.78g/1.5=0.52 g. This value is 0.78 g if the structure is at the intact state.

The impact of flood hazard on the seismic fragility of bridges can be quantified using the scour depth induced by flooding events. Expected scour depths caused by various flood discharge levels are determined and provided by Prasad and Banerjee (51) for the case study bridge (see Table 3-2). For retrofit options with no scour countermeasure, the scour depth will accumulate as the number of flood events increases.

Table 3-2 Expected scour depths caused by various discharge values for the case study bridge (51)

Discharge Value (m^3/s)	60	305	900	1300	1900	2200
Induced Scour Depth (m)	0.73	2.16	2.84	3.11	3.42	3.55

3.4.3. Cost of Retrofit Alternatives

In case of retrofitting or performing a scour countermeasure plan, an initial cost will be added to the total LCC of the case study bridge.

The material, equipment and technician costs associated with CFRP wrappings are estimated as 12.48$/ft2 (57). After updating the cost values to 2017, this value becomes

13.24$/ft2. This cost is considered for two layers of CFRP wrap around the columns as a common practice (100). According to Caltrans (74), this value is increased by 30% to account for the mobilization and contingency costs. Additionally, based on the procedure and number of days reported for constructing CFRP wraps by Teng et al. (101) for an area of 3300 ft^2, two days (can be estimated as 1.5 days) are estimated for wrapping the entire four columns of the case study bridge with the wrapping area of 600ft^2. This time comprises one day for the mobilization of the equipment and material, and surface reparation of concrete columns for the CFRP wrapping, and one day for applying the wrapping on the columns. During this time, the bridge is considered fully open, since it is assumed that the shoulders of the road provide sufficient space for the required crew and material for retrofit actions on elements under the bridge. However, for safeguarding the work zone, speed limit is reduced from 60mph to 50mph. It should be noted that for repairing slight seismic-induced damages one lane of the bridge is assumed to be closed; since necessary repairs may be required for structural damages on the deck or on superstructure elements that should be accessed from the top of the bridge. Additionally, identical number of days, i.e. two days, is considered for conducting the scour countermeasure plan, considering that the bridge bents are single-column. When both FRP wrapping and scour countermeasures are executed, due to availability of crew and material and simultaneous execution of these plans, the duration of the project becomes less than the sum of individual duration of the two plans (65,102). This duration is considered as three days in this study. On this basis, the user cost of DVE, economic losses, and

environmental damages are added to calculate the total cost incurred by these retrofit projects.

The scour countermeasure plan considered for this bridge is concrete-grouting the voids of the loose soil underneath each pile foundation and the soil surrounding bent foundations together with 1 m layer of Rock Slope Protection (RSP) material. Based on Caltrans (74) and engineering judgment, the cost of the scour countermeasure plan for the four foundations of the case study bridge as of 2017 becomes $260,000.

3.5. Numerical Results

Numerical results of the application of the proposed LCC framework to the case study bridge are provided in this section. The objective is to determine the optimal action, i.e. the action that minimizes the LCC of the bridge during its service life. The considered set of actions are listed below:

1) Status quo plan: The bridge structure is planned to operate as is.
2) CFRP wrapping (CFW) with no scour countermeasure (ScC) plan: All bridge columns will be entirely wrapped with two layers of CFRPs, but no scour countermeasure will be performed on bridge foundations.
3) CFRP wrapping and scour countermeasures plan: All bridge columns will be entirely wrapped with two layers of CFRPs, and ScC actions will be performed on bridge foundations.
4) Scour countermeasures with no CFRP wrapping plan: Only scour countermeasures will be performed on bridge foundations.

The rest of this section presents results of a convergence study for the proposed numerical framework, demonstrates impacts of incorporating multiple types of hazards and their multiple occurrences on the LCC of the bridge, and finally, discusses how repair time variations can impact the optimal strategy.

3.5.1. Convergence Analysis

The convergence of the proposed framework for LCC assessment of the case-study bridge with respect to the number of hazard incidents is investigated here. A relative tolerance of 0.005 is considered here. When the relative difference of the total hazard-induced cost from two consecutive steps becomes less than the specified tolerance value, the analysis is considered as converged. Results of convergence analysis for a wide range of lifetimes are presented in Figure 3-6. Generally, as the time horizon increases, the number of hazard incidents required for the framework to converge increases. This can be explained by the fact that the expected number of hazard incidents following a Poisson process is linearly proportional to the lifetime, i.e. $E(i|T_{LC}) = \upsilon_U \times T_{LC}$ where $\upsilon_U = \upsilon_1 + \upsilon_2$ for the case-study system subjected to two hazard types. The likelihood of number of occurrences significantly decreases in the Poisson occurrence model as the considered number of hazard occurrences becomes larger than the expected number. Therefore, as seen in Figure 3-6, the required number of hazard incidents for convergence is slightly larger than the expected number of hazard incidents for all alternatives. Leveraging this property here results in a numerical framework that is accurate and computationally efficient. In addition, it appears that the four retrofit actions require nearly the same number of hazard

incidents to converge. Results of this analysis also indicate that a reliable estimation of the LCC of systems requires consideration of the possibility of multiple hazard occurrences throughout the lifetime. This consideration, however, is neglected in some existing loss assessment studies.

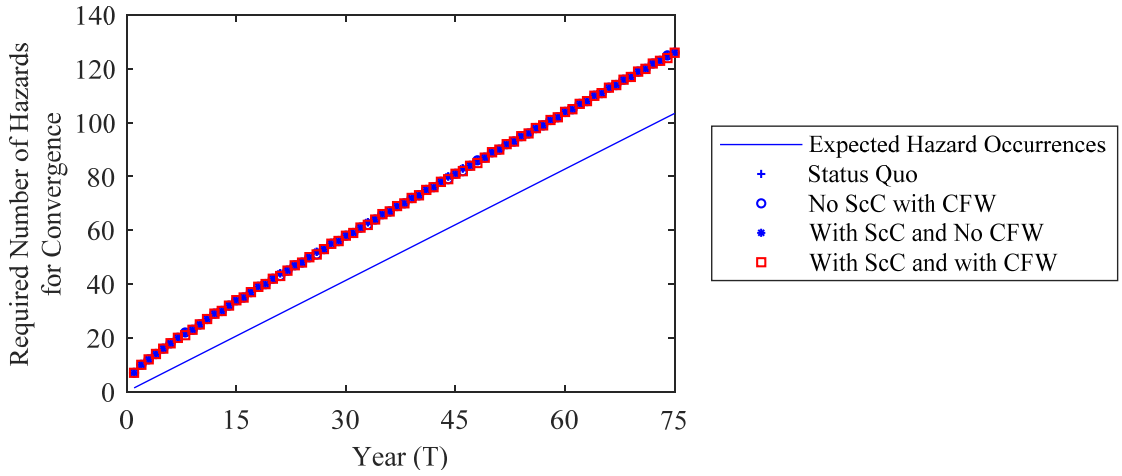

Figure 3-6 Required number of hazard incidents to be considered in the framework for convergence

3.5.2. Lifecycle Cost Analysis and Optimal Decision-Making across Predetermined Alternatives

Using the proposed framework for the case-study bridge, the LCC for the considered set of retrofit alternatives are estimated as a function of lifetime. The results of this study identify the best retrofit option to take at the current time for a wide range of remaining service lifetimes, considering that the seismic and scour condition state at the current time

of decision-making is intact. For these results, mean values of the probabilistic repair time models for the recovery paths in Table 2-11 are considered. LCC values are provided separately for repair, maintenance and total costs in Figure 3-7. As can be seen from Figure 3-7-c, the LCCs of maintenance are close in value for the four retrofit alternatives. However, since maintenance cost directly depends on the cost of bridge construction and the implemented retrofit plan, it is larger for alternatives with more costly retrofit plans. Figure 3-7-b shows the hazard-induced LCC for the case study bridge. Results show that this cost is more than the LCC of maintenance, if no retrofit action is applied to the bridge. These indicate that the risk of hazards contributes considerably to the total LCC, and thus highlights the neccessity of considering the risk of hazard occurrences for optimal decision-making. Figure 3-7-b also shows that the hazard-induced LCC is largest for status quo compared to other alternatives. This outcome is expected, since the bridge rehabilitated with any of the considered alternatives is less vulnerable to hazards compared to the status quo bridge case. The achieved enhancement varies for different retrofit actions. As Figure 3-7-b indicates, the extent of enhancement is larger for the CFW retrofit action compared to the ScC plan (more than two times for 75 years lifetime). In addition, the initial cost of CFW plan is less than that for the ScC strategy. This results in the CFW plan being more favorable than the ScC retrofit action for all lifetimes. Considering all alternatives, status quo is found to be the optimal option for time horizons less than 26 years. This can be mostly attributed to the fact that the total hazard risk cost for short lifetimes is less costly than the sum of the implementation cost of retrofit plans and the reduced hazard risk costs due to higher seismic capacity achieved by those

retrofits. For lifetimes more than 26 years, CFW plan results in the least incurred expected total LCC.

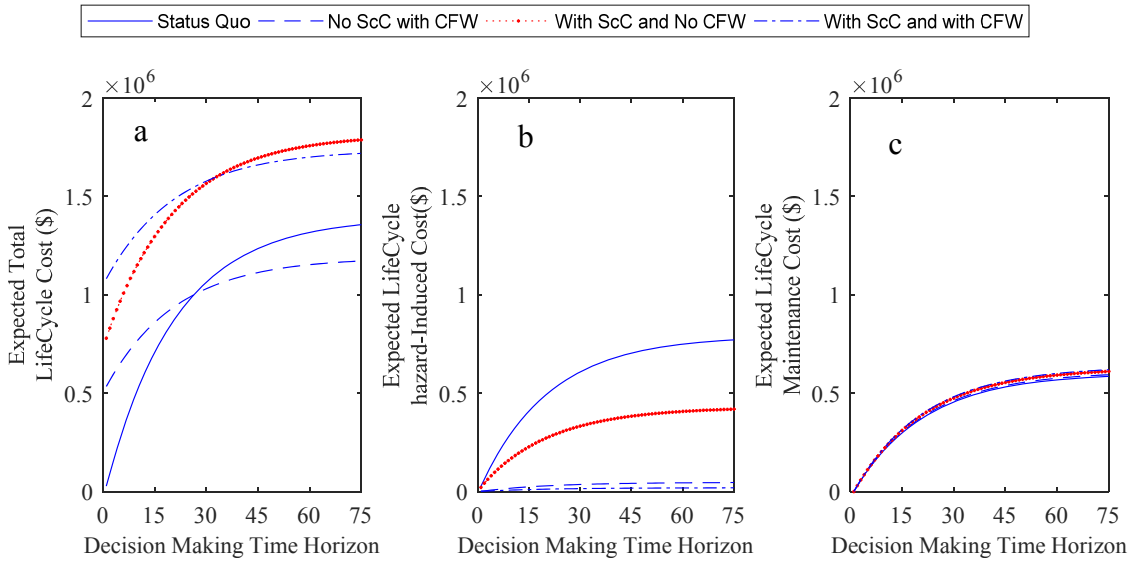

Note: ScC=Scour countermeasure, CFW=Carbon FRP wrap.

Figure 3-7 a) Total, b) Repair, and c) Maintenance LCCs for the considered retrofit alternatives

3.5.3. Significance of Considering Multiple Types of Hazards in Lifecycle Optimal Decision-Making across Predetermined Alternatives

In case flood hazard is not considered in LCC analysis, impacts of scouring on seismic vulnerabilities together with the associated costs will not be accounted for. Figure 3-8 shows that this scenario may not only result in a considerable underestimation of total LCC, but also may lead to false identification of the optimal strategy as the impact of neglecting flood hazard on the LCC of retrofit plans is not uniform. As can be seen when

the effect of scouring is ignored, the optimal retrofit strategy is identified as the status quo option for all lifetimes, whereas comparing status quo and CFW plans, the correct optimal action for time horizons longer than 26 years is the CFW plan (Figure 3-7-a). For lifetime of 75 years, this false identification of the optimal plan would incur an extra cost of $184,000 to the society. Furthermore, consideration of only seismic hazard in the analysis will result in an underestimation of total LCC of approximately 26% for the status quo retrofit plan, when the lifetime is 75 years. This error for the case of CFW strategy is small (2%). As shown in Figure 3-7-b, CFW plan is an effective strategy that considerably reduces the risk of seismic-induced losses. As a result, the contribution of the hazard-induced LCC to the total LCC and consequently the impact of the error associated with neglecting flood hazard becomes less significant for the case of CFW plan.

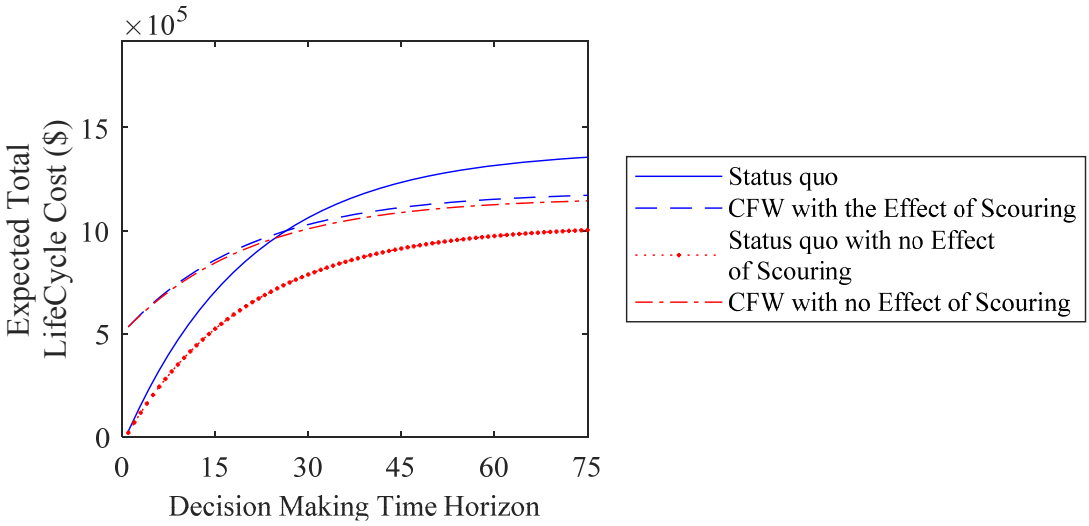

Note: ScC=Scour countermeasure, CFW=Carbon FRP wrap.

Figure 3-8 Total LCC of status quo and CFW retrofit alternatives, with and without the effect of scour in the analyses

3.5.4. Significance of Repair Time Variation and Damage-Dependencies in Lifecycle Cost Analysis

The importance of repair time for the LCC assessment and optimal decision-making across predetermined retrofit alternatives is illustrated in Figure 3-9. Multiple factors can lead to delays in the recovery process of the bridge, including:

- Crew and materials are temporarily not available.
- The bridge is owned by an agency that has a slow response time for repair preparations.
- Damage to the nearby infrastructure, e.g. transportation systems, power supply, etc., is to the extent that it causes extra delays in the recovery of the bridge.

In these scenarios, elongated repair times not only increase the overall cost because of time-dependent consequences such as user costs and economic losses, but also will increase hazard risk costs due to the higher likelihoods of other hazards occurring before the bridge is completely repaired. The latter effect consequently increases the expected hazard-induced and the total LCC. As presented in Chapter 2, each item in the recovery path for all damage-states has a lognormal distribution with statistical parameters presented in Table 2-11. Following identical procedure explained in Chapter 2, the total recovery time for each damage-state n, T_{total}^{n}, is the sum of the times it takes to finish each involved step. Using Monte Carlo simulation technique based on Latin Hypercube sampling, three recovery times for each damage-state are identified: T_{0}^{n}, $T_{0.5}^{n}$ and $T_{0.95}^{n}$. These values are derived such that $P[T_{total}^{n} \leq T_{\alpha}^{n}] = \alpha$, where $\alpha = \{0, 0.5, 0.95\}$ as noted in Chapter 2 is referred to as Non-Exceedance Probability (NEP). Figure 3-9-a shows the total LCC and the hazard-induced LCC for the status quo strategy, when recovery times of T_{0}^{n}, $T_{0.5}^{n}$ and $T_{0.95}^{n}$ are considered for each damage-state. It is seen that, as the recovery time increases, the LCCs increase as well. For 75 years of service lifetime, the expected total LCC increases by 51%, as the recovery times increase from instant repair (T_{0}^{n}) to a delayed repair process corresponding to the NEP of 0.95 ($T_{0.95}^{n}$). These results highlight the significance of considering repair times in LCC analysis. Furthermore, disregarding repair times in damage accumulations, i.e. neglecting dependencies between damages from consecutive hazards, can result in non-optimal decisions. Considering status quo and CFW retrofit plans, Figure 3-9-b indicates that if the proposed LCC framework is employed without considering such dependencies, the status quo strategy will be

identified as the optimal option for lifetimes less than 37 years. However, in reality, for service lifetimes more than 26 years, applying CFW is the optimal policy. If the status quo is incorrectly identified as the optimal plan for the bridge with an expected service life of 37 years, an extra cost of $83,000 is expected to incur within these years to the community. This cost can be precluded, if the true optimal plan of retrofitting with CFW is performed. Moreover, neglecting dependencies between seismic-induced damages from consecutive hazards results in $98,000 underestimation of the total LCC, which may lead to improper allocation of budget for lifetime repairs of the case study bridge.

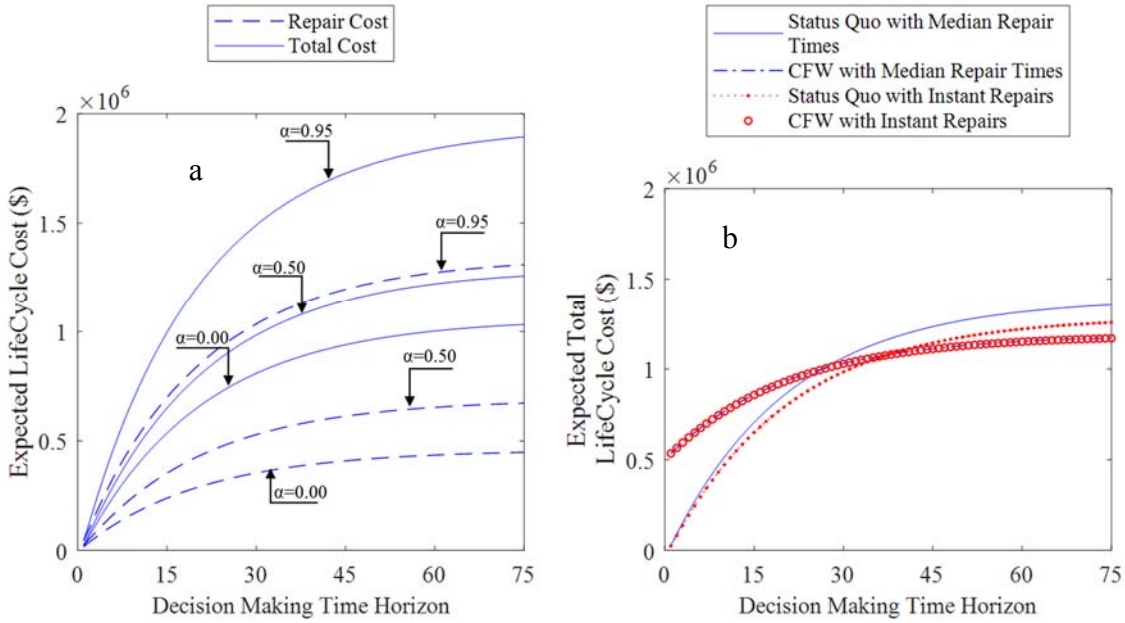

Note: ScC=Scour countermeasure, CFW=Carbon FRP wrap.

Figure 3-9 a) Variation of the total LCC and the hazard-induced LCC for recovery times corresponding to NEPs of 0, 0.5 and 0.95. b) Total LCC for the status quo and retrofitting with CFW alternatives, with and without considering the effect of repair time

3.6. Concluding Remarks

This chapter proposed a framework for LCC assessment of structures and infrastructure systems considering the potential for multiple occurrences of multiple types of hazards. The expected total LCC comprises initial cost of construction/retrofit, expected LCC of system maintenance, and expected LCC of hazard-induced consequences, i.e. hazard risk costs. The proposed method offers the following features and assumptions:

- Using the total probability theorem, the risk costs for all possibilities of different hazard types and number of hazard occurrences were included. Moreover, probability models of uncertain model and hazard variables are discretized into mutually exclusive and collectively exhaustive set of events. These variables include intensity of hazard incidents (probability models obtained from hazard curves), extent of induced-damage from various hazard types (probability models obtained from damage-state dependent fragility curves), and the time of hazard occurrences (modeled through probability models of multiple hazard occurrences) through which the randomness in the state of repair (complete or incomplete) is modeled for the incurred damage.
- Using damage-state dependent fragility curves, the damage-state probabilities after the occurrence of each hazard event is computed based on the joint damage-state probabilities calculated for the previous hazard and the repair status after the previous hazard. The latter depends on the recovery time of the incurred damage-state and the probability model of multiple hazard occurrences.

- The framework can incorporate all direct and indirect costs of consequences and account for the dependency of these costs to the duration of repair. In the present chapter, agency repair costs, user costs of imposed delay and vehicle operation, economic losses, and cost of human casualties were considered as a function of incurred damage-states. Moreover, the damage incurred by traffic delays to the environment was considered explicitly.
- Damage-state probabilities after each hazard occurrence are computed through a dynamic programming procedure. This recursive function is a key to the time efficiency of the framework as it substitutes numerous simulations that would have been required otherwise.

Similar to the framework developed for one type of hazard in Chapter 2, the proposed method in this chapter requires limited input data including hazard curves, cost values, damage-state dependent fragility curves and repair times.

The framework was demonstrated for the realistic case study bridge system presented in Chapter 2, which is exposed to floods, in addition to earthquake hazards during its lifetime. These hazard types can potentially induce scouring and seismic damage to the structure. In the estimation of the hazard-induced LCC, the joint effect of earthquake and flood hazards are considered through analyzing the likelihood of different combinations of damage-states that arise from these two types of hazard. Derivation of these likelihoods in the proposed method accounts for the repair time required for each considered damage-state. Four retrofit alternatives were considered and the proposed

framework was utilized to compute the LCC of each alternative for various expected service lifetimes. Results showed that:

- To achieve high accuracy in the estimation of the hazard-induced LCC, the proposed method requires only slightly more than the expected number of hazard incidents in the considered timespan to converge. This attribute leads to the computational efficiency of the framework in estimating LCC of systems subjected to multiple occurrences of multiple types of hazards.
- Hazard-induced LCC contributes significantly to the total LCC of the bridge system; highlighting the importance of considering this cost term in decision-making problems.
- Applying CFRP Wrapping to the bridge reduces hazard risk costs significantly. This reduction for 75 years of expected service lifetime is more than twice the enhancement gained from performing a Scour Countermeasure (ScC) plan for the bridge foundations. This indicates that the developed method is able to quantify the effects of various hazard mitigation plans for optimal decision-making across predetermined alternatives.
- Based on the rankings provided for the considered retrofit alternatives, for lifetimes less than 26 years, the status quo plan is the optimal strategy. However, if the lifetime exceeds 26 years, CFRP Wrapping retrofit plans results in the least expected total LCC for the community.
- The recovery times following each damage-state have significant impact on the hazard-induced LCC and the total LCC; the slower the recovery process, the more the

expected hazard-induced LCC. This highlights the necessity of including the required time of recovery in the evaluation of hazard risk costs.

- Ignoring dependencies between damages induced by consecutive hazards lead to false identification of optimal actions and incurs an extra cost of about $83,000 for 37 years of service lifetime.

The above set of conclusions indicates that the developed framework presented in this chapter provides a comprehensive, accurate, and computationally efficient method that can help decision makers to find optimal strategies for a structures or an infrastructure system exposed to multiple occurrences of multiple types of hazards. The enhancements offered by this framework over existing methods for LCC analysis of systems exposed to multi-hazards will lead to solutions with higher confidence in their effectiveness. This is significant especially for structures and infrastructure systems located in hazard-prone regions or those where damage may cause significant adverse consequences.

Chapter 4: Integrating Gradual Deterioration in Risk-Based Lifecycle Cost Analysis with Multiple Types and Occurrences of Hazards

4.1. Summary

In hazard-prone regions, structures and infrastructure systems can experience multiple hazards with various intensities and inter-arrival times during their lifetime. As elaborated in previous chapters, the potential of damage accumulation due to the possibility that a damage is not fully repaired before the occurrence of a next hazard increases the vulnerability of these assets against hazard incidents. In addition, gradual deterioration due to environmental stressors may reduce their capacity against such hazard events. In light of these compounding effects, it is important to evaluate the lifecycle cost (LCC) of structures and infrastructure systems to select design or retrofit alternatives that maximize their safety and serviceability.

This chapter extends the framework proposed in Chapter 3 and develops a probabilistic LCC framework that properly incorporates the foregoing effects in order to arrive at optimal decisions across predetermined design or retrofit alternatives for structures and infrastructure systems. The development of a recursive function significantly reduces the computational runtime, while enables calculation of damage-state probabilities at each time and hazard occurrences in the presence of deterioration.

The framework is demonstrated for the case study bridge in previous chapters, which is stochastically exposed to multiple earthquake and flood hazards. Furthermore, the bridge is assumed to be exposed to a marine environment, which induces gradual deterioration in the structural system of the bridge. Results indicate that such deterioration significantly increases expected hazard-induced and total LCCs. Hence, disregarding deterioration in LCC analysis could lead to substantial underestimation of the expected costs, which could adversely impact the allocation of repair budget for management purposes. In addition, optimal retrofit decisions may be incorrectly identified if deterioration is overlooked in LCC analysis. As shown, this could result in significant additional costs for communities.

The demonstrated features in this chapter suggest that the proposed framework can be beneficial to responsible agencies for risk-informed decision-making across predetermined design or retrofit alternatives for vulnerable aging structures and infrastructure systems.

4.2. Introduction

In hazard-prone regions, structures and infrastructure systems can experience multiple hazards with various intensities during their lifetime. As elaborated in previous chapters, the potential of damage accumulation due to the possibility that a damage is not fully repaired before the occurrence of a next hazard increases the vulnerability of these assets against hazard incidents (30,102,103). In addition, gradual deterioration due to environmental stressors may significantly reduce their capacity against such hazard

events. In light of these compounding effects, it is important to evaluate the lifecycle cost of these assets to select design or retrofit alternatives that maximize their safety and serviceability.

In the literature, there are only a handful of studies that conducted lifecycle cost analysis for structures and infrastructure systems subjected to both random hazards and gradual deterioration due to environmental stressors (40). For example, Ghosh (33) utilized a non-homogenous exponential function to calculate hazard-induced risk costs of bridges considering gradual degradation in the capacity of those bridges against earthquakes. Salman and Stewart (34) also presented a framework to calculate the LCC of aging power distribution lines exposed to hurricane loads during their lifetime. The hazard-induced LCC is calculated by summing over the discounted annual expected hurricane risk costs. In these studies, however, the potential of damage accumulation induced by successive hazards is overlooked. As supported by historical events and discussed in previous chapters, disregarding this effect can result in overestimation of the system reliability against extreme hazards, underestimation of hazard-induced LCCs, and identification of false optimal decisions for lifecycle management of these assets. On the other hand, a few studies attempted to include the effect of damage accumulation in the context of renewal theory. For example, Kumar and Gardoni (31) suggested a risk-based LCC framework based on renewal theory. The renewal instances are considered at the times of completion of repairs or replacements. Repair and replacement decisions are made when the probability of failure of the system is more than a certain threshold. Jia and Gardoni (32) also implemented this framework for the estimation of some lifecycle

performance measures of infrastructure systems, such as availability, and instantaneous probability of being in-service. This renewal LCC method, however, embeds simplifications and several assumptions that limits its application to realistic systems, including:

- After any of such repair/replacement instances, the system is assumed to perform identical to when it has just rebuilt. This assumption brings error in the estimation of the LCC when the system is repaired, which may happen frequently in hazard-prone regions, since the gradual deterioration of infrastructure systems, due to phenomena such as corrosion, may continue even after these systems are repaired.
- All damages are considered to be repaired when failure threshold is violated. For systems that experience different damage types, this assumption is not realistic; since an agency may repair just one type of damage and leave the other damage types untreated. For instance, for the case study bridge system in this dissertation, repairing scour-induced damages are not conducted every time a seismic-induced damage is intended to be repaired. On this basis, even if seismic-induced damages are repaired after each earthquake incident, the vulnerability of the system against earthquake excitations increases with respect to time, as more flood events occur.
- A system is completely out of service during any repair process. However, in reality, many infrastructure systems, including the case study bridge system, may be partially in service while being repaired. Considering the possibility of damage accumulation due to the intervention of further hazards during repair processes, estimation of user cost in the renewal-based LCC framework is a challenge.

- In the estimation of repair or replacement initiation times in the renewal process, demand increases and capacity reductions due to multiple hazard occurrences seems to be separated and independently calculated, while in reality these events are dependent.

Moreover, none of the proposed methods in the literature incorporate more than one type of hazard, which is essential for proper management of structures or infrastructure systems in regions susceptible to multiple types of hazards. For this purpose, this chapter proposes a stochastic LCC framework that addresses the foregoing limitations, and calculates the expected LCC of individual structures or infrastructure systems against multiple types of hazards considering the dependencies among induced damages in the presence of gradual deterioration. In addition, the method facilitates stochastic incorporation of both instantaneous and time-variant damage-state costs.

4.3. Analytical Framework

In this section, the development of the proposed method is presented in detail.

4.3.1. Expected Total Lifecycle Cost

As expressed in previous chapters, the net present value of the expected total LCC of a structure or an infrastructure system, i.e. $\bar{C}_{T,NPV}$, comprises the following costs.

$$\bar{C}_{T,NPV} = \bar{C}_0 + \bar{C}_{M,NPV} + \bar{C}_{R,NPV} \tag{4-1}$$

where $\bar{C}_0$ is the initial construction or retrofit cost, $\bar{C}_{M,NPV}$ is the net present value of the expected LCC of maintenance, and $\bar{C}_{R,NPV}$ is the net present value of the expected hazard-

induced LCC. $\bar{C}_{M,NPV}$ can be articulated as:

$$\bar{C}_{M,NPV} = \sum_{t=1}^{T_{LC}} \gamma^t \times \bar{C}_{m,t} \tag{4-2}$$

where T_{LC} is the considered lifecycle for the system, γ is the discount factor expressed as $\frac{1}{1+\delta}$ with δ as the discount rate, and $\bar{C}_{m,t}$ stands for the expected cost of maintenance at time *t*. Implementing the theorem of total probability and the conditional probability chain rule over the entire possibilities of the number of hazard occurrences during the system lifetime, the term $\bar{C}_{R,NPV}$ can be expanded as follows:

$$\bar{C}_{R,NPV} = \sum_{i=1}^{\infty} P(i, T_{LC}) \times \left(\bar{C}_{R,NPV} \middle| i, T_{LC}\right) \tag{4-3}$$

where $P(i, T_{LC})$ is the probability of *i* hazards occurring during the lifetime of the system, and $\left(\bar{C}_{R,NPV} \middle| i, T_{LC}\right)$ is the net present value of the expected hazard-induced LCC conditioned on the occurrence of *i* hazards during system lifetime. The term *i* in Equation (4-3) should start from 1, since no hazard-induced costs are incurred associated with zero hazards in the lifetime of the system. Evidently, the total hazard-induced costs due to *i* hazard occurrences is the sum of the expected incurred costs after each of the *i* hazards. Therefore, $\left(\bar{C}_{R,NPV} \middle| i, T_{LC}\right)$ can be written as:

$$\left(\bar{C}_{R,NPV} \middle| i, T_{LC}\right) = \sum_{j=1}^{i} \left(\bar{C}^{j}_{R,NPV} | i, T_{LC}\right) \tag{4-4}$$

where $\left(\bar{C}^{j}_{R,NPV} | i, T_{LC}\right)$ is the expected incurred costs after *j*th hazard incident, given the occurrence of *i* hazards during the lifetime of the system. When the system is exposed to

multiple types of hazards that induce *M* different damage types, each having a number of mutually exclusive and collectively exhaustive damage-states, any combination of these damage-states could be experienced by the system after the *j*th hazard. Each of the possibilities of these damage-state combinations incur a particular expected cost until the occurrence of the next hazard (*j*+1th hazard). Applying the theorem of total probability for the entire space of damage-state combinations and the associated expected costs, $\left(\bar{C}_{R,NPV}\middle|i,T_{LC}\right)$ can be expanded as follows:

$$\left(\bar{C}_{R,NPV}\middle|i,T_{LC}\right) = \sum_{j=1}^{i}\sum_{n_1=1}^{N_1}\dots\sum_{n_M=1}^{N_M} P\left(DS^{j}_{[n_1,\dots,n_M]}|i,T_{LC}\right) \times \bar{C}^{j\sim j+1}_{R,NPV}(DS^{j}_{[n_1,\dots,n_M]}|i,T_{LC}) \quad (4\text{-}5)$$

where $N_1,\dots,N_M$ are the total number of damage-states for damage types 1…*M*, respectively, $P\left(DS^{j}_{[n_1,\dots,n_M]}|i,T_{LC}\right)$ is the probability of sustaining damage-state combination $[n_1,\dots,n_M]$ at *j*th hazard given the occurrence of *i* hazards during the system lifetime, and $\bar{C}^{j\sim j+1}_{R,NPV}(DS^{j}_{[n_1,\dots,n_M]}|i,T_{LC})$ is the expected cost of damage-state combination $[n_1,\dots,n_M]$ sustained at *j*th hazard event incurred until the occurrence of the next hazard (*j*+1th hazard) conditioned on the occurrence of *i* hazards during the lifetime of the system.

Decomposing $\bar{C}^{j\sim j+1}_{R,NPV}$ to an instant cost of $\bar{C}^{Inst}_{R}$ as a result of damage-state $[n_1,\dots,n_M]$ which is incurred at *j*th hazard, and a continuous cost of $\bar{C}^{Cont}_{R}(t)$, which is incurred between *j*th and *j*+1th hazards, Equation (4-5) can be written as:

$$\left(\bar{C}_{R,NPV}\middle|i,T_{LC}\right)$$

$$= \sum_{j=1}^{i} \sum_{n_1=1}^{N_1} \dots \sum_{n_M=1}^{N_M} P\left(DS^{j}_{[n_1,\dots,n_M]}|i,T_{LC}\right)$$

$$\times \left(\gamma^{t_j} \times \bar{C}_R^{Inst} \right. \tag{4-6}$$

$$\left. + \int_{t_j}^{\min(t_{j+1},t_j+t_h)} \gamma^{t} \times \bar{C}_R^{Cont}(t|DS^{j}_{[n_1,\dots,n_M]},i,T_{LC}) \,.\, dt \right)$$

To account for impacts of gradual deteriorations due to environmental stressors on the structural performance of the system, it is important to know how much time is passed from the pristine state of the system at the time of *j*th incident. Often, the time at which the system has a pristine state is the construction or replacement time of the system. In this research, for demonstration purposes and to avoid more complexity in the formulations, it is considered that the system has the pristine state only at time 0, i.e. the current time, and it will not be replaced during its lifetime. While this assumption is true for many systems, it imposes error in the estimation of the lifecycle hazard-induced costs. However, as it will be shown in the example section of this chapter, the associated error is negligible, i.e. less than 1%, for the typical case study bridge.

Based on the foregoing explanation, the time of *j*th hazard occurrence, t_j, needs to be added to the formulations. Considering the entire possible space for the time of *j*th incident, in addition to the space of time for the subsequent *j*+1th hazard, $\left(\bar{C}_{R,NPV}\middle|i,T_{LC}\right)$ can be presented as:

$$
\begin{aligned}
&\left(\bar{C}_{R,NPV}\middle|i,T_{LC}\right)\\
&\quad=\sum_{j=1}^{i}\sum_{n_1=1}^{N_1}\cdots\sum_{n_M=1}^{N_M}\int_{t_j=0}^{T_{LC}}\int_{t_{j+1}=t_J}^{T_{LC}} f(t_j,t_{j+1}|i,T_{LC})\\
&\quad\times P\left(DS^{j}_{[n_1,\ldots,n_M]}|i,T_{LC},t_j\right)\\
&\quad\times\Bigg(\gamma^{t_j}\times\bar{C}_R^{Inst}\\
&\quad+\int_{t_j}^{\min(t_{j+1},t_j+t_h)}\gamma^{t}\\
&\quad\times\bar{C}_R^{Cont}(t|DS^{j}_{[n_1,\ldots,n_M]},i,T_{LC})\,.\,dt\Bigg).dt_{j+1}.dt_j
\end{aligned}
\tag{4-7}
$$

where $f\left(t_j,t_{j+1}|i,T_{LC}\right)$ is the probability density function for the occurrence of *j*th and *j*+1th hazards, at times t_j and t_{j+1}, respectively. Noticeably, the term $f\left(t_j,t_{j+1}|I,T_{LC}\right).dt_{j+1}.dt_j$ in Equation (4-7) can be expanded based on Bayes rule as follows:

$$
f(t_j,t_{j+1}|i,T_{LC})=\frac{f(t_j,t_{j+1},i,T_{LC})}{f(i,T_{LC})} \tag{4-8}
$$

Then, inserting Equation (4-8) into Equation (4-7), the term $f(t_j,t_{j+1},i,T_{LC}).dt_{j+1}.dt_j$ for $j\neq i$ can be calculated based on a timeline of events presented in Figure 4-1.

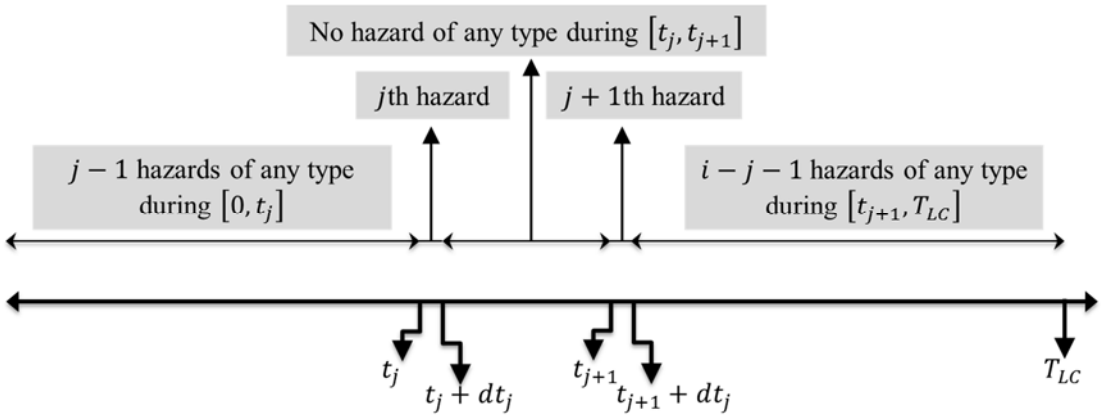

Figure 4-1 Timeline of events for multiple hazard occurrences of hazards, with *j*th and *j*+1th occurring at times t_j and t_{j+1}

Consequently, based on the timeline of events provided in Figure 4-1, $f(t_j, t_{j+1}, i, T_{LC}).dt_{j+1}.dt_j$ for $j \neq i$ can be calculated as:

$$\begin{aligned} & f(t_j, t_{j+1}, i, T_{LC}).dt_{j+1}.dt_j \\ & = P\big(j-1, [0 \;\; t_j]\big) \times P\big(0, [t_j \;\; t_{j+1}]\big) \\ & \times P\big(i-j-1, [t_{j+1} \;\; T_{LC}]\big) \times \upsilon_T{}^2 \times dt_{j+1}.dt_j \end{aligned} \tag{4-9}$$

where υ_T is the combined rate of hazards of different types as $\upsilon_T = \sum_{h=1}^{N_H} \upsilon_h$ with N_H denoting the total number of hazard types. According to the timeline of events used for the calculation of $f(t_j, t_{j+1}, i, T_{LC})$, the term $f(i, T_{LC})$ is the probability of i hazards occurring in the lifetime of the structure. Since this event is not conditioned on the occurrence times of *j*th and *j*+1th hazards, $f(i, T_{LC})$ is independent of $dt_{j+1}.dt_j$. Thus, $f(i, T_{LC})$ can be drawn out of the integrations in Equation (4-7) and expressed as $P(i, T_{LC})$.

Then, integrating Equations (4-7), (4-8), and (4-9) into (4-3), $\bar{C}_{R,NPV}$ can be expressed as:

$$\begin{aligned}\bar{C}_{R,NPV} = \sum_{i=1}^{\infty}\sum_{j=1}^{i}\sum_{n_1=1}^{N_1}\dots\sum_{n_M=1}^{N_M}\int_{t_j=0}^{T_{LC}} P\left(DS^{j}_{[n_1,\dots,n_M]}|i,T_{LC},t_j\right) \\ \times \int_{t_{j+1}=t_j}^{T_{LC}} P\left(j-1,[0\ \ t_j]\right)\times P\left(0,[t_j\ \ t_{j+1}]\right) \\ \times P\left(i-j-1,[t_{j+1}\ \ T_{LC}]\right)\times \upsilon_T{}^2 \\ \times\Bigg(\gamma^{t_j}\times \bar{C}_R^{Inst} \\ +\int_{t_j}^{\min(t_{j+1},t_j+t_h)}\gamma^{t} \\ \times \bar{C}_R^{Cont}(t|DS^{j}_{[n_1,\dots,n_M]},i,T_{LC})\,.\,dt\Bigg).dt_{j+1}.dt_j\end{aligned} \tag{4-10}$$

With a similar analogy, for $j = i$ in Equation (4-7), $\bar{C}_{R,NPV}$ can be written as:

$$\bar{C}_{R,NPV} = \sum_{i=1}^{\infty}\sum_{j=1}^{i}\sum_{n_1=1}^{N_1}\dots\sum_{n_M=1}^{N_M}\int_{t_i=0}^{T_{LC}} P\left(DS^{j}_{[n_1,\dots,n_M]}|i,T_{LC},t_j\right)$$
$$\times P\left(j-1,[0\ \ t_j]\right)\times P\left(0,[t_j\ \ T_{LC}]\right)\times \upsilon_T$$
$$\times\left(\gamma^{t_j}\times \bar{C}_R^{Inst}\right. \tag{4-11}$$
$$\left.+\int_{t_j}^{\min(T_{LC},t_j+t_h)}\gamma^{t}\right.$$
$$\left.\times \bar{C}_R^{Cont}(t|DS^{j}_{[n_1,\dots,n_M]},i,T_{LC})\,.\,dt\right).dt_i$$

Based on Equation (3-13) presented in Chapter 4, the term $P\left(DS^{j}_{[n_1,\dots,n_M]}|i,T_{LC},t_j\right)$ can be expressed as:

$$PP\left(DS^{j}_{[n_1,\dots,n_M]}|i,T_{LC},t_j\right)$$
$$= P(LS^{j}_{[n_1,\dots,n_M]}|i,T_{LC},t_j)$$
$$-\bigcup_{\substack{i_1,\dots,i_M\in\{0,1\}\\(i_1,\dots,i_M)\neq(0,\dots,0)}} P(LS^{j}_{[n_1+i_1,\dots,n_M+i_M]}|i,T_{LC},t_j) \tag{4-12}$$

As explained in the previous chapters, $P\left(LS^{j}_{[n_1,\dots,n_M]}|i,T_{LC},t_j\right)$ is the probability of exceeding limit-state $[n_1,\dots,n_M]$ at jth hazard at the time of t_j given the occurrence of i hazards during the system lifetime. Then, each of the terms $P\left(LS^{j}_{[n_1,\dots,n_M]}|i,T_{LC},t_j\right)$ can be expanded according to Equation (3-15) presented in Chapter 3, as follows:

$$
\begin{aligned}
&P\left(LS^{j}_{[n_1,\dots,n_M]}|i,T_{LC},t_j\right)\\
&=\sum_{n'_1=1}^{N'_1}\dots\sum_{n'_M=1}^{N'_M}\sum_{h=1}^{N_H}\sum_{RP}\sum_{IM_h}P(LS^{j}_{[n_1,\dots,n_M]}\left|\left[RP_{[n'_1,\dots,n'_M]},DS^{j-1}_{[n'_1,\dots,n'_M]},i,T_{LC}\right.\right.\\
&\times P\left(\left[RP_{[n'_1,\dots,n'_M]}\middle|DS^{j-1}_{[n'_1,\dots,n'_M]},HT_h,i,T_{LC},t_j\right]\right)\\
&\times P(DS^{j-1}_{[n'_1,\dots,n'_M]}|i,T_{LC},t_j)\times P(HT_h)\times P(IM_h)
\end{aligned}
\tag{4-13}
$$

As explained in the previous chapter, $RP_{[n'_1,\dots,n'_M]}$ represents the repair status, either 0 (incomplete) or 1 (complete), associated with damage-state $[n'_1,\dots,n'_M]$ that is sustained at j-1th hazard, HT_h is the hazard of type h, and IM_h is the intensity measure of the hazard of type h.

Since the time of jth hazard is a given parameter in the term $P(DS^{j-1}_{[n'_1,\dots,n'_M]}|i,T_{LC},t_j)$ in Equation (4-13), j-1th hazard can happen any time less than t_j from 0 to t_j. Through the application of the total probability theorem and conditional probability chain rule for t_{j-1}, $P(DS^{j-1}_{[n'_1,\dots,n'_M]}|i,T_{LC},t_j)$ can be expanded as follows:

$$
\begin{aligned}
&P(DS^{j-1}_{[n'_1,\dots,n'_M]}|i,T_{LC},t_j)\\
&\quad=\int_{t_{j-1}=0}^{t_j}P(DS^{j-1}_{[n'_1,\dots,n'_M]}|i,T_{LC},t_j,t_{j-1})\\
&\quad\times f\left(t_{j-1}|i,T_{LC},t_j\right).dt_{j-1}
\end{aligned}
\tag{4-14}
$$

Considering that probability of sustaining damage-state $[n'_1,\dots,n'_M]$ due to the j-1th hazard is independent of the time at which the next hazard occurs, the term

$P(DS^{j-1}_{[n'_1,\ldots,n'_M]}|i, T_{LC}, t_j, t_{j-1})$ can be simplified to $P(DS^{j-1}_{[n'_1,\ldots,n'_M]}|i, T_{LC}, t_{j-1})$. With the same analogy provided for the calculation of $f(t_j, t_{j+1}|i, T_{LC})$, the term $f(t_{j-1}|i, T_{LC}, t_j).dt_{j-1}$ in Equation (4-14) can be expressed as $\frac{f(t_{j-1}, i, T_{LC}|t_j).dt_{j-1}}{P(i, T_{LC}|t_j)}$. Based on the timeline of event presented in Figure 4-2, the term $f(t_{j-1}, i, T_{LC}|t_j).dt_{j-1}$, is calculated as follows:

$$\begin{aligned} & f(t_{j-1}, i, T_{LC}|t_j).dt_{j-1} \\ & \quad = P(j-2, [0 \;\; t_{j-1}]) \times P(0, [t_{j-1} \;\; t_j]) \\ & \quad \times P(i-j, [t_j \;\; T_{LC}]) \times \upsilon_T \times dt_{j-1} \end{aligned} \tag{4-15}$$

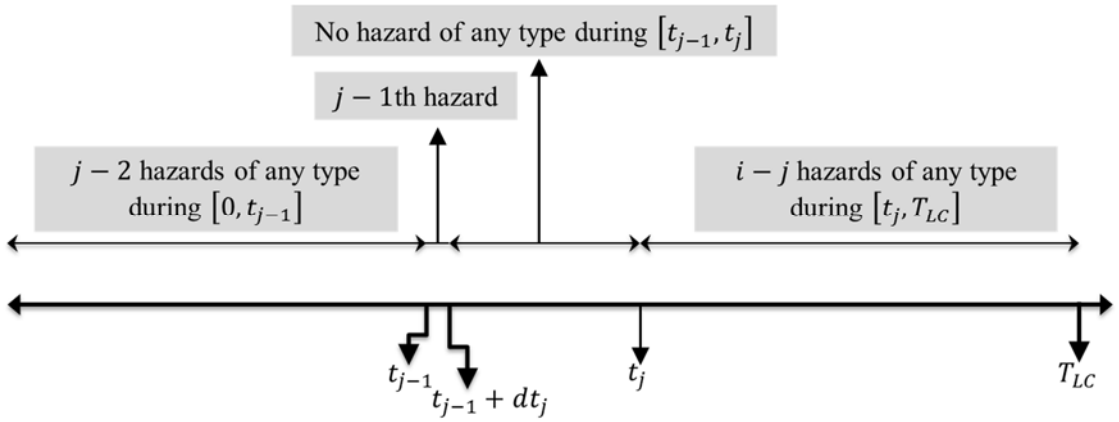

Figure 4-2 Timeline of events for the calculation of the probability of the $f(t_{j-1}, i, T_{LC}|t_j).dt_{j-1}$, with *j*th hazard occurring at time t_j

Based on a timeline of events similar to Figure 4-2, the term $P\left(i, T_{LC} \middle| t_j\right)$ can be expressed as follows:

$$P\left(i, T_{LC} \middle| t_j\right) = P\left(j-1, \left[0 \;\; t_j\right]\right) \times P\left(i-j, \left[t_j \;\; T_{LC}\right]\right) \tag{4-16}$$

Thus, inserting Equations (4-14), (4-15), and (4-16) into Equation (4-13), $P\left(LS^{j}_{[n_1,\ldots,n_M]} | i, T_{LC}, t_j\right)$ can be expressed as:

$$\begin{aligned} & P\left(LS^{j}_{[n_1,\ldots,n_M]} | i, T_{LC}, t_j\right) \\ & = \sum_{n'_1=1}^{N'_1} \ldots \sum_{n'_M=1}^{N'_M} \sum_{h=1}^{N_H} \sum_{RP} \sum_{IM_h} P(LS^{j}_{[n_1,\ldots,n_M]} \left| \left[RP_{[n'_1,\ldots,n'_M]}, DS^{j-1}_{[n'_1,\ldots,n'_M]}, i, T_{LC}, t_j\right], H\right. \\ & \times P\left(\left[RP_{[n'_1,\ldots,n'_M]} \middle| DS^{j-1}_{[n'_1,\ldots,n'_M]}, HT_h, i, T_{LC}, t_j\right]\right) \times P(HT_h) \times P(IM_h) \\ & \times \int_{t_{j-1}=0}^{t_j} P(DS^{j-1}_{[n'_1,\ldots,n'_M]} | i, T_{LC}, t_{j-1}) \times f\left(t_{j-1} \middle| i, T_{LC}, t_j\right). dt_{j-1} \end{aligned} \tag{4-17}$$

It is worthy to note that when hazards occur independently, $P\left(LS^{j}_{[n_1,\ldots,n_M]} | i, T_{LC}, t_j\right) = P\left(LS^{j}_{[n_1,\ldots,n_M]} | i', T_{LC}, t_j\right) \; \forall i, i'$. This is due to the fact that if *j*th hazard takes place at t_j, independent of the total number of hazards occurring in the lifetime of the system, *j*-1 hazards need to occur before t_j. This fact is useful in reducing the computational runtime of the framework.

According to Bayes rule, $P\left(\left[RP_{[n'_1,\ldots,n'_M]} \middle| DS^{j-1}_{[n'_1,\ldots,n'_M]}, HT_h, i, T_{LC}, t_j\right]\right)$ in Equation (4-17) can be articulated as follows:

$$P\left(\left[RP_{[n'_1,\dots,n'_M]}\middle|DS^{j-1}_{[n'_1,\dots,n'_M]},HT_h,i,T_{LC},t_j\right]\right)$$

$$=\frac{P\left(\left[RP_{[n'_1,\dots,n'_M]},HT_h,i,T_{LC}\middle|DS^{j-1}_{[n'_1,\dots,n'_M]},t_j\right]\right)}{P\left(\left[HT_h,i,T_{LC}\middle|DS^{j-1}_{[n'_1,\dots,n'_M]},t_j\right]\right)} \tag{4-18}$$

Considering independent repair processes for each damage type, $P\left(\left[RP_{[n'_1,\dots,n'_M]},HT_h,i,T_{LC}\middle|DS^{j-1}_{[n'_1,\dots,n'_M]},t_j\right]\right)$ in the above equation can be expanded as:

$$P\left(\left[RP_{[n'_1,\dots,n'_M]},HT_h,i,T_{LC}\middle|DS^{j-1}_{[n'_1,\dots,n'_M]},t_j\right]\right)$$

$$=P\left(\left[RP_{[n'_1]},HT_h,i,T_{LC}\middle|DS^{j-1}_{[n'_1,\dots,n'_M]},t_j\right]\right)\times\dots\times \tag{4-19}$$

$$\times P\left(\left[RP_{[n'_M]},HT_h,i,T_{LC}\middle|DS^{j-1}_{[n'_1,\dots,n'_M]},t_j\right]\right)$$

In addition, since two repair statuses are considered for the repair of each damage-state, i.e. complete (1) or incomplete (0), the following holds true:

$$P\left(\left[RP_{n'_k}=0,HT_h,i,T_{LC}\middle|DS^{j-1}_{[n'_1,\dots,n'_M]},t_j\right]\right)+$$

$$P\left(\left[RP_{n'_k}=1,HT_h,i,T_{LC}\middle|DS^{j-1}_{[n'_1,\dots,n'_M]},t_j\right]\right)=1\quad\forall k\in\{1,\dots,M\} \tag{4-20}$$

Calculation of $P\left(\left[RP_{n'_k}=0,HT_h,i,T_{LC}\middle|DS^{j-1}_{[n'_1,\dots,n'_M]},t_j\right]\right)$ with k=1:M, depends on the time difference between t_j and the last time a damage of this type, n'_k, was imposed to the system. Noticeably, this process is not entirely Markovian, since any number of damages of different types can occur between t_J and the last occurrence of a damage of type k before t_j. Since the occurrence of a damage of type k depends on the occurrence of

a hazard that induces this damage type, $P\left(\left[RP_{n'_k}=0, HT_h, i, T_{LC}\middle|DS^{j-1}_{[n'_1,\dots,n'_M]}, t_j\right]\right)$ can be expended as:

$$P\left(\left[RP_{n'_k}=0, HT_h, i, T_{LC}\middle|DS^{j-1}_{[n'_1,\dots,n'_M]}, t_j\right]\right)=$$

$$\sum_{j_1=0}^{j-1}\dots\sum_{j_H=0}^{j-1-\sum_{k=1}^{H-1}j_k} P_H(j_1,\dots,j_H)\times$$

$$P\left(\left[RP_{n'_k}=0, HT_h, i, j_1,\dots,j_H, T_{LC}\middle|DS^{j-1}_{[n'_1,\dots,n'_M]}, t_j\right]\right), \quad \text{with} \quad \sum_{k=1}^{H}j_k = j-1 \tag{4-21}$$

where $P_H(j_1,\dots,j_H)$ is the probability that $j_1, \dots, j_H$ mutually exclusive hazards of types 1, …, H, with $\sum_{k=1}^{H}j_k = J-1$ occurr during [0 t_j). Notably, if zero number of hazards of a hazard type occurs, the probability of incomplete repairs associated with the damage induced by that type of hazard is zero. As can be seen, $P\left(\left[RP_{n'_k}=0, HT_h, i, j_1,\dots,j_H, T_{LC}\middle|DS^{j-1}_{[n'_1,\dots,n'_M]}, t_j\right]\right)$ depends on the hazard types followed by the type of damage that they potentially induce on the system, among others. As explained in the previous chapter, some hazards may induce more than one type of damage. For instance, hurricanes can induce both structural and non-structural damages to buildings. Yet, for many systems, each hazard type induces a particular type of damage. For instance, for the realistic bridge system used as a case study in this dissertation, floods induce scour around foundations or piles, and earthquakes cause structural damages in terms of residual deformation in piers. Thus, scour depth and residual deformation in structural elements can be considered as two types of hazard-induced damages for this bridge. Considering independent hazard occurrences, and that each hazard type induces a

particular type of damage, the term $P_H(j_1, \dots, j_H)$ can be calculated based on the multinomial distribution function as (Hines et al., 2003):

$$P_H(j_1, \dots, j_H) = \frac{j-1!}{j_1! \dots j_H!} P(HT_1)^{j_1} \dots P(HT_H)^{j_H} \tag{4-22}$$

As explained in previous chapters, incomplete repair for a damage-state occurs if the time of the next hazard event is less than the required repair time for that damage-state. On this basis, according to the series of timeline of events shown in Figure 4-3, $P\left(\left[RP_{n'_k} = 0, HT_h, i, j_1, \dots, j_H, T_{LC} \middle| DS^{j-1}_{[n'_1,\dots,n'_M]}, t_j\right]\right)$ can be calculated as follows:

$$\begin{aligned} &P\left(\left[RP_{n'_k} = 0, HT_h, i, j_1, \dots, j_H, T_{LC} \middle| DS^{j-1}_{[n'_1,\dots,n'_M]}, t_j\right]\right) \\ &= \int_{t_{j_k}=\max[t_j-\tau_{n'_k},0]}^{t_j} P_{U-k}(j-1-j_k, [0 \;\; t_j]) \\ &\times P_k(j_k - 1, [0 \;\; t_{j_k}]) \times P_k(0, [t_{j_k} \;\; t_j]) \\ &\times P_U(i-j, [t_j \;\; T_{LC}]) \times \upsilon_k . dt_{j_k} \end{aligned} \tag{4-23}$$

where $\tau_{n'_k}$ is the required time for the repair of damage-state n'_k. Additionally, considering independent hazard occurrences, the probability terms in Equation (4-23) can be calculated using Poisson process. The rate of hazard incidents for these events are given in the subscript of these probability terms, with the following notations: k is the rate of the hazard of type *k*, U is the union (or sum in this case) of the rates of all hazard types, and $U-k$ is the union (or sum in this case) of the rates of all hazard types, excluding (or subtracting in this case) the rate of the hazard of type *k*.

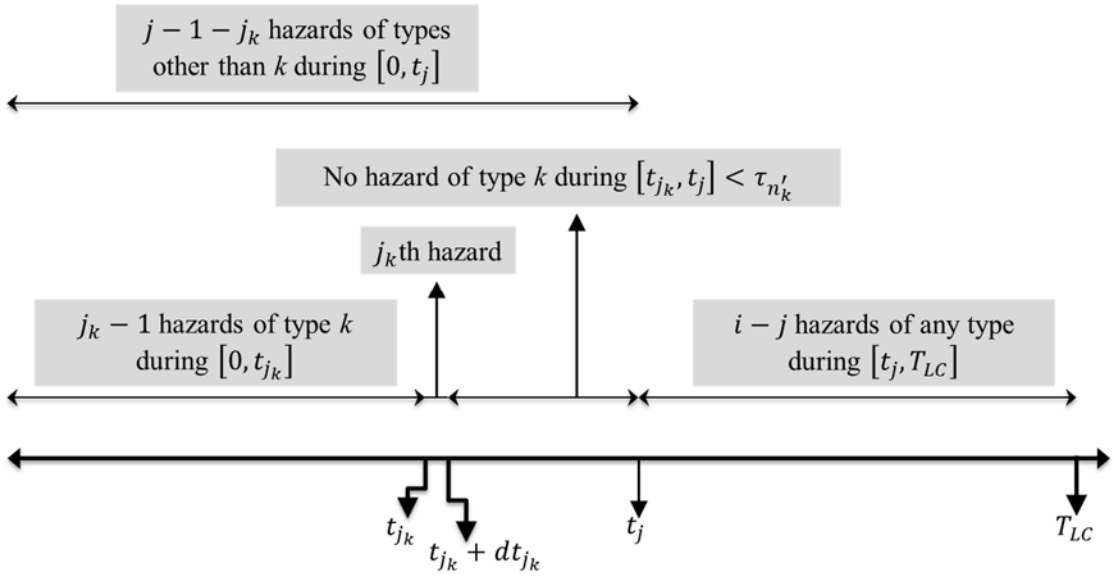

Figure 4-3 Timeline of events for the calculation of the probability of incomplete repair of type k with jth hazard occurring at times t_j

4.3.2. Time-dependent Annual Rate of Collapse and Lifetime Probability of at least One Collapse

Despite the capability of incorporating injuries and casualty losses, among other cost terms, in the proposed hazard-induced LCC framework, some may argue against the consideration of this cost for decision-making in LCC analysis (46,47). As a substitute, some structural guidelines identify minimum acceptable annual probability of collapse or minimum acceptable annual reliability index for structural systems.

In addition, some recent guidelines recommend minimum lifetime collapse probabilities for newly designed structural systems. For example, AASHTO LRFD bridge design specification (104) recommends that the target reliability index for 75 years lifetime of a bridge should be 3.5 for 75 years of lifetime. This value corresponds to the probability of 2.3263e-04 for at least one collapse in 75 years. Thus, Section 4.3.2 and 4.3.3 present methods to calculate the probability of minimum annual rate of collapse and at least one system collapse, respectively, considering damage and repair time dependencies, structural deterioration, and multiple hazard occurrences.

4.3.2.1. Time-Dependent Mean Annual Rate of Collapse

For structures under multiple hazard occurrences, Chapter 2 presented a probabilistic model for time-dependent annual rate of collapse. This section extends that model to account for the impacts of multiple types of hazards, as well as gradual deterioration in the structural system.

As mentioned before, the probability of collapse of a structure or an infrastructure at the time of a hazard depends on the history of seismic events that have happened before the hazard event of interest and whether repairs are complete by this time. Considering i hazards occurring during the lifetime of the system, the hazard for which the reliability of the system should be calculated can vary from the first to the ith hazard. Therefore, for the calculation of the annual rate of collapse, at least one hazard needs to have occurred. Evidently, the worst state of the system occurs at the ith hazard due to the likelihood of damage accumulation. On this basis, mean annual collapse rate of the system should be

evaluated against the *i*th hazard, which can range from one to a large value (theoretically infinity). Considering system deterioration, this event can occur at any time from 0 to the end of the system lifetime.

The mean annual rate of collapse of the system at *i*th hazard occurring at time t_i, given *i* hazards happening during the structural lifetime, i.e. $\lambda\left(DS^{i}_{[n_1,\dots,n_M]}|i,T_{LC},t_i\right)$, can be calculated identical to $P\left(DS^{i}_{[n_1,\dots,n_M]}|i,T_{LC},t_i\right)$ according to Equations (4-12) and (4-17), except that in Equation (4-17), the term $P(IM_h)$ should be replaced by $\lambda(IM_h)$. Considering the variations in the total number of hazards, *i*, the time of the *i*th hazard incident, and all combinations of damage-states that are considered as collapse for the system due to the potential exposure of the system to multiple types of hazards, the mean annual rate of collapse corresponding to the lifetime of the system, $\lambda_F^{T_{LC}}$, can be calculated as:

$$\begin{aligned}\lambda_F^{T_{LC}} &= \lambda^{T_{LC}}\left(DS_{[n_1,\dots,n_M]\in\Omega_F}\right)\\ &= \sum_{i=1}^{\infty} P(i,T_{LC},i\geq 1)\\ &\times \sum_{[n_1,\dots,n_M]\in\Omega_F}\int_{t_i=0}^{T_{LC}} \lambda\left(DS^{i}_{[n_1,\dots,n_M]}|i,T_{LC},t_i\right)\\ &\times f(t_i|i,T_{LC}).\,dt_i\end{aligned} \tag{4-24}$$

where Ω_F is the domain of collapse that entails the entire combinations of damage-states that represent the collapse of the system, and $P(i,T_{LC},i\geq 1)$ is the probability of *i* hazards happening during the lifetime T_{LC}, given that at least one hazard occurs in this period.

Based on Bayes rule, $P(i, T_{LC}, i \geq 1) = \frac{P(i,T_{LC})}{P(i\geq 1)}$, $f(t_i|i, T_{LC})$ can be expressed as $\frac{f(t_i,i,T_{LC})}{P(i,T_{LC})}$. For independent hazard occurrences, $P(i \geq 1)$ can be determined as $1 - e^{-\upsilon_T \times T_{LC}}$. Subsequently, Equation (4-24) can be simplified as:

$$\lambda_F^{T_{LC}} = \sum_{i=1}^{\infty}(1 - e^{-\upsilon_T \times T_{LC}}) \times \sum_{[n_1,\ldots,n_M]\in\Omega_F} \int_{t_i=0}^{T_{LC}} \lambda\left(DS^i_{[n_1,\ldots,n_M]}|i, T_{LC}, t_i\right) \times f(t_i, i, T_{LC}).dt_i \quad (4\text{-}25)$$

Based on the timeline of events is presented in Figure 4-4, the term $f(t_i, i, T_{LC})$ can be computed as follows:

$$f(t_i, i, T_{LC}) = P(I-1, [0\ \ t_i]) \times P(0, [t_i\ \ T_{LC}]) \times \upsilon_T \quad (4\text{-}26)$$

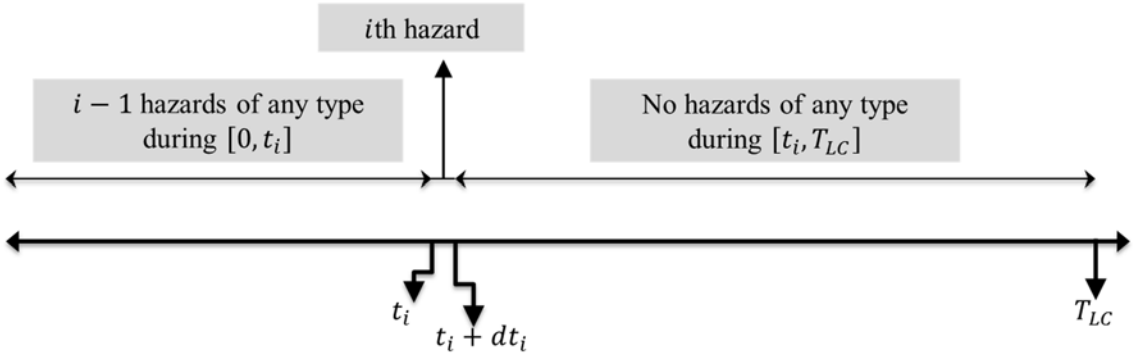

Figure 4-4 Timeline of events for the calculation of $f(t_i, i, T_{LC})$

4.3.2.2. Lifetime Probability of at least One Collapse

The probability of at least one system collapse can be calculated from the complementary event i.e. no lifetime collapse as follows:

$$P([n_1, \dots, n_M] \in \Omega_F) = 1 - P([n_1, \dots, n_M] \notin \Omega_F) \tag{4-27}$$

Considering the entire possibilities for the number of hazards that can occur in the lifetime of the system as well as their occurrence time, the probability that the system does not experience a collapse damage-state during its lifetime can be expressed as:

$$\begin{aligned} &P([n_1, \dots, n_M] \notin \Omega_F) \\ &= \sum_{i=0}^{\infty} \int_{t_i=0}^{T_{LC}} P([n_1, \dots, n_M] \notin \Omega_F | i, T_{LC}, t_i) \\ &\times f(i, T_{LC}, t_i).dt_i \end{aligned} \tag{4-28}$$

where $f(i, T_{LC}, t_i)$ is calculated according to Equation (4-25). The term $P([n_1, \dots, n_M] \notin \Omega_F | i, T_{LC}, t_i)$ is the probability that at no instance during the *i* hazards the system sustains a collapse damage-state. On this basis, this term can be expanded as follows:

$$\begin{aligned} &P([n_1, \dots, n_M] \notin \Omega_F | i, T_{LC}, t_i) \\ &= P\left(DS^1_{[n_1,\dots,n_M]} \notin \Omega_F, \dots, DS^i_{[n_1,\dots,n_M]} \notin \Omega_F \,\middle|\, i, T_{LC}, t_i\right) \end{aligned} \tag{4-29}$$

where $DS^j_{[n_1,\dots,n_M]} \notin \Omega_F$ indicates experiencing a damage-state other than collapse at *j*th hazard. According to Equations (4-12) and (4-17), the probability of a damage-state at each hazard occurrence depends on the state of damage from the previous hazard, among

others. Considering this fact and employing the conditional probability chain rule, Equation (4-29) can be expressed as:

$$\begin{aligned} &P\left(DS^{1}_{[n_1,\dots,n_M]} \notin \Omega_F, \dots, DS^{i}_{[n_1,\dots,n_M]} \notin \Omega_F \,\middle|\, i, T_{LC}, t_i\right) \\ &\quad = P\left(DS^{i}_{[n_1,\dots,n_M]} \notin \Omega_F \,\middle|\, i, T_{LC}, DS^{i-1}_{[n_1,\dots,n_M]} \notin \Omega_F, t_i\right) \\ &\quad \times P\left(DS^{i-1}_{[n_1,\dots,n_M]} \notin \Omega_F \,\middle|\, i, T_{LC}, DS^{i-2}_{[n_1,\dots,n_M]} \notin \Omega_F, t_{i-1}\right) \\ &\quad \times \dots \times P\left(DS^{1}_{[n_1,\dots,n_M]} \notin \Omega_F \,\middle|\, i, T_{LC}, t_1\right) \end{aligned} \tag{4-30}$$

The term $P\left(DS^{j}_{[n_1,\dots,n_M]} \notin \Omega_F \,\middle|\, i, T_{LC}, DS^{j-1}_{[n_1,\dots,n_M]} \notin \Omega_F, t_j\right)$ takes into consideration all possible damage-states that the system can experience, except for damage-states in the collapse domain. Considering the mutually exclusive and collectively exhaustive space of damage-states, this term can be expanded as follows:

$$\begin{aligned} &P\left(DS^{j}_{[n_1,\dots,n_M]} \notin \Omega_F \,\middle|\, i, T_{LC}, DS^{j-1}_{[n_1,\dots,n_M]} \notin \Omega_F, t_j\right) \\ &= \sum_{[n_1,\dots,n_M] \notin \Omega_F} P\left(DS^{j}_{[n_1,\dots,n_M]} \,\middle|\, i, T_{LC}, DS^{j-1}_{[n_1,\dots,n_M]} \notin \Omega_F, t_j\right) \end{aligned} \tag{4-31}$$

Using Equation (4-12), this term can be expressed in terms of probability of limit-state exceedances. Each of these exceedance probabilities, i.e. $P\left(LS^{j}_{[n_1,\dots,n_M]} \,\middle|\, i, T_{LC}, DS^{j-1}_{[n_1,\dots,n_M]} \notin \Omega_F, t_j\right)$, can then be recursively calculated based on Equation (4-17), except that the possibility of $DS^{j-1}_{[n_1,\dots,n_M]} \in \Omega_F$ should be excluded. In mathematical terms:

$$P\left(LS^{j}_{[n_1,\dots,n_M]}\left|i,T_{LC},DS^{j-1}_{[n_1,\dots,n_M]}\notin\Omega_F,t_j\right.\right)$$

$$=\sum_{[n'_1,\dots,n'_M]\notin\Omega_F}\sum_{h=1}^{N_H}\sum_{RP}\sum_{IM_h}P(LS^{j}_{[n_1,\dots,n_M]}\left|\left[RP_{[n'_1,\dots,n'_M]},DS^{j-1}_{[n'_1,\dots,n'_M]},i,T_{LC},t_j\right],HT_h\right.$$

$$\times P\left(\left[RP_{[n'_1,\dots,n'_M]}\left|DS^{j-1}_{[n'_1,\dots,n'_M]},HT_h,i,T_{LC},t_j\right.\right]\right)\times P(HT_h)\times P(IM_h) \qquad (4\text{-}32)$$

$$\times\int_{t_{j-1}=0}^{t_j}P(DS^{j-1}_{[n'_1,\dots,n'_M]}\left|i,T_{LC},t_{j-1}\right.)\times f\left(t_{j-1}\left|i,T_{LC},t_j\right.\right).dt_{j-1}$$

As mentioned before, in the calculation of the expected lifecycle hazard risk costs, it is considered that the deterioration of the system is not renewed during its lifetime. In practical words, the assumption is that the system is not replaced during its lifetime, since system replacement improves the state of the system to its pristine condition. Thus, it is necessary to estimate the imposed error due to neglecting renewals in the deterioration performance of the system. Typically, infrastructure systems are renewed during their lifetime only after experiencing collapse. On this basis, the error associated with disregarding the renewals in the system deterioration is equal to $P([n_1,\dots,n_M]\notin\Omega_F)$, which can be calculated from Equation (4-28). It will be shown in the Result section that this error is negligible for the typical case study bridge.

4.4. Case Study: Five Span Concrete Bridge

For the illustration of the enhanced framework in this Chapter, the same case study bridge as the one evaluated in Chapter 3 is considered. In this section, in addition to the effect of damage-dependencies due to subsequent hazards of floods and earthquakes, the impact of

deterioration on the capacity of the bridge against seismic excitations is also incorporated for the hazard-induced LCC analysis.

As mentioned in Chapter 3, since the bridge is located over a river in the city of Sacramento with a Mediterranean weather (105), a marine environment can be considered for the bridge. In this environment, bridge piers are exposed to deterioration, primarily as a result of corrosion in steel rebar due to chloride penetration (33,94). Therefore, the capacity of the case study bridge against seismic excitations deteriorates over time, which is integrated into the proposed LCC analysis framework presented in this Chapter.

It is worthy to remind that the following four retrofit alternatives, which are identical to the ones considered in the previous chapter, are evaluated in this chapter as well.

1) Status quo plan: The bridge structure is planned to operate as is.
2) CFRP wrapping (CFW) with no scour countermeasure (ScC) plan: All bridge piers will be entirely wrapped with two layers of CFRPs, but no scour countermeasure will be performed on bridge foundations.
3) CFRP wrapping and scour countermeasures plan: All bridge piers will be entirely wrapped with two layers of CFRPs, and ScC actions will be performed on bridge foundations.
4) Scour countermeasures with no CFRP wrapping plan: Only scour countermeasures will be performed on bridge foundations.

4.4.1. Reduction in the Median of Fragility Curves of Piers due to Deterioration

For RC piers of some typical multi-span concrete bridges, Ghosh (33) derived median values for seismic fragility curves for "slight", "moderate", "extensive", and "complete" damage-state. Those values are presented under different environmental conditions. As mentioned in the previous section, the location of the case study bridge has a Mediterranean weather, which has the closest characteristics to the "marine atmospheric exposure condition" considered by Ghosh (33). Based on this study, for RC piers in the marine atmospheric condition, the amount of reduction in the median values of the seismic fragility curves for 0, 25, 50, and 75 years, compared to the pristine median values, are derived as the values are derived and presented in Table 4-1. For instance, the median of the fragility curve for the extensive limit-state 50 years after the pristine condition of the pier is (1-0.272)=0.728 times the median value of this limit-state when the pier is at the pristine condition. Since the seismic capacity of the case study bridge depends only on the seismic capacity of the four RC piers (51), the reductions presented in Table 4-1 are considered as the reductions in the seismic capacity of this bridge.

Table 4-1 The amount of reduction (%) in the median value of the seismic fragility curves for 0, 25, 50, and 75 years (33)

Time from pristine condition (years)	Damage-State			
	Slight	Moderate	Extensive	Complete
0	0	0	0	0
25	20.3	19.2	19.0	18.2
50	28.1	27.3	27.2	25.8
75	29.7	29.3	29.8	29.3

Plots of fragility curves for the case study bridge for moderate, extensive, and complete limit-states are shown in Figure 4-5. These curves are plotted for the case where the bridge is in the slight seismic-induced and intact scour-induced damage-state. As expected, the median of fragility curves, i.e. the PGAs associated with 50% probability of exceeding limit-states, decreases over time for the three limit-states; indicating that the capacity of the bridge against earthquake loads decreases over time due to gradual environmental deterioration.

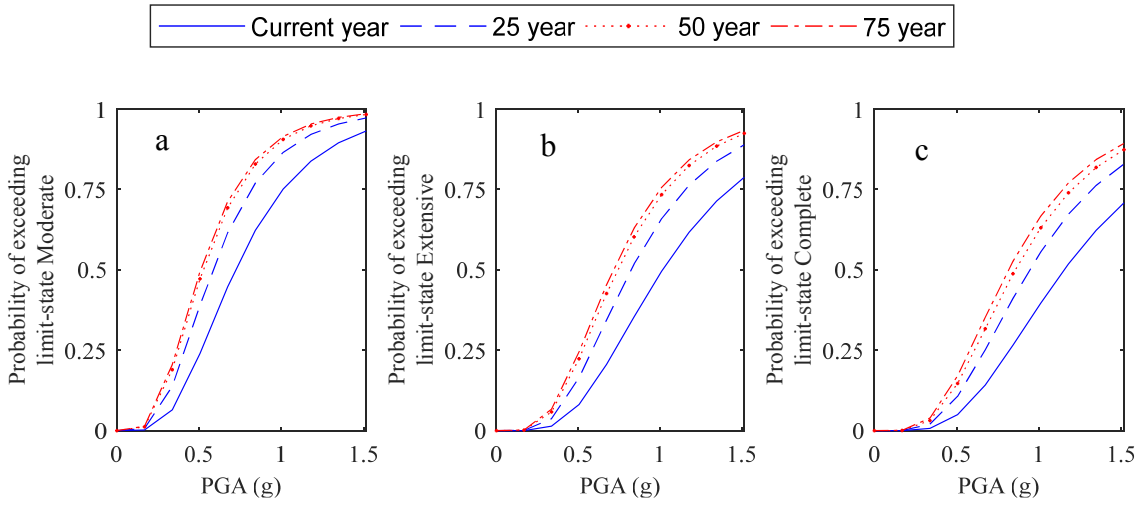

Figure 4-5 Time-variant fragility curves for a) moderate, b) extensive, and c) complete limit-states when the bridge is at the slight seismic-induced damage-state

4.4.2. Reduction in the Median of Fragility Curves of Piers Wrapped with CFRP due to Deterioration

For evaluating the durability of concrete members against corrosion, Green et al. (106) conducted a number of experiments on concrete piers wrapped with CFRP and compared the results with those without wrappings. Their results showed that the typical corrosion rate, i_{corr}, for CFRP retrofitted piers is around 25 percent of the unwrapped ones. According to Stewart (94), for the case of general corrosion, the effective steel area remaining after *t* years of corrosion, $A^r{}_{st}(t)$, can be expressed as follows:

$$A^r{}_{st}(t) = \frac{n\pi(D_0 - 0.0232 i_{corr} t)^2}{4} \tag{4-33}$$

where n is the number of steel rebars, D_0 is the initial rebar diameter, and i_{corr} is the corrosion rate. As can be seen, reduction in the effective area of steel rebar in concrete elements is correlated with the square of the corrosion rate of the steel rebar. On the other hand, the flexural capacity of concrete piers is linearly proportionate to the area of the steel rebar. Thus, considering that the ductility capacity of the bridge is linearly proportionate to the flexural capacity of those piers, the amount of reduction in the median values of fragility curves for limit-state *n* for concrete piers retrofitted with CFRP wraps over time, $MR_n^{CFRP}(t)$, can be derived as:

$$MR_n^{CFRP}(t) = \left(\frac{i_{corr}^{CFRP}}{i_{corr}^{unwrapped}}\right)^2 \times MR_n^{unwrapped}(t) \tag{4-34}$$

where i_{corr}^{CFRP} and $i_{corr}^{unwrapped}$ are the corrosion rates in concrete piers when they are not wrapped, and when they are wrapped with CFRPs, respectively. The term $MR_n^{unwrapped}$

is also the amount of reduction in the median of fragility curves of concrete piers due to deterioration when piers are not wrapped. These values are presented in Table 4-1.

4.4.3. The Impact of Routine Maintenance on the Deterioration of Bridge Piers

Generally, in the case of preventive maintenance, power washing and/or crack sealing may be performed on bridge piers (107). Based on the research study by Pincheira and Dorshorst (108) sealing cracks have a negligible impact on chloride penetration, and consequently corrosion rate of concrete piers. Thus, in this research, it is assumed that conducting maintenance on bridge piers does not affect corrosion deterioration of bridge piers over its lifetime.

4.4.4. Cost Function for Damage-State Combinations of the Case Study Bridge

Considering the list of damage-state dependent costs presented in the previous chapters for the case study bridge, the injury and casualty loss, $\bar{C}_{R,Cas}^{Inst}$, is the only cost that is incurred instantly after the occurrence of a seismic-induced damage-state. Other costs are caused gradually in time. Therefore, $\bar{C}_{R}^{Cont}(t)$ in Equation (4-6) can be split into the following terms:

$$\bar{C}_{R}^{Cont}(t) = \bar{C}_{R,Rep}^{Cont}(t) + \bar{C}_{R,DVE}^{Cont}(t) + \bar{C}_{R,E-Loss}^{Cont}(t) + \bar{C}_{R,Env}^{Cont}(t) \quad (4\text{-}35)$$

where $\bar{C}_{R,Rep}^{Cont}$, $\bar{C}_{R,DVE}^{Cont}$, $\bar{C}_{R,E-Loss}^{Cont}$, and $\bar{C}_{R,Env}^{Cont}$ are the gradual costs of physical repair, DVE, economic losses, and environmental losses as a function of time. For the purpose of demonstration, here it is assumed that the repair/replacement costs are incurred linearly

with respect to time, from the time of damage occurrence until the end of the required repair time.

The user costs of DVE and environmental losses depend on the accessibility of the case study bridge to the users after the bridge sustains damage. According to the formulations presented for the calculation of the DVE cost, depending on the extent of the induced seismic damage-states, the functionality of the bridge increases according to the step functions presented in Figure 2-19. Based on the presented graphs in this figure for extensive and complete damage-states, the entire bridge is closed until fully repaired and reopened for service. For the slight damage-state, one lane of the bridge is closed. However, for the moderate damage-state, there are two stages of recovery: first, the entire bridge is closed for inspection, then two lanes are closed for necessary repairs. For simplification, since the inspection time of the bridge is relatively small compared to the total recovery time of this damage-state, it is assumed that two lanes of the bridge are closed at all times during the recovery of the bridge at the moderate damage-state. On this basis, similar to the gradual repair/replacement costs, the costs of DVE and environmental losses are considered to be linearly increasing from the time of damage occurrence until the end of the required repair time. This consideration holds for the last cost term, i.e. economic losses, as well, since this cost is considered as a multiplication of the DVE cost by two. Therefore, all the unit-in-time costs of physical repair, DVE, economic losses, and environmental losses can be summed together to determine the unit-in-time total cost of $\bar{C}_R^{Cont}$. On this basis, the term $\left(\bar{C}_R^{Inst} + \int_{t_j}^{\min(t_{j+1}, t_j+t_h)} \gamma^t \times \bar{C}_R^{Cont}(t|DS^j_{[n_1,\dots,n_M]}, i, T_{LC}) \,.\, dt\right)$ in Equation (4-6) can be simplified as:

$$\left(\gamma^{t_j} \times \bar{C}_R^{Inst} + \int_{t_j}^{\min(t_{j+1}, t_j+t_h)} \gamma^t \times \bar{C}_R^{Cont}(t|DS^j_{[n_1,\dots,n_M]}, i, T_{LC}) \,.\, dt\right)$$
$$= \gamma^{t_j} \times \bar{C}_R^{Inst} + \frac{\bar{C}_R^{Cont}}{\ln \gamma} \times \left(\gamma^{\min(t_{j+1}, t_j+t_h)} - \gamma^{t_j}\right) \quad (4\text{-}36)$$

Notably, earthquake events may incur instant casualty loss at *j*th hazard, whereas the potential occurrence of a flood does not impose any casualties. On this basis, Equation (4-36) is modified according to Equation (4-37), which is used for hazard-induced LCC calculations of the case study bridge.

$$\left(\gamma^{t_j} \times \bar{C}_R^{Inst} + \int_{t_j}^{\min(t_{j+1}, t_j+t_h)} \gamma^t \times \bar{C}_R^{Cont}(t|DS^j_{[n_1,\dots,n_M]}, i, T_{LC}) \,.\, dt\right)$$
$$= P(HT_{Eq}) \times (\gamma^{t_j} \times \bar{C}_R^{Inst}) + \frac{\bar{C}_R^{Cont}}{\ln \gamma} \quad (4\text{-}37)$$
$$\times \left(\gamma^{\min(t_{j+1}, t_j+t_h)} - \gamma^{t_j}\right)$$

It is worth noting that Equation (4-37) assumes that the initial time of the repair process for the damage-state at *j*th hazard is equal to the occurrence time of this hazard, whereas the repair process may have started earlier and interrupted by this incident. This assumption is considered to avoid further complexities in cost calculations, which can be released in future studies.

4.5. Numerical Results

The numerical results of applying the developed LCC framework in this chapter to the case study bridge is presented in the following sections.

4.5.1. Convergence Analysis

The required number of hazards to consider for the calculation of hazard-induced LCCs as a function of lifetime horizon is displayed in Figure 4-6. These numbers are derived after convergence in hazard-induced LCCs is achieved. Identical to the consideration for the bridge case study in previous chapters, convergence is achieved when the relative difference of the expected hazard-induced cost from two consecutive steps becomes less than 0.005. Similar to the results of convergence analyses in the previous chapters, the required number of hazards to consider increases with the lifetime of the bridge. Additionally, the required number of hazards to achieve convergence is slightly larger than the expected number of hazard occurrences for those lifetimes.

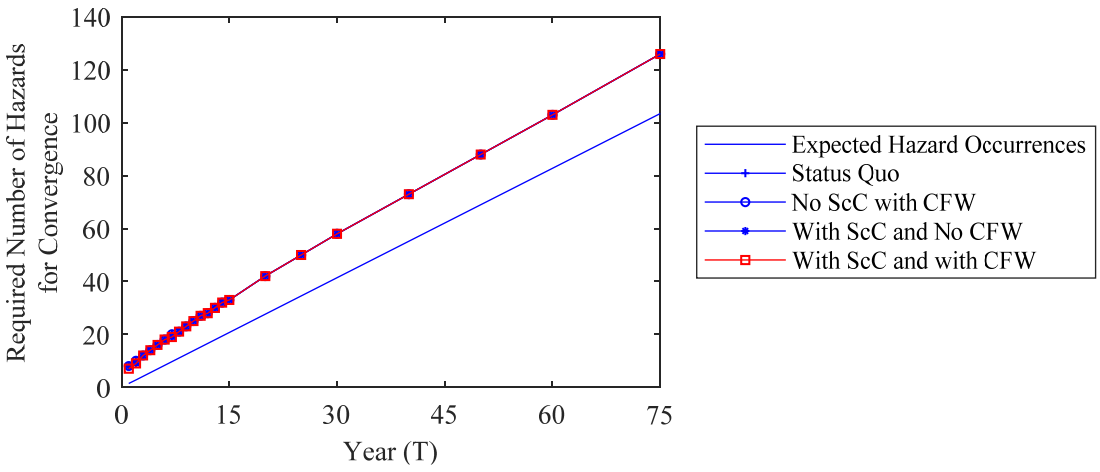

Note: ScC=Scour countermeasure, CFW=Carbon FRP wrap.

Figure 4-6 Required number of hazard incidents to consider in the framework for convergence in lifecycle hazard-induced costs

4.5.2. Lifecycle Cost Analysis and Optimal Decision-Making across Predetermined Alternatives

Considering both user and agency costs, the initial implementation cost of the retrofit plans including status quo, CFRP wrapping with no scour countermeasure, CFRP wrapping and scour countermeasure, and scour countermeasures with no CFRP wrapping are calculated as $0, $532,000, $758,000, and $1,080,000, respectively. The expected maintenance, hazard-induced, and total LCCs of the four retrofit plans are also plotted in Figure 4-3 for lifetime horizons from 0 to 75 years. Similar to the results of Chapter 3, where deterioration is disregarded, the expected hazard-induced LCCs become significantly small when CFRP wrapping is applied to bridge piers. This is expected, since CFRP wrapping not only increases the capacity of the bridge against seismic excitations, but also it considerably decreases the reduction in the seismic capacity of the bridge over time due to steel corrosion. As can be seen, the amount of reduction in the expected hazard-induced LCCs for the scour countermeasure plan is not as high as this reduction for the case of the CFRP wrapping strategy. The implementation cost of the scour countermeasure plan is also higher than the CFRP wrapping strategy. Conclusively, the scour countermeasure plan may not be a cost-effective strategy for improving the seismic performance of the bridge. This is also in line with the results presented in Figure 4-7-a, which does not identify scour countermeasure plan as the optimal decision for any lifetime horizons. According to this figure, performing no retrofit action is optimal for service lifetimes less than 20 years, whereas retrofitting bridge piers with CFRP wrapping is the optimal decision for lifetime horizons equal to or longer than 20 years. These optimal

strategies incur the least expected total LCC on the community among all of the four alternatives.

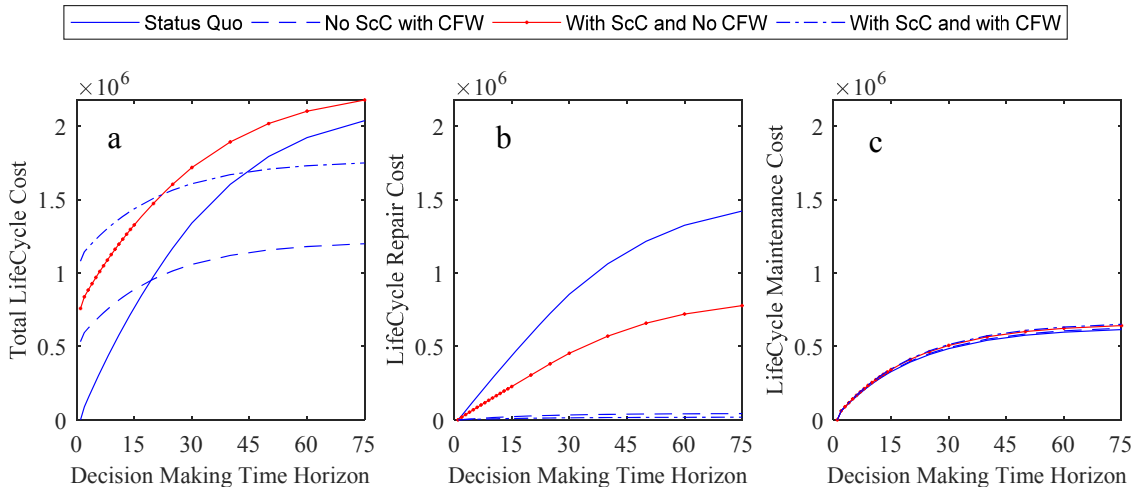

Note: ScC=Scour countermeasure, CFW=Carbon FRP wrap.

Figure 4-7 a) Total, b) Repair, and c) Maintenance LCCs for the considered retrofit alternatives

4.5.3. Significance of Considering Deterioration in Lifecycle Optimal Decision-Making across Predetermined Alternatives

This section demonstrates the importance of considering the effect of deterioration in LLC estimation and optimal decision-making across predetermined retrofit alternatives.

Figure 4-8 presents the results of the expected total LCC of the four retrofit alternatives, with and without considering the effect of deterioration. The former case is also shown in Figure 4-7-a. As can be seen, the expected total LCC for all retrofit alternatives is larger when the effect of capacity reduction against seismic loads due to

gradual deterioration is considered. As an interesting observation, the difference in the expected total LCCs between the cases of considering and disregarding deterioration is substantially large for alternatives that do not enhance (i.e. status quo) or slightly enhance (i.e. scour countermeasures) the seismic capacity of the bridge. This can be explained based on the following two reasons:

1) The bridge has a lower capacity against earthquakes in the presence of gradual deterioration compared to the case where such deterioration is disregarded. This increases the probability of sustaining more severe seismic-induced damage-states, which are more costly. This is a direct impact of deterioration on the vulnerability of the bridge against seismic events.
2) The incurred more severe damage-states, as well as the longer required time to repair those damages increase the likelihood of severe damage-states against upcoming earthquake incidents. This is an indirect impact of deterioration on the vulnerability of the bridge against seismic events.

As a result, deterioration in bridge piers increases the expected total LCC of the case study bridge by 70%. Hence, disregarding deterioration in the LCC analysis could lead to a substantial underestimation of the expected costs, which could adversely impact the allocation of repair budgets for management of bridges.

On the contrary, the difference in the total LCCs between the cases of considering and disregarding deterioration is small for retrofit plans that involve CFRP wrapping, which significantly improve the seismic capacity of the bridge and substantially decrease the gradual deterioration of bridge piers.

Additionally as Figure 4-8 shows, disregarded deterioration in the LCC analysis can lead to misidentification of the optimal decision. For instance, for 50 years expected lifetime, status quo is determined as the optimal plan if the effect of gradual deterioration is overlooked, whereas in reality in the presence of gradual deterioration, the optimal decision is to apply CFRP wrapping to bridge piers. As a consequence of this improper decision, a substantial extra cost of $635,000 is incurred to the society.

It should be noted that one may expect to see identical LCC values in Figure 4-8-b, where the effect of deterioration is overlooked, to those presented for the case study bridge in the previous chapter, i.e. Figure 3-7. Comparing these two figures, the expected total LCC values are close; e.g. there is only 10%, -2%, 5%, and -2% difference between the LCCs of Figure 4-8-b and Figure 3-7-a for the status quo, CFW, ScC, and ScC with CFW retrofit plans, respectively, for 75 years of service lifetime. Notably, the LCCs in Figure 4-8-b, corresponding to status quo and ScC strategies are slightly higher. This can be attributed to the following factor:

- The accumulation of hazard risk costs is more accurately calculated following the method of Chapter 4. In this chapter, the time-variant user and agency costs for the repair of seismic-induced damages are added gradually from the time of damage occurrences until the end of the repair time. However, in the method developed in Chapter 3, these costs are added as a lump sum cost at the time those damages occur. Since the expected inter-arrival time of earthquakes is larger than the required time for the repair of all damage-states, the hazard-induced costs are lumped together in the LCC formulation in Chapter 3. However, these repair processes may be

interrupted by subsequent hazards, in which case lower user and agency costs due to such repairs are incurred. This is taken into account in the framework developed in Chapter 4. For this reason, there is a slight overestimation of the hazard-induced LCCs, for the status quo and ScC alternatives that have higher likelihood of costly and time-consuming hazard-induced damages.

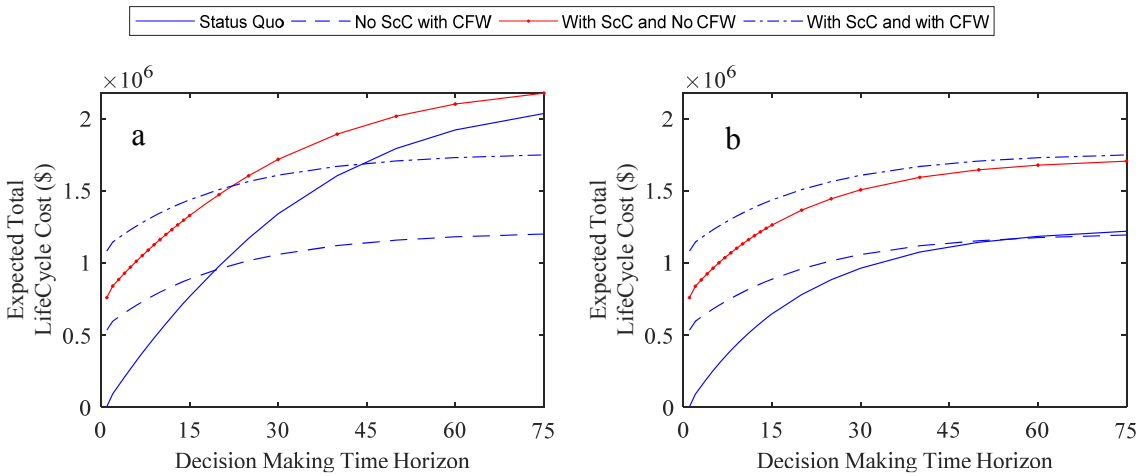

Note: ScC=Scour countermeasure, CFW=Carbon FRP wrap.

Figure 4-8 The expected total LCC of the four retrofit alternatives, a) with and b) without considering the effect of deterioration

4.5.4. The Impacts of Deterioration on the Significance of Damage-Dependencies in Lifecycle Cost Analysis

As demonstrated in previous chapters, a major contribution of the developed LCC frameworks is the incorporation of damage-dependencies in the LCC analysis and optimal decision-making across predetermined retrofit or repair alternatives. This section shows

that the significance of incorporating such dependencies is even more in the presence of deterioration.

For both scenarios of considering and disregarding deterioration, Figure 4-9 presents the expected total LCCs for the status quo and CFRP wrapping strategies considering two cases: 1) when the potential of flood- and earthquake-induced damage-dependencies from consecutive hazards are incorporated, and 2) when such dependencies are overlooked. It is worthy to note that ignoring these damage-dependencies is equivalent to considering instant repairs at the times of damage occurrences for any type of damage, which is a simplified assumption in many existing LCC frameworks.

According to Figure 4-9, neglecting damage-dependencies results in a considerable underestimation of the expected total LCC. For instance, this underestimation is around 34% and 27% for the status quo alternative when gradual deterioration is considered or disregarded, respectively, for 75 years of service lifetime.

Noticeably, this underestimation is larger when deterioration is present. As discussed in the previous section, due to the indirect effect of deterioration on the vulnerability of the bridge against seismic events, expected total LCCs are larger in the presence of deterioration. This indirect effect can only be captured when damage-dependencies are integrated in the LCC analysis procedure. Therefore, disregarding such damage-dependencies overlooks the additional costs as a result of the indirect effect of deterioration, which leads to large differences in the expected total LCCs between the cases of considering and disregarding damage-dependencies when deterioration is present.

Furthermore, in the presence of deterioration, the service lifetime after which the optimal retrofit decision changes from the status quo to implementing CFRP wrapping incorrectly shifts from 20 years to 45 years if damage-dependencies are neglected. On the other hand when deterioration is not incorporated in LCC estimations, the status quo is incorrectly identified as the optimal plan for all service lifetimes for the case where damage-dependencies are neglected. However when deterioration effects are considered, applying CFRP wrapping is found to be the decision with the least expected LCC for lifetimes greater than 50 years.

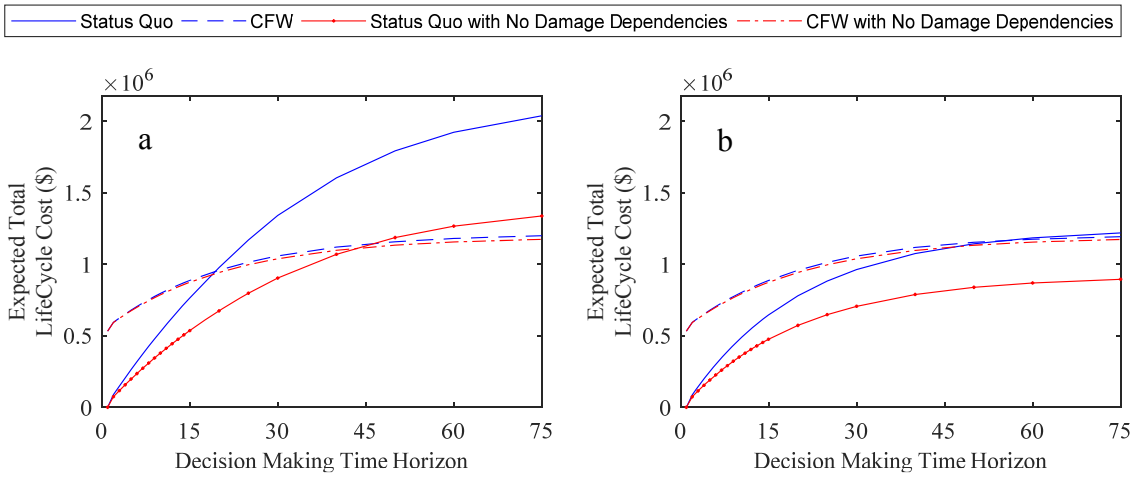

Note: CFW=Carbon FRP wrap.

Figure 4-9 The impact of deterioration on the significance of damage-dependencies in lifecycle cost estimation, a) considering deterioration b) disregarding deterioration

4.5.5. Lifecycle Probability of at least One System Collapse (Replacement)

Considering the state of practice, the system collapse corresponds to the occurrence of the seismic-induced "complete" damage-state for the case study bridge. This damage-state can be joint with any level of flood-induced damage-state.

Additionally, as mentioned in the previous section, AASHTO LRFD bridge design specification (104) recommends 2.3263e-04 as the target probability of at least one collapse for bridge systems that are designed for 75 years of service life. This corresponds to the annual rate of collapse of 3.1021e-06 for bridges. On this basis, the target probability of at least one collapse during the lifetime of a bridge can be determined as $1 - e^{-3.1021\text{e}-06 \times T_{LC}}$ for any time horizon T_{LC}. Results of this target collapse probability are plotted in Figure 4-10 for 1 to 75 years of service lifetimes. Additionally, the plot of the actual probability of at least one collapse for the case study bridge is calculated using Equation (4-27) and shown in Figure 4-10.

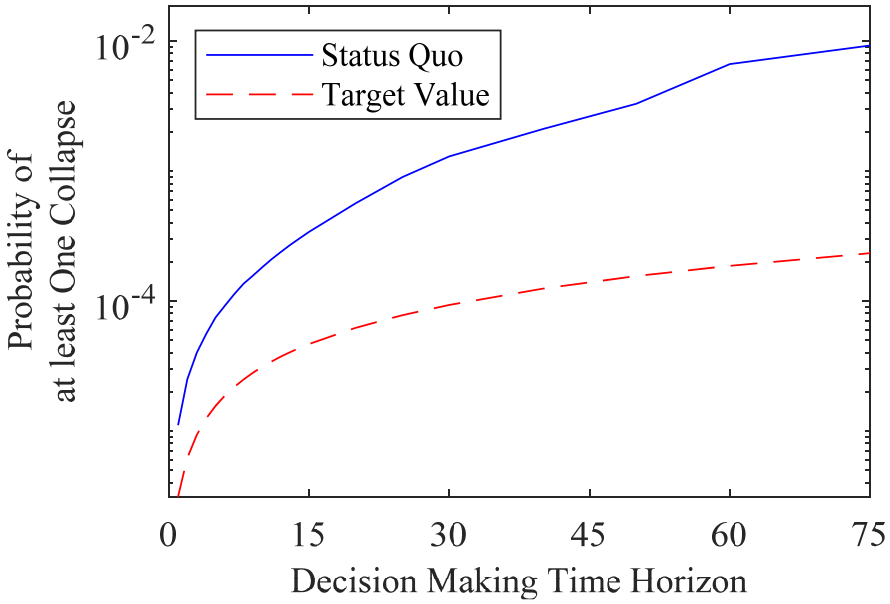

Figure 4-10 The target and actual probability of at least one collapse for the case study bridge

As Figure 4-10 shows, for short lifetimes, the probability of at least one collapse for the case study bridge is close to the target value that is recommended by the AASHTO LRFD bridge design specification (104). However, multiple occurrences of floods and earthquakes with the potential of damage accumulation due to incomplete repairs, as well as capacity reduction due to gradual deterioration increase the collapse probability of the case study bridge over time. This indicates that in order to maintain acceptable reliability for the bridge, it needs to be retrofitted over its lifetime.

As mentioned in the methodology section, the error of disregarding renewals in the deterioration performance of the bridge can also be assessed from the curve presented in Figure 4-10. As expected, the probability of at least one replacement due to structural

collapse increases over time. For the last considered lifetime, i.e. 75 years, this value is still as low as 0.9%. This indicates that the developed framework has a negligible error of less than 1% in assessing the expected total LCC of the case study bridge.

Additionally through this feature, agencies are able to determine error in LCC estimates, and therefore realize the confidence in the calculated costs.

4.5.6. Lifecycle Reliability Analysis

Following Chapter 2, the minimum acceptable annual collapse probability for the case study bridge is derived from the relationship in Bhattacharya et al. (61) and Lazar and Dolsek (62). For the building structure investigated in Chapter 2, the relationship in Bhattacharya et al. (61) and Lazar and Dolsek (62) yielded the minimum acceptable annual probability of collapse of 0.001. For the case study bridge, following the calculation procedures presented in Chapter 3 for casualty losses, the expected number of people at risk for the highest severity level is estimated as $75.7 \times 0.07 = 5.3$ for the complete damage-state. In addition, following Bhattacharya et al. (61), the type of activity, A, and the nature of warning for bridges, W, can be considered as 3.0 and 1.0, respectively. Thus, according to Equation (2-46), the minimum acceptable annual probability of collapse for the case study bridge is calculated as 1.3032e-5. As a common practice in the field of structural engineering, annual probability of collapse of a structure is expressed equivalently by annual reliability index. In mathematical terms, this index is equal to the negative of the value of the standard normal cumulative distribution function evaluated at

the annual collapse probability. On this basis, the acceptable annual reliability index for the case study bridge is calculated as 4.2054.

It is worth mentioning that the minimum acceptable annual probability of collapse or reliability index that is used in this section should be satisfied at all times. However, as noted in the prior section, AASHTO LRFD bridge design specification (104) considers limitation on the reliability of the bridge that varies over time. A potential reason is that in the AASHTO guideline the structural system is designed for lifetime hazards, in addition to the durability of the system elements against corrosive environments (104). In other words, this guideline accounts for reduced capacity of the bridge over time, and ensures that as the bridge deteriorates, its reliability remains acceptable. For this reason, AASHTO LRFD bridge design specification (104) has more strict limitation on the acceptable reliability thresholds, i.e. the target annual probability of collapse according to AASHTO LRFD bridge design specification (104) is 3.1021e-06, while this value is identified as 1.3032e-5 followed by the relationship in Bhattacharya et al. (61) and Lazar and Dolsek (62). For the purpose of evaluating the annual safety reliability of the bridge in this section, the latter relationship is utilized.

Figure 4-11compares the reliability index of the case study bridge for two retrofit alternatives considering various lifetime horizons. As expected, the annual reliability index of the bridge retrofitted with CFRP wrapping is higher compared to the status quo of the bridge. This indicates that CFRP wrapping provides a safer condition against hazards. Furthermore, the reliability index of the bridge falls below the acceptable value for all lifetimes if no retrofit action is taken on the bridge. If this minimum acceptable

reliability index is chosen as the decision-making criterion, the bridge needs to be retrofitted to meet the acceptable level of safety for any service lifetimes.

However, when casualty losses are incorporated in LCC assessments, , no retrofit plans are recommended for time horizons less than 20 years (see Figure 4-7). Figure 4-11also shows that performing CFRP wrapping on piers maintains an acceptable value of reliability index for the bridge for the entire lifetimes ranging from 0 to 75 years.

Finally, it can be seen that the reliability index of the bridge for the two retrofit plans for all service lifetimes is identified as acceptable if the effects of damage-dependencies and gradual deterioration are disregarded. Considering that the un-retrofitted bridge has a reliability less than the minimum acceptable threshold, this leads to the improper decision that performing no retrofit action is also a safe alternative for entire lifetimes. As shown in the results of the LCC analysis, this inappropriate decision may have catastrophic and costly consequences on the community. Thus, it is significant to incorporate the effects of damage-dependencies and gradual deterioration for retrofit decision-making across predetermined alternatives based on the annual reliability index.

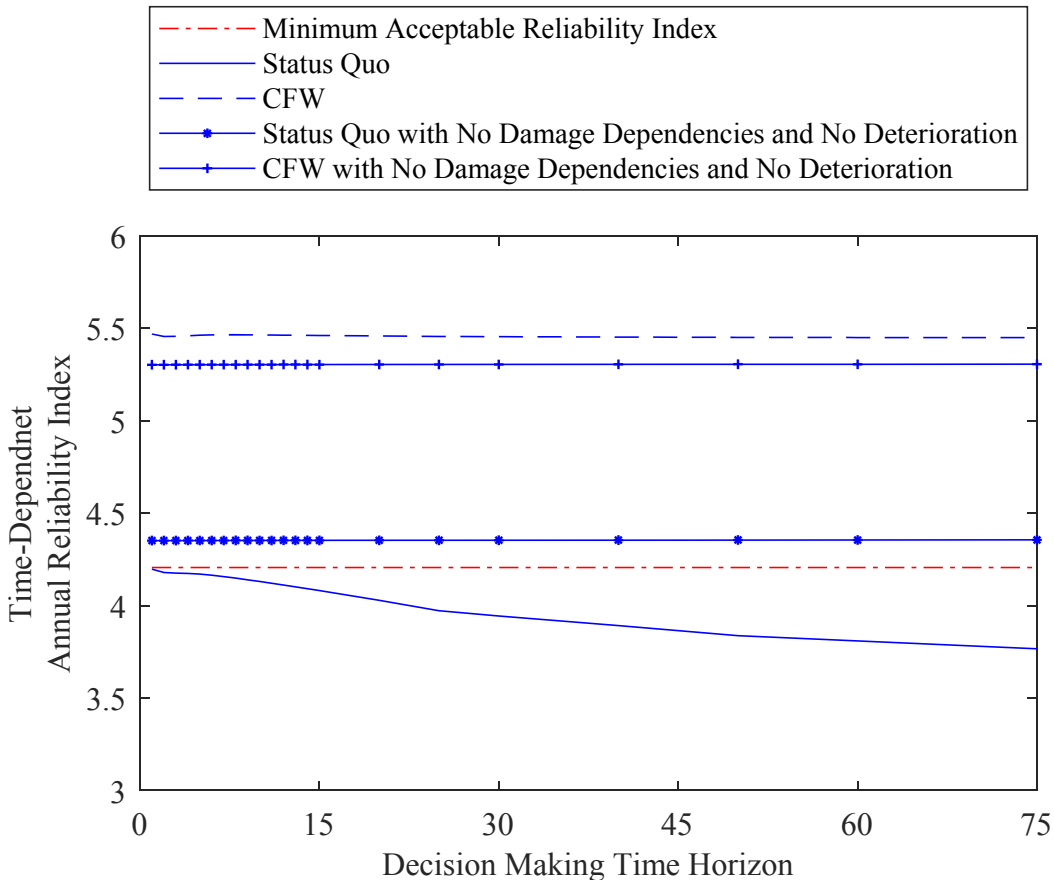

Figure 4-11 Time-dependent annual reliability index of the case study bridge for two retrofit alternatives

4.6. Discussion

In this chapter, effects of gradual deterioration due to environmental stressors were integrated with the potential of multiple types and occurrences of hazards to arrive at a reliable and comprehensive LCC analysis framework for aging infrastructure systems. The expected total LCC in the proposed framework comprises the initial construction or retrofit cost, the net present value of the LCC of maintenance, and the net present value

of the expected hazard-induced LCC. For the latter cost, the framework considers the uncertainties in hazards and structural properties, all possibilities for the time and intensities of hazards, the potential of damage accumulation caused by consecutive hazards as a result of incomplete repairs, and the effect of gradual deterioration due to environmental stressors in the capacity reduction of structures and infrastructure systems against hazard events. To achieve these features, the developed method implements the theorem of total probability, conditional probability chain rule at multiple levels, Bayes rule, and a recursive function for the calculation of damage-state probabilities at each time and hazard occurrences. In addition, the method is capable of stochastically considering both instantaneous and time-variant damage-state costs.

The framework was demonstrated for the case study bridge in previous chapters, which is stochastically exposed to multiple earthquake and flood hazards. In addition, due to the atmospheric marine environment of the bridge, gradual deterioration as a result of corrosion in steel rebar reduces the capacity of the bridge against seismic hazards over time.

Results indicated that degradation due to the imposed environmental stressors significantly increases expected hazard-induced and total LCCs. Hence, disregarding deterioration in the LCC analysis can lead to substantial underestimation of the expected costs, which could adversely impact the allocation of repair budget for management purposes. Results also indicated that applying retrofit plans that have a proper resistance against environmental stressors in addition to considerably improving the seismic capacity of the bridge can substantially decrease hazard-induced costs even for long lifetimes. As

demonstrated, the significance of incorporating damage-dependencies from consecutive hazards is higher in the presence of deterioration. In this case, if damage-dependencies are overlooked, the implications of false decisions on the community are larger. These adverse consequences will not be captured at its full extent if deterioration is not considered in the LCC analysis. In addition, the maximum error associated with disregarding renewals in the system deterioration due to system replacement was found to be less than 1% for the case study bridge. This finding indicates the high accuracy of the proposed framework in the estimation of the hazard-induced LCC.

Finally, if casualty losses are preferred to be excluded from the LCC analysis, the result of the time-dependent annual probability of collapse for the bridge showed an unsafe state for the bridge when no retrofit action is planned to be applied. This critical finding is not observed if the effects of deterioration and damage-dependencies are disregarded.

The foregoing features demonstrate that the proposed method is a comprehensive, reliable, and time-efficient framework for the assessment of the LCCs of hazard mitigation strategies for structures and infrastructure systems. This method can be particularly beneficial to responsible agencies and community decision-makers.

Chapter 5: Summary, Conclusions, and Future Research Directions

In this chapter, summaries of the proposed methods in chapters 2 to 5, together with the associated findings are presented, first. Then, suggestions for future directions of these research studies are provided.

5.1. Summary and Conclusions

Chapter 2 proposed a risk-based lifecycle cost assessment framework that incorporates the possibility of multiple occurrences of an extreme type of hazard in the lifetime of a structure or an infrastructure system. The framework considers uncertainties in hazards and structural properties, all possibilities for the time and intensities of hazards, and the potential of damage accumulation caused by consecutive hazards, among others. Moreover, this framework requires limited input data including hazard curves, cost values, damage-state dependent fragility curves and repair times. In general, the proposed method utilizes the total probability theorem, conditional probability chain rule at multiple levels, Bayes rule, and a developed recursive function for damage-state transition probabilities to arrive at accurate estimations of the expected lifecycle hazard-induced risk costs.

The developed lifecycle cost framework was demonstrated for the selection of the best retrofit and repair plan decisions among a list of alternatives for two realistic case studies, i.e. a four story building and a five span reinforced concrete bridge. For the building structure, six retrofit alternatives were explored and their impacts on the lifecycle

cost were evaluated and ranked for various ranges of building lifetimes. Results showed that neglecting repair times leads to identification of the status quo strategy as safe, while this hypothesis was found to be false with the probability of 50% when repair times are considered. This signifies the importance of incorporating repair times into LCC analysis, and that neglecting repair times leads to considerable overestimation of the reliability of structures or infrastructure systems over their lifetime. The results of the framework on the bridge case study with a high traffic volume indicated that ignoring damage-dependencies leads to considerable underestimation of hazard-induced LCC by as large as 20%. This can have negative consequences for proper allocation of repair budgets during the lifetime of the bridge. Additionally, results showed that investing on fast repair technologies decreases the expected hazard-induced LCC costs, despite the higher costs of implementing these methods. These findings cannot be observed, if damage-dependencies are ignored.

Additionally, Chapter 2 enhanced the formulation of the existing resilience index, which is a common measure in disaster recovery assessment following hazard occurrences, to accurately incorporate the foregoing damage-dependencies from consecutive hazards. Unlike the existing resilience indexes, the developed index, called Risk-based Lifecycle Resilience Index (RLRI), probabilistically accounts for 1) the relative time between stochastic hazard occurrences and 2) damage accumulations due to incomplete repairs, or untreated structural damages. These factors are incorporated using the theorem of total probability, conditional probability chain rule at multiple levels,

Bayes rule, the foregoing recursive function for damage-state transition probabilities, and time-variant reward functions for system recovery at different damage-states.

Implementation of the proposed RLRI framework for the case study bridge showed that disregarding couplings between damages from consecutive earthquakes can result in significant overestimation of the resilience index. This can be misleading, especially for in-advance planning for post hazard recovery of infrastructure systems. In addition, considering a wide range of service lifetimes for the case study bridge, expected RLRIs and LCCs were calculated for multiple repair alternatives with various extents and working speeds of repair actions. Based on this framework and considering limitations on agency's budget and a designated lifetime, optimal repair plans that lead to the highest expected resiliency were proposed. It was demonstrated that a combined application of the proposed LCC and RLRI frameworks can assist agencies to effectively enhance the lifecycle functionality of their structures and infrastructure assets.

Chapter 3 extended the LCC framework presented for multiple occurrences of one hazard type in Chapter 2 to multiple occurrences of multiple types of hazards that may occur at any time and order during the lifetime of a structure or an infrastructure system. In this approach, the damage-state space was extended to a multi-dimensional space of mutually exclusive and collectively exhaustive damage-states. This facilitates the calculation of joint transition probabilities containing damage-states of different types. In addition, to realistically model repair processes in practice, the space of the timeline of events for the calculation of the probability of complete/incomplete repairs is developed

in such a way that the complete/incomplete repair of a damage type depends only on the inter-arrival time of a successive hazard that causes or aggravates that type of damage.

The framework was demonstrated for the case study bridge used in previous chapters. This time the bridge, which is assumed to cross over a river, was exposed to not only earthquake hazards, but also to flood incidents. These flooding events can potentially induce scouring, and therefore increase the vulnerability of the bridge. Four retrofit alternatives were considered for the bridge. It was observed that to achieve a high accuracy in the hazard-induced LCC, the framework requires only slightly more than the expected number of hazards in the considered timespan to converge. This indicates the computational efficiency of the proposed framework. It was demonstrated that the framework is able to quantify the effects of various hazard mitigation plans and identify those that result in the least expected total LCC for various lifetime horizons. The recovery times following each damage-state were found to have significant impact on the hazard-induced LCC, which highlights the necessity of including the required time of recovery in the evaluation of hazard risk costs. Finally, it was demonstrated that ignoring dependencies between damages induced by consecutive hazards may lead to false identification of optimal actions, which can incur considerable additional costs to communities.

Chapter 4 enhanced the framework presented in Chapter 3 by probabilistically integrating the effects of gradual deterioration due to environmental stressors with the potential of multiple types and occurrences of hazards to arrive at a reliable and comprehensive LCC analysis framework for aging structures and infrastructure systems.

Releasing the lump sum cost assumption for the consequences of hazard-induced damages in the previous LCC frameworks, the method developed in this chapter is capable of stochastically considering both instantaneous and time-variant costs. In order to include this feature as well as effects of deterioration in hazard-induced LCCs, the probabilistic structure of the LCC analysis method is modified and the dimension of time is added to the transition probabilities, the recursive function, and the framework for calculating the probability of complete/incomplete repairs.

For the case study bridge, it was observed that degradation due to the imposed environmental stressors significantly increases expected hazard-induced and total LCCs. Results also indicated that retrofit plans that have a proper resistance against environmental stressors in addition to improving the seismic capacity of the bridge can substantially decrease hazard-induced costs even for long lifetimes. Results demonstrated that the vulnerability of infrastructure systems against hazards due to the potential of damage accumulations is amplified in the presence of environmental deterioration. Finally, even when casualty losses are excluded from LCC analysis, the estimated time-dependent annual probability of failure showed that the bridge is unsafe if no retrofit action is applied. This critical finding cannot be observed if the effects of deterioration and damage-dependencies are not considered.

In summary, the above set of conclusions indicate that the developed frameworks presented in this dissertation provide a comprehensive, accurate, and computationally efficient methods that can assist decision makers in finding optimal strategies for individual structures and infrastructure systems exposed to multiple hazards. When the

system is exposed to only one hazard type during its lifetime, the LCC framework proposed in Chapter 2 is suggested to be utilized. When the functionality of systems in such settings is the priority, agencies can benefit from the resilience index formulation proposed in this chapter. For optimal decision-making across predetermined alternatives for systems susceptible to more than one type of hazard, the LCC framework developed in Chapter 3 is recommended. It is noteworthy that the framework in this chapter is also applicable for systems under one type of hazard, however, the computational runtime is slightly higher than the framework presented in Chapter 2. Finally, if the system is vulnerable to gradual degradation due to environmental stressors, in addition to multiple occurrences of hazards of one or different types, the LCC framework in chapter 4 can be employed.

The enhancements offered by these frameworks over existing methods for lifecycle cost analysis of systems will lead to solutions with higher confidence in their effectiveness. This is significant especially for structures and infrastructure systems located in hazard-prone regions or those where damage may cause significant adverse consequences.

5.2. Future Research Directions

Based on the identified assumptions and their limitations (see Section 1.3), in addition to the findings and developments of this dissertation, the following future directions are recommended:

- Considering dependencies among hazard occurrences of either the same or different types, such as mainshock-aftershock events, in the developed lifecycle cost methods.
- Adjusting the developed methods to facilitate the consideration of probability distributions for the current damage-state of the system. This is a more realistic consideration especially for facilities that have been in service for some time, in the light of measurement and sampling errors.
- Performing sensitivity analysis for highly uncertain parameters such as the probabilities of hazard intensities and occurrences, which are difficult to quantify reliably. This assists in evaluating the uncertainties of the expected lifecycle costs for a more reliable design or retrofit alternative decision-making.
- Enhancing the developed methods to incorporate proactive decisions throughout the lifetime of the system, based on the sustained damage-state of the system following hazard occurrences. It is worthy to mention that proactive decision-making frameworks have been developed in the literature in the context of gradual deterioration.
- Applying optimization techniques to identify optimal design, retrofit or repair plans among a wide range of possible alternatives.
- Extending the proposed frameworks to interdependent infrastructure systems in order to capture interdependencies in the evaluation of the performance of systems and optimal decision-making.

- Upgrading the resilience index formulation to incorporate more than one type of hazard in its formulation.
- Developing damage-state dependent fragility curves for various combinations of damage types in regions prone to multiple types of hazards.
- Implementing the proposed frameworks for the design and retrofit of new or existing buildings and infrastructure portfolios.

Bibliography

1. Insurance Journal. Chubb. Hurricanes Harvey, Irma Losses to Top $1 Billion [Internet]. 2017. Available from: https://www.insurancejournal.com/news/national/2017/09/28/465904.htm

2. Insurance Journal. Chubb. Lloyd's Expects $4.5 Billion Hit from Hurricanes Harvey, Irma [Internet]. 2017. Available from: https://www.insurancejournal.com/news/national/2017/09/28/465904.htm

3. Risk Management Solutions. RMS Estimates Hurricane Matthew Insured Losses for the U.S. Will Be Between $1.5 billion and $5 billion [Internet]. Newsroom; 2016. Available from: https://www.rms.com/newsroom/press-releases/press-detail/2016-10-21/rms-estimates-hurricane-matthew-insured-losses-for-the-us-will-be-between-15-billion-and-5-billion

4. Zimmaro P, Stewart J. Engineering Reconnaissance following the October 2016 Central Italy Earthquakes. a report of the NSF-Sponsored GEER Association Team; 2017 Jan.

5. City of Sierra Madre Municipality. 2017. Earthquake [Internet]. Available from: http://www.cityofsierramadre.com/residents/emergency_management/disaster_preparedness/earthquake/

6. Dreger D. The large aftershocks of the Northridge earthquake and their relationship to mainshock slip and fault-zone complexity. Bulletin of the Seismological Society of America. 1997;87(5):1259–1266.

7. BBC news. Strong earthquake rocks New Zealand's South Island [Internet]. 2010. Available from: http://www.bbc.com/news/world-asia-pacific-11183685

8. New Zealand Police. Christchurch earthquake. List of deceased [Internet]. 2012. Available from: http://www.police.govt.nz/major-events/previous-major-events/christchurch-earthquake/list-deceased

9. Matthews P. Death Zone [Internet]. Stuff, Fairfax New Zealand Limited; 2011 Apr. Available from: http://www.stuff.co.nz/the-press/news/christchurch-earthquake-2011/4867859/Death-Zone

10. Macfie R. Collapse of accountability: Christchurch's CTV building [Internet]. Published in Noted; 2014 Feb. Available from: http://www.listener.co.nz/currently/social-issues/collapse-of-accountability-christchurchs-ctv-building/

11. United States Geological Survey (USGS). Magnitude 9.03 – Near The East Coast Of Honshu, Japan". 2015.

12. Syed S. Japan quake: Infrastructure damage will delay recovery. BBC News. 2011;

13. Blake E, Zelinsky D. National Hurricane Center Tropical Cyclone Report: Hurricane Harvey (AL092017) [Internet]. National Hurricane Center; 2018. Available from: https://www.nhc.noaa.gov/data/tcr/AL092017_Harvey.pdf

14. Padgett J, Ebad Sichani M, Vishnu N, Misra S, Kameshwar S, Panakkal P, et al. Post-Harvey Houston-Galveston Roadway Bridge Reconnaissance. DesignSafe-CI, doi:10.17603/DS2HM4H; 2018.

15. FEMA 445. Next-generation performance-based seismic design guidelines program plan for new and existing buildings. 2006.

16. Chang S, Shinozuka M. Life-cycle cost analysis with natural hazard risk. Journal of Infrastructure Systems. 1996;2 (3):118–126.

17. Goulet C, Haselton C, Mitrani-Reiser J, Beck J, Deierlein G, Porter K, et al. Evaluation of the seismic performance of a code-conforming reinforced-concrete frame building—from seismic hazard to collapse safety and economic losses. Earthquake Engineering & Structural Dynamics. 2007;36(13):1973–97.

18. Padgett JE, Dennemann K, Ghosh J. Risk-based seismic life-cycle cost–benefit (LCC-B) analysis for bridge retrofit assessment. Structural Safety. 2010;32(3):165–173.

19. Frangopol D. Life-cycle performance, management, and optimisation of structural systems under uncertainty: accomplishments and challenges. 1 Structure and Infrastructure Engineering. 2011;7(6):389–413.

20. Vanmarcke E, Guerrero J. Markov Decision Models in Seismic Design. MIT Department of Civil Engineering: Cambridge,; 1971.

21. Yeo G, Cornell C. Post-quake decision analysis using dynamic programming. Earthquake Engineering & Structural Dynamics. 2009;38(1):79–93.

22. Veneziano D, Agarwal A, Karaca E. Decision making with epistemic uncertainty under safety constraints: an application to seismic design. Probabilistic Engineering Mechanics. 2009;24(3):426–37.

23. Freddi F, Padgett J, Dall'asta A. Life cycle cost analysis of low ductility RC frame buildings retrofitted by modern retrofit techniques. In Genoa, Italy: 5th European Conference on Structural Control; 2012.

24. Junca M, Sanchez-Silva M. Optimal maintenance policy for permanently monitored infrastructure subjected to extreme events. Probabilistic Engineering Mechanics. 2013;33:pp.1-8.

25. Yilmaz T, Banerjee S, Johnson PA. Performance of two real-life California bridges under regional natural hazards. Journal of Bridge Engineering. 2015;21(3):04015063.

26. Chandrasekaran S, Banerjee S. Retrofit optimization for resilience enhancement of bridges under multihazard scenario. Journal of Structural Engineering. 2015;142(8):C4015012.

27. Wen YK, Kang YJ. Minimum building life-cycle cost design criteria. II: Applications. Journal of Structural Engineering. 2001;127(3):338–346.

28. Decò A, Frangopol DM. Risk assessment of highway bridges under multiple hazards. Journal of Risk Research. 2011;14(9):1057–1089.

29. Jalayer F, Asprone D, Prota A, Manfredi G. Multi-hazard upgrade decision making for critical infrastructure based on life-cycle cost criteria. Earthquake Engineering & Structural Dynamics. 2011;40(10):1163–1179.

30. Fereshtehnejad E, Shafieezadeh A. Multiple hazard incidents lifecycle cost assessment of structural systems considering state-dependent repair times and fragility curves. Earthquake Engineering & Structural Dynamics. 2016;45(14):2327–2347.

31. Kumar R, Gardoni P. Renewal theory-based life-cycle analysis of deteriorating engineering systems. Structural Safety. 2014 Sep;50:94–102.

32. Jia G, Tabandeh A, Gardoni P. Life-Cycle Analysis of Engineering Systems: Modeling Deterioration, Instantaneous Reliability, and Resilience. In: Gardoni P, editor. Risk and Reliability Analysis: Theory and Applications [Internet]. Cham:

Springer International Publishing; 2017 [cited 2018 Mar 29]. p. 465–94. Available from: http://link.springer.com/10.1007/978-3-319-52425-2_20

33. Ghosh J. Parameterized seismic reliability assessment and life-cycle analysis of aging highway bridges [PhD Thesis]. 2013.

34. Salman AM, Li Y, Stewart MG. Evaluating system reliability and targeted hardening strategies of power distribution systems subjected to hurricanes. Reliability Engineering & System Safety. 2015;144:319–333.

35. Ouyang M, Dueñas-Osorio L, Min X. A three-stage resilience analysis framework for urban infrastructure systems. Structural safety. 2012;36:23–31.

36. Ouyang M, Duenas-Osorio L. Multi-dimensional hurricane resilience assessment of electric power systems. Structural Safety. 2014;48:15–24.

37. Burton H, Deierlein G, Lallemant D, Lin T. Framework for incorporating probabilistic building performance in the assessment of community seismic resilience. Journal of Structural Engineering. 2015;(DOI:10.1061/(ASCE) ST.1943-541X.0001321):1–11.

38. Karamlou A, Bocchini P. Computation of bridge seismic fragility by large□scale simulation for probabilistic resilience analysis. Earthquake Engineering & Structural Dynamics. 2015;44(12):pp.1959-1978.

39. Frangopol D, Estes A. Optimum lifetime planning of bridge inspection and repair programs. In Structural Engineering International; 1999. p. 219–23.

40. Bruneau M, Chang SE, Eguchi RT, Lee GC, O'Rourke TD, Reinhorn AM, et al. A framework to quantitatively assess and enhance the seismic resilience of communities. Earthquake spectra. 2003;19(4):733–752.

41. Cimellaro GP, Reinhorn AM, Bruneau M. Framework for analytical quantification of disaster resilience. Engineering structures. 2010;32(11):3639–3649.

42. Bocchini P, Frangopol DM. Optimal resilience-and cost-based postdisaster intervention prioritization for bridges along a highway segment. Journal of Bridge Engineering. 2010;17(1):117–129.

43. Decò A, Bocchini P, Frangopol DM. A probabilistic approach for the prediction of seismic resilience of bridges. Earthquake Engineering & Structural Dynamics. 2013;42(10):1469–1487.

44. Petersen M, Frankel A, Harmsen S, Mueller C, Haller K, Wheeler R, et al. Documentation for the 2008 update of the United States National Seismic Hazard Maps. U.S. Geological Survey Open-File Report 2008-1128; 2008.

45. Der Kiureghian A. Non-ergodicity and PEER's framework formula. Earthquake Engineering & Structural Dynamics. 2005;34(13):1643–52.

46. Morrow R, Bryant J. Health policy approaches to measuring and valuing human life: conceptual and ethical issues. American Journal of Public Health. 1995;85(10):1356–60.

47. Holguín-Veras J, Pérez N, Jaller M, Van Wassenhove L, Aros-Vera F. On the appropriate objective function for post-disaster humanitarian logistics models. Journal of Operations Management. 2013;31(5):262–80.

48. Abo El Ezz A. Deformation and strength based assessment of seismic failure mechanisms for existing RC frame buildings [Master's dissertation,]. [Italy]: ROSE School; 2008.

49. Abad J, Ulrich T, Réveillere A, Gehl P. Development of damage-state-dependent fragility functions for a MDOF structure through dynamic analyses with successive un-scaled time-histories. In Vienna; 2013.

50. Mfawy A, Elkholy S. Comparative vulnerability assessment of retrofit techniques for pre-code RC structures. In: In Proceedings of the 15th World Conference on Earthquake Engineering. 2012.

51. Prasad G, Banerjee S. The impact of flood-induced scour on seismic fragility characteristics of bridges. Journal of Earthquake Engineering. 2013;17(6):803–28.

52. Bai J. Seismic fragility and retrofitting for a reinforced concrete flat-slab structure [Doctoral dissertation]. Texas A&M University; 2004.

53. Akbarii R, Aboutalebi M, Maheri M. Seismic fragility assessment of steel X-braced and chevron-braced RC frames. Asian Journal Of Civil Engineering (Bhrc). 2015;16(1):13–27.

54. NIBS, FEMA. Multi-Hazard Loss Estimation Methodology. Earthquake Model, HAZUS® MH Technical Manual, National Institute of Building Sciences and Federal Emergency Management Agency. Washington DC; 2007. Report No.: 2003; 690.

55. Liel A, Deierlein G. Cost-benefit evaluation of seismic risk mitigation alternatives for older concrete frame buildings. Earthquake Spectra. 2013;29(4):1391–1411.

56. DASSE. Cost advantages of buckling restrained braced frame buildings. DASSE Design Inc. Structural Engineers; 2007.

57. Less T. Structural performance and corrosion resistance of fiber reinforced polymer wrapped steel reinforcing bars [MSc Thesis]. The Ohio State University,; 2013.

58. Gwartney T. Estimating Land Values. Arden,Delaware; 1999 p. 1–25.

59. Joint Committee on Structural Safety, JCSS. Probabilistic Model Code. Part 1 - Basic of Design. Technical University of Denmark; 2000.

60. Allen D. Criteria for design safety factors and quality assurance expenditure. In: In Proc of the 3rd Int. 1981. p. 667–78.

61. Bhattacharya B, Basu R, Ma K. Developing target reliability for novel structures: the case of the mobile offshore base. Marine Structures. 2001;14(1):37–58.

62. Lazar N, Dolšek M. Risk-based seismic design—an alternative to current standards for earthquake-resistant design of buildings. In: In Proceedings of the 15th World. 2012.

63. FEMA 227. A benefit–cost model for the seismic rehabilitation of buildings. In 1992.

64. Thomas W. Ryan, P.E., J. Eric Mann, P.E., Zachary M. Chill, E.I.T., Bryan T. Ott. Bridge Inspector's Reference Manual (BIRM). National Highway Institute (NHI); Report No.: Publication No. FHWA NHI 12-050.

65. Fereshtehnejad E, Shafieezadeh A. OPTIMAL RETROFIT DECISION-MAKING FOR BRIDGE SYSTEMS BASED ON MULTI-HAZARD LIFECYCLE COST ANALYSIS. In: Eleventh International Bridge and Structures Management Conference. 2017. p. 160.

66. Earthquake Track. 2018. Recent Earthquakes Near Sacramento, California, United States [Internet]. Available from: https://www.earthquaketrack.com/us-ca-sacramento/recent?mag_filter=6

67. Furtado M, Alipour A. Cost assessment of highway bridge network subjected to extreme seismic events. Transportation Research Record: Journal of the Transportation Research Board. 2014;42(10):1469–87.

68. Decò A, Bocchini P, Frangopol DM. A probabilistic approach for the prediction of seismic resilience of bridges. Earthquake Engineering & Structural Dynamics. 2013;42(10):1469–1487.

69. Kelly D. Seismic Site Classification for Structural Engineers. Structure. 2006;21.

70. Prasad G. Analysis of bridge performance under the combined effect of earthquake and flood-induced scour [Master Thesis]. The Pennsylvania State University; 2011.

71. Raghunandan M, Liel AB, Luco N. Aftershock collapse vulnerability assessment of reinforced concrete frame structures. Earthquake Engineering & Structural Dynamics. 2015;44(3):419–439.

72. Gordin E. Performance-based decision-making in post-earthquake highway bridge repair [PhD Thesis]. UC Berkeley; 2010.

73. Shinozuka M, Murachi Y, Dong X, Zhou Y, Orlikowski MJ. Seismic performance of highway transportation networks. In: Proceedings of China-US Workshop on protection of urban infrastructure and public buildings against earthquakes and man-made disasters. 2003.

74. Caltrans. Historic Bridge Inventory, Sample Plans of Actions. Division of Maintenance, Structure Maintenance [Internet]. 2005. Available from: http://www.dot.ca.gov/hq/structur/strmaint/poa_samp.pdf

75. LuAnn Copeland. User`s manual for QYEWZ-98. Texas Transportation Institute. The Texas A&M University System; 1998.

76. Ohio Department of Transportation (ODOT). Innovative Contracting Manual. Division of Construction Management; 2010.

77. Zegeer JD, Vandehey M, Blogg M, Nguyen K, Ereti M. NCHRP report 599: Default values for highway capacity and level of service analyses. Transportation Research Board of the National Academies, Washington, DC. 2008;

78. Caltrans. Annual Average Daily Truck Traffic on the California State Highway System. Traffic Data Branch; 2014.

79. Caltrans. California Manual on Uniform Traffic Control Devices. Part 6 Temporary Traffic Control [Internet]. 2014. Available from: http://www.dot.ca.gov/trafficops/camutcd/docs/CAMUTCD2014_rev1.pdf

80. Kliesen K, Mill J. The economics of natural disasters. The regional economist. Federal Reserve Bank of St. Louis; 1994 Apr. Report No.: 332.

81. Porter K, Shoaf K, Seligson H. Value of injuries in the Northridge earthquake. Earthquake Spectra. 2006;22(2):555–563.

82. Caltrans. High Occupancy Vehicle Lanes Status Report. Sacramento Metropolitan Area. Sacramento: District 3. Office of Freeway Operations; 2011.

83. Soliman M, Frangopol DM. Life-cycle cost evaluation of conventional and corrosion-resistant steel for bridges. Journal of Bridge Engineering. 2014;20(1):06014005.

84. Dong Y, Frangopol DM, Saydam D. Time-variant sustainability assessment of seismically vulnerable bridges subjected to multiple hazards. Earthquake Engineering & Structural Dynamics. 2013;42(10):1451–1467.

85. Gallivan F, Ang-Olson J, Papson A, Venner M. GREENHOUSE GAS MITIGATION MEASURES FOR TRANSPORTATION CONSTRUCTION, MAINTENANCE, AND OPERATIONS ACTIVITIES. 2010;

86. Kendall A, Keoleian GA, Helfand GE. Integrated life-cycle assessment and life-cycle cost analysis model for concrete bridge deck applications. Journal of Infrastructure Systems. 2008;14(3):214–222.

87. Darestani YM, Shafieezadeh A, DesRoches R. Effects of Adjacent Spans and Correlated Failure Events on System-Level Hurricane Reliability of Power Distribution Lines. IEEE Transactions on Power Delivery. 2017;

88. Jeon J-S, Shafieezadeh A, Lee DH, Choi E, DesRoches R. Damage assessment of older highway bridges subjected to three-dimensional ground motions: characterization of shear–axial force interaction on seismic fragilities. Engineering Structures. 2015;87:47–57.

89. Shafieezadeh A, Burden LI. Scenario-based resilience assessment framework for critical infrastructure systems: Case study for seismic resilience of seaports. Reliability Engineering & System Safety. 2014;132:207–219.

90. Lehman DE. Seismic performance of well-confined concrete bridge columns. 2000;

91. Chapter 6. Probability, Unions and Intersections [Internet]. 2018. Available from: https://math.dartmouth.edu/archive/m19w03/public_html/Section6-2.pdf

92. Kiureghian AD. Non-ergodicity and PEER's framework formula. Earthquake engineering & structural dynamics. 2005;34(13):1643–1652.

93. George MR. Mediterranean Climate. UC Rangelands Research and Education Archive. UC Cooperative Extension [Internet]. 2018. Available from: http://rangelandarchive.ucdavis.edu/Annual_Rangeland_Handbook/Mediterranean_Climate/

94. Stewart MG. Spatial variability of pitting corrosion and its influence on structural fragility and reliability of RC beams in flexure. Structural Safety. 2004;26(4):453–470.

95. Rai GL. Different Strengthening Techniques for RC Columns. R&M International.

96. Gallardo B, Gabriel RA. Achieving Operational Seismic Performance of RC Bridge Bents Retrofitted With Buckling-Restrained Braces [Doctoral dissertation]. Portland State University; 2017.

97. Toutanji H, Balaguru P. Durability characteristics of concrete columns wrapped with FRP tow sheets. Journal of materials in civil engineering. 1998;10(1):52–57.

98. Shinozuka M, Zhou Y, Kim S-H, Murachi Y, Banerjee S, Cho S, et al. Socio-economic effect of seismic retrofit implemented on bridges in the Los Angeles highway network. Final report to the California Department of Transportation, Division of Research and Innovation. 2005;

99. Billah AM, Alam MS, Bhuiyan MR. Fragility analysis of retrofitted multicolumn bridge bent subjected to near-fault and far-field ground motion. Journal of Bridge Engineering. 2012;18(10):992–1004.

100. Manukonda S. Cost Estimation of FRP Wrapping for Bridge Rehabilitation Using Regression Analysis. West Virginia University Libraries; 2011.

101. Teng M, Sotelino E, Chen W. Monitoring of Long-Term Performance of Highway Bridge Columns Retrofitted by Advanced Composite Jackets in Indiana. 2000;

102. Fereshtehnejad E, Shafieezadeh A. A multi-type multi-occurrence hazard lifecycle cost analysis framework for infrastructure management decision making. Engineering Structures. 2018;167:504–517.

103. Shokrabadi M, Burton HV. Building service life economic loss assessment under sequential seismic events. Earthquake Engineering & Structural Dynamics. 2018;47(9):1864–1881.

104. American Association of State Highway and Transportation Officials (AASHTO). AASHTO LRFD Bridge Design Specifications. 2012.

105. UC Rangelands Research and Education Archive. Mediterranean Climate [Internet]. Available from: http://rangelandarchive.ucdavis.edu/Annual_Rangeland_Handbook/Mediterranean_Climate/

106. Green MF, Bisby LA, Fam AZ, Kodur VK. FRP confined concrete columns: Behaviour under extreme conditions. Cement and concrete composites. 2006;28(10):928–937.

107. Ohio Department of Transportation. Structure Management System (SMS) [Internet]. 2017. Available from: https://www.dot.state.oh.us/Divisions/Engineering/Structures/Pages/Structure-Management-System.aspx

108. Pincheira JA, Dorshorst MA. Evaluation of concrete deck and crack sealers. Wisconsin Highway Research Program; 2005.